7.1
High Nuclearity Clusters: Iso and Heteropolyoxoanions and Relatives

L. CRONIN
University of Glasgow, UK

7.1.1 INTRODUCTION

Since the early 1980s the field of polyoxometalate chemistry has undergone a revolution. This has been characterized by the synthesis of ultra-large clusters that have nuclearities as high as 368 metal atoms in a single molecular cluster.[1] Of course, such discoveries have only been possible thanks to the advances of the instrumentation used to collect the diffraction data coupled with the advent of cheap and powerful computing power for structure solution and refinement. Much of the interest in these molecules has arisen because such clusters represent a paradigm in the discovery of systems that can be encouraged to grow from the molecular to the nanoscale. Polyoxometalates have also generated interest in areas as diverse as catalysis,[2–13] magnetism,[14–23] synthesis of molecular devices,[24] synthesis of new materials,[25–51] and have even found potential application as anti-viral agents.[52–55]

7.1.1.1 Scope

In this article the field of polyoxometalate chemistry will be reviewed and discussed as it has progressed from the 1980s to its position at the start of the new millennium. In embarking on this journey special attention will be given to the synthesis, structure, and properties of discrete polyoxometalate clusters with a nuclearity that is greater than 12 metal atoms. In nearly all cases the frameworks of these clusters are based upon V, Mo, and W. There is a rich chemistry with iso and heteropolyanions with nuclearities 12 and below (see also Chapters 4.10 and 4.11), but these will not be treated in this chapter unless they are used as fragments in the construction of larger clusters or have interesting physical properties.[56,57]

7.1.1.2 Fundamental Units and Building Blocks

Polyoxometalate cluster anions are comprised of aggregates of metal–oxygen units where the metal can be best visualized as adopting the center of a polyhedron and the oxygen ligands defining the vertices of this polyhedron. Therefore, the overall structures of the cluster can be represented by a set of polyhedra that have corner- or edge-sharing modes (face sharing is also possible but rarely seen), see Figure 1 for examples of corner- and edge-sharing polyhedra.

It is not surprising therefore that there are, at least theoretically, a bewildering number of structurally distinct clusters available for a given nuclearity. However, it will become evident that it is extremely useful, at least conceptually, to regard these metal-centered polyhedra and aggregates of these $\{MO_x\}$ polyhedra as structural building blocks that can be used to help both understand and perhaps even manipulate the synthesis of cluster. The structures can then be considered to form via a self-assembly process involving the linking or aggregation of these polyhedra.[58,59] However, although such concepts will be widely considered here, care must be taken to distinguish between a structurally repeating building block and an experimentally available building block that can be proved to be present and incorporated during the construction of a given cluster.[60]

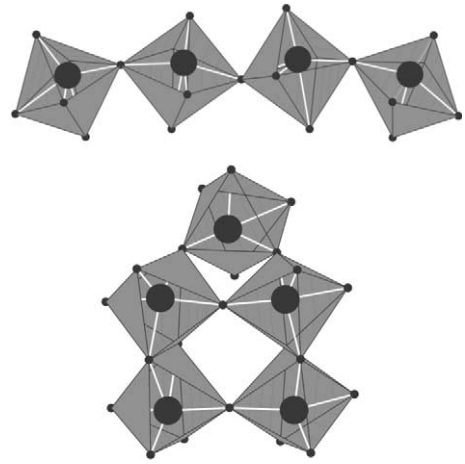

Figure 1 A representation of corner- and edge-sharing polyhedra found in polyoxometalate clusters. The metal ions at the center of the open polyhedra are shown by the black spheres and the oxygen ligands at the vertexes of the polyhedra are shown by smaller black circles. The top image shows exclusively a corner-sharing mode whereas the bottom image shows a combination of edge and corner-sharing polyhedra.

7.1.1.3 Basic Principles in Polyoxometalate Cluster Synthesis

Before outlining the general approach to the synthesis of polyoxometalate clusters it is informative to consider the most useful synthetic results thus far discovered for derivatization and functionalization of fragments leading to a huge variety of structures. These are given below:

- The potential of the system to generate a versatile library of linkable units.
- The ability to generate groups (intermediates) with high free enthalpy to drive polymerization or growth processes, e.g., by formation of H_2O.
- The possibility for structural change in the building units or blocks.
- The ability to include hetero-metallic centers in the fragments.
- The possibility to form larger groups that can be linked in different ways.
- The ability to control the structure-forming processes using templates.
- The ability to generate structural defects in reaction intermediates (e.g., leading to lacunary structures) for example by removing building blocks from (large) intermediates due to the presence of appropriate reactants.
- The ability to localize and delocalize electrons in different ways in order to gain versatility.
- The ability to control and vary the charge of building parts (e.g., by protonation, electron transfer reactions, or substitution) and to limit growth by the presence of appropriate terminal ligands.
- The possibility of generating fragments with energetically low-lying unoccupied molecular orbitals.
- The ability to selectively derivatize both the outside and inside of clusters with sizable cavities.

Generally, the approaches used to produce high nuclearity polyoxometalate-based clusters are extremely simple, consisting of acidifying an aqueous solution containing the relevant metal oxide anions (molybdate, tungstate, and vanadate). In the case of the acidification of the metal oxide-containing solution (see Figure 2) for example, the acidification of a solution of sodium molybdate gives rise to fragments, which increase in nuclearity as the pH of the solution decreases (see Section 7.1.4).[56,57] These isopolyanions have been extremely well investigated in the case of molybdenum, vanadium, and tungsten. However the tungsten cases are limited due to the time required for the system to equilibrate, which is of the order of weeks.[56] Another class of cluster can be synthesized when hetero atoms are introduced, heteropolyanions (see Section 7.1.3) and these are extremely versatile. Indeed, heteroanions based on tungsten have been used in the assembly of extremely large clusters (see Section 7.1.3.2.7).[61] In the case of molybdenum the acidification of solutions of molybdate followed by its subsequent reduction yields new classes of clusters with interesting topologies and very large nuclearities (see Section 7.1.4).[62,63]

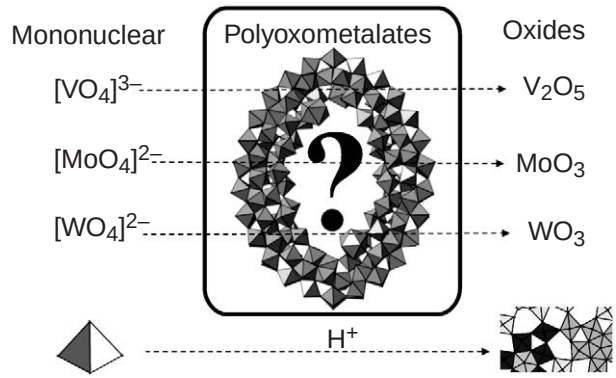

Figure 2 Polyoxometalates are formed in experimental conditions that allow linking of polyhedra. Discrete structures are formed as long as the system is not driven all the way to the oxide. One such example, in this case a part of a $\{Mo_{256}Eu_8\}$ cluster unit, is depicted in the square (see Section 7.1.4.6.2).

The synthetic variables of greatest importance in synthesizing such clusters may be outlined as follows:

concentration/type of metal oxide anion;
pH and type of acid;
type and concentration of electrolyte;
heteroatom concentration;
possibility to introduce additional ligands (reducing ligands);
reducing agent (in the case of the Mo systems);
temperature; and
solvent.

Often such syntheses are done in a single pot and this can mask the extraordinary complexity of the assembly event(s) leading to the high nuclearity cluster. Specific reaction variables and considerations will be discussed at the relevant points throughout this chapter.

7.1.2 VANADATES

The vanadates are structurally very flexible and as such can be based on a large number of different types of polyhedra $\{VO_x\}$ where $x = 4$, 5, 6 whereby the pyramidal $O{=}VO_4$ polyhedra show a tendency to form cluster shells or cages which have topological similarities to the fullerenes and comprise aspects that are structurally analogous to the layers of V_2O_5.[64,65] The bulk of the polyoxovanadates reported so far possess a variable number of vanadium ions bridged by μ_2-, μ_3-oxo, and μ-arseniato groups to yield complex structures ranging from approximate spherical to elliptical geometries.[66,67] The geometry around the vanadium ions can be square pyramidal, octahedral, or tetrahedral. In the tetrahedral case the ion is almost always vanadium(V), while in the square pyramidal/octahedral geometries the metal ion can either be in the +4 or +5 oxidation state. The resulting structures range from quite compact forms, for example, in the case of $[V_{10}O_{28}]^{6-}$ to open ribbon, basket, shell, and cage-like host systems,[64] suitable for the uptake of neutral[68,69] and ionic guests.[70–73] In addition, two-dimensional layered materials,[74,75] as well as three-dimensional host structures,[76] have been described in recent years. Interestingly, simple vanadates have even been found useful to replace insulin in some mammals.[77–79]

The identification of the oxidation state of the square pyramidal vanadium ions is not always easy, especially when extensive electron delocalization is present. However valence bond summations can greatly aid the assignment in those cases where sufficiently high quality structural data have been obtained. Such assignments can be further checked by EPR and magnetic investigations. Indeed, one of the most exciting aspects of polyoxovanadate chemistry is the prospect of synthesizing topologically[80–82] interesting clusters that can behave as nanoscale magnets.[19,83–88] Such clusters are synthesized in aqueous solution with the appropriate precursor, anion templates and, in the case of the mixed valence species, reducing agents. However vanadates have also been synthesized under hydrothermal conditions,[89] and even in vanadium oxide sol–gel systems.[30,90]

7.1.2.1 $\{V_{12}\}$ Clusters

A number of heterotungstates and molybdates adopt either the Keggin ion structure or a structure derived from fragments of it.[56,91] However for heteropolyvanadates, the realization of the normal Keggin ion-type structure of the form $XV_{12}O_{40}$ is limited by the generation of a high negative charge. The stabilization of such clusters appears to be facilitated by the incorporation of VO^{3+} or AsO^{3+} groups.

For example, the compound $K_6[H_3KV_{12}As_3O_{39}(AsO_4)]\cdot 4H_2O$ (**1**)[87,92] is a good example of a mixed valence vanadium cluster with both localized and delocalized vanadium centers (Figure 3). Compound (**1**) is formally built up by nine VO_6 octahedra, three VO_4 tetrahedra, and four AsO_4 tetrahedra, one of the latter being a central AsO_4^{3-} group. The terminal O atoms of each of the peripheral AsO_4 groups are protonated and a potassium ion crowns the fragment. The number of vanadium(IV) centers, expected to be four, was confirmed by Barra *et al.* by manganometric titration.[93]

The identification of the vanadium(IV) centers in the structure is not a trivial endeavor. Bond valence sum (BVS) investigations[94] suggest that V10, V11, and V12 are localized vanadium(IV) centers, however the fourth vanadium(IV) ion is delocalized over the positions V1, V2, and V3, i.e., a $\{V_{3+1}\}$ cluster, see Figure 3. The oxovanadium ions V10, V11, and V12 are connected by long O–As–O bridges and the delocalized vanadium(IV) spread on positions V1, V2, and V3 are connected by μ_2-oxo bridges. The connection between the localized and delocalized vanadium(IV) ions are long and involve more atoms, so their interaction is negligible. The $\{V_{3+1}\}$ electronic structure was also confirmed by magnetic measurements giving a room-temperature effective magnetic moment of $3.17\mu_B$, which corresponds to four unpaired electrons. The magnetic moment decreases smoothly with decreasing temperature giving a small plateau at $2.36\mu_B$ in the range 10–20 K. This was modeled by including an exchange coupling constant, J, for the localized and J' for the localized–delocalized interaction. The best-fit values were reported as being $J = 63\,cm^{-1}$ and $J' = 1.0\,cm^{-1}$. It would appear that this case provides useful information for the analysis of more complex systems, namely those in which there is ambiguity when judging the extent of delocalization vs. localization using the BVS approach. In addition the data indicate that the delocalization is extremely fast and thus one averaged coupling constant can be used.[87,92]

Synthesis of the isostructural clusters $[V_{12}As_8O_{40}(KCO_2)]^{n-}$ (when $n = 3$ (**2a**) the cations are $2[HNEt_3]^+$ and $1[HNH_2Me]^+$ and when $n = 5$ (**2b**) the cations are five sodium ions) gave an opportunity to compare two isostructural clusters that have different ratios of $V^{IV/V}$ ions in the cluster framework, see Figure 4. (**2a**) contains six noninteracting and (**2b**) eight antiferromagnetically coupled V^{IV} (d^1) centers.

Both cluster anions have D_{4h} symmetry and consist of 12 distorted tetragonal VO_5 pyramids and four As_2O_5 groups, which together link to form a hollow cavity that encapsulates a

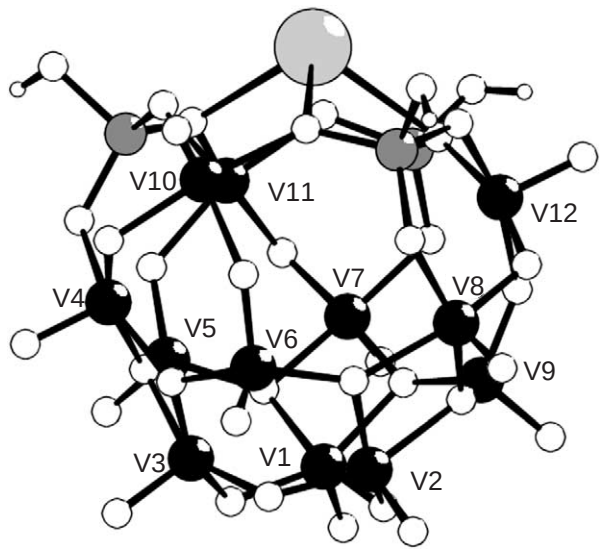

Figure 3 A representation of the crystal structure of the $\{V_{12}\}$ cluster (**1**). The vanadium ions are shown as black spheres, the arsenate ions by dark gray spheres and the potassium ion by the large light gray sphere. The small white spheres are oxygen atoms and the smaller white spheres are hydrogen atoms.

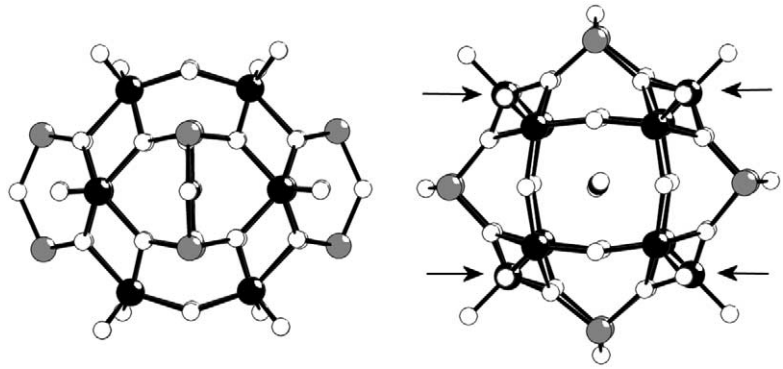

Figure 4 Structure of the cluster (**2a**) and (**2b**) (left-hand side (LHS) = side view; right-hand side (RHS) = top view) with an encapsulated disordered formate ion (center of the RHS view). The trapped V^{IV} centers are shown by the arrows in the RHS view. The vanadium ions are shown as black spheres, the arsenate ions by dark gray spheres and the oxygen atoms as white spheres.

disordered formate ion.[95,96] The 12 VO_5 pyramids can be divided into two types that differ with respect to their position relative to the As_2O_5 groups. The first consists of four pyramids that are bridged through edges by the As_2O_5 groups forming the middle section of the anion where four V^{IV} centers are trapped, see Figure 4, while two V^{IV} centers in (**2a**) and four in (**2b**) are delocalized over eight sites, the remaining ions being formally V^{V} ions, i.e., $\{V_{4+2}\}$ and $\{V_{4+4}\}$, respectively. Although the magnetic analysis is quite complex it has been shown that the magnetic behavior correlates with the geometry and the topology of the cluster.[96] The four localized vanadium(IV) ions are bridged by μ-O–As–O groups, while the delocalized sites are bridged by μ-O and μ-O–As–O groups, and the mixed localization sites are bridged by either double μ_2-OAs or single μ-O–As–O groups, see Table 1. The room-temperature effective magnetic moment of $\{V_{4+2}\}$ is $4.05\mu_B$ and the $\{V_{4+4}\}$ is $2.97\mu_B$, indicating that in both cases there are many electrons with antiparallel spins. Overall, magnetic properties of $\{V_{4+4}\}$ can be explained by assuming that the two vanadium(IV) ions in the delocalized sites are strongly antiferromagnetically coupled, so that the observed effective magnetic moment can be attributed to the four localized vanadium(IV) ions. Using this model the temperature dependence of the effective magnetic moment can be fitted with $J = 10\,cm^{-1}$. The magnetic properties of the $\{V_{4+2}\}$ are more problematic as the data cannot be fitted with only antiferromagnetic coupling constants. However, if one constant is assumed to be ferromagnetic then a good fit is obtained, but the pathway that gives rise to this is difficult to assign.

Table 1 Exchange pathways and coupling constants in some vanadates—see reference[87] for a more advanced and complete discussion.

Cluster	*Atom 1*	*Atom 2*	*Bridge 1*	*Bridge 2*	*Distance*	*Coupl*	*Value*
$\{V_{15}\}$ (**7**)	V_1	V_2	μ_3-O	μ_3-O	2.87	J	556
	V_1	V_2'	μ_3-O	μ_2-OAs	3.05	J'	104
	V_1	V_3	μ_3-O	μ_2-OAs	3.02	J_1	104
	V_2	V_2'	μ_3-O		3.68	J''	208
	V_2	V_3'	μ_3-O		3.73	J_2	208
$\{V_{14}\}$ (**8**)	V_1	V_2	μ_2-OAs	μ_2-OAs	3.06	J_1	19
	V_3	V_4	μ_3-O	μ_2-OAs	3.01	J_2	124
	V_2	V_4	μ_3-O	μ_3-O	284	J	507
	V_2	V_3	μ_3-O		3.60	J_3	55
$\{V_{3+1}\}$ (**1**)	V_{10}	V_{11}	μ-OAsO		5.70	J	63
$\{V_{4+2}\}$ (**2a**)	V_{10}	V_{11}	μ-OAsO	μ-OAsO	5.25	J	10
$\{V_{4+4}\}$ (**2b**)	V_{10}	V_8	μ_2-OAsO	μ_2-OAs	3.16		
	V_{10}	V_9	μ_2-OAsO		5.28	J'	−12
	V_8	V_9	μ	μ	3.42		

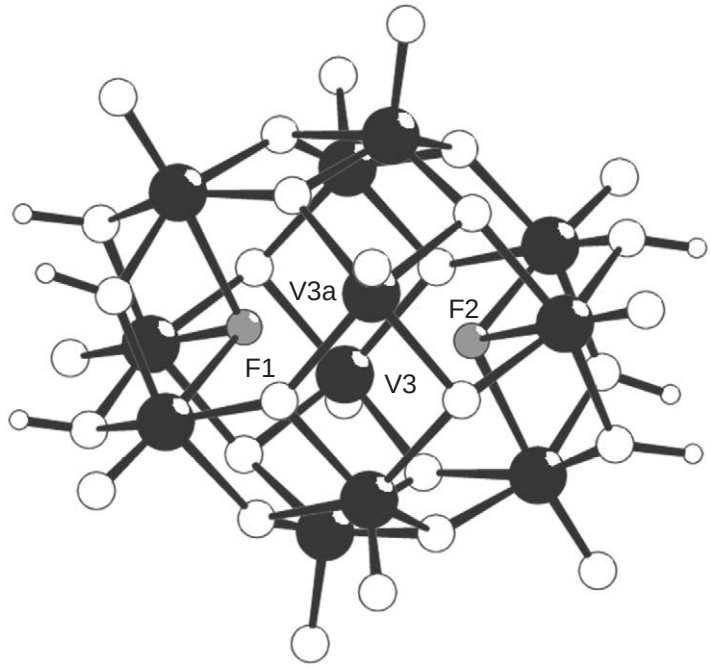

Figure 5 Structure of the cluster anion $[H_6V_{12}O_{30}F_2]^{6-}$. The vanadium ions are shown as black spheres, the fluoride atoms by the gray spheres. The small white spheres are oxygen atoms and the smaller white spheres are hydrogen atoms.

The anionic cluster[83,97] $[H_6V_{12}O_{30}F_2]^{6-}$ (**3**) contains 10 V^{IV} and two localized V^V centers and as such, this compound offers another test for the validity of valence bond summations, which suggest all the charges are trapped. Standard BVS calculations clearly indicate that the localized V^V centers are those shown as V3 and V3a in Figure 5.

It is also possible to synthesize somewhat more open clusters. For example Klemperer *et al.* synthesized a topologically interesting vanadate, a $[V_{12}O_{32}]^{4-}$ basket[64,68] (**4**) which comprises 12 V^V ions. Interestingly the basket holds an acetonitrile molecule, see Figure 6.

This result was extended with the inclusion of C_6H_5CN in the molecular bowl (**5**), see Figure 7.[98] This result offers the possibility that vanadium oxide bowls could be used as molecular containers and may help capture and stabilize interesting molecules.

Indeed this approach was extended by Ozeki and Yagasaki[99] in 2000 when they managed to crystallize a $\{V_{12}\}$ bowl (**6**) analogous to those reported before, but this time encapsulating a NO^- anion, see Figure 8.

This is the first example of the NO^- anion trapped in the solid phase and it is notable that the NO^- anion appears to rest deeper in the cavity than any of the previous guest molecules. This is of interest as an example of an anionic guest being isolated in an anionic host, but is by no means without precedent (see Section 7.1.4.4.3).

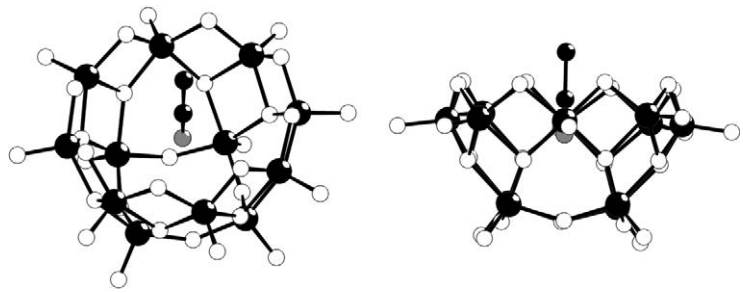

Figure 6 Representation of the vanadate basket cluster, $[V_{12}O_{32}]^{4-}$ (LHS = top view; RHS = side view). The acetonitrile solvent molecule can be seen in the center of the cavity. The vanadium ions are shown as black spheres and the white spheres are oxygen atoms.

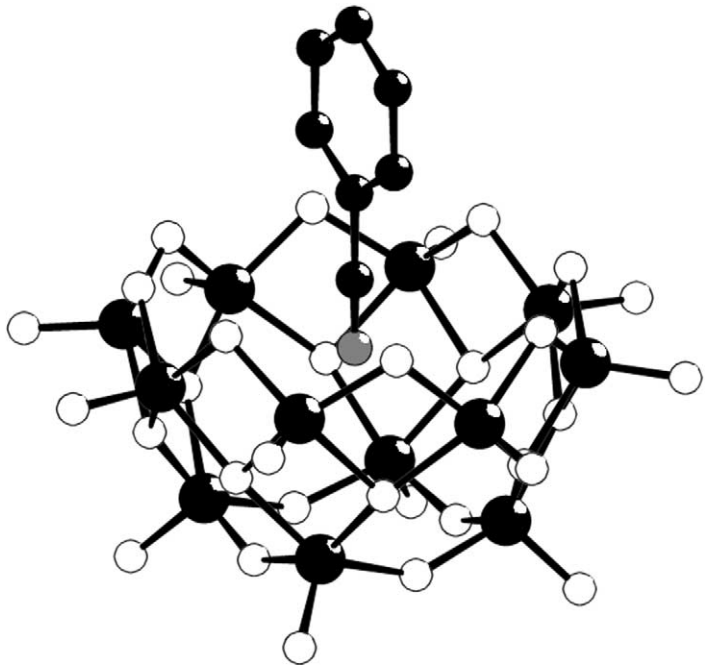

Figure 7 A representation of the vanadate basket cluster, $[V_{12}O_{32}]^{4-}$ including a C_6H_5CN molecule. The vanadium ions are shown as the large black spheres and the white spheres are oxygen atoms. The smaller black spheres and the gray sphere indicated the C_6H_5CN molecule.

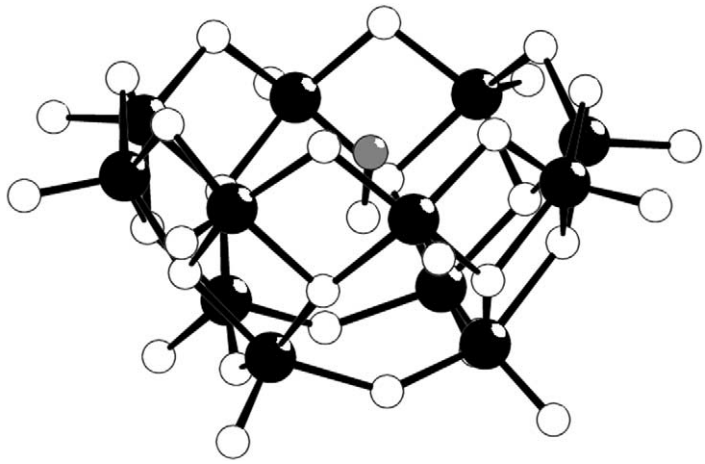

Figure 8 A representation of the crystal structure of the NO^- anion in a vanadate-based molecular bowl. The vanadium ions are shown as the large black spheres and the white spheres are oxygen atoms. The NO^- molecule is shown as the linked gray and white sphere in the center of the cavity.

7.1.2.2 $\{V_{14}\}$ and $\{V_{15}\}$ Clusters

One of the most interesting aspects of cluster synthesis is the possibility of engineering, by accident or design,[100] clusters with large but finite numbers of spins, which are coupled to each other. In this respect the cluster anion $[V_{15}As_6O_{42}(H_2O)]^{6-}$ (**7**) comprising 15 V^{IV} ions,[87,101] offers interesting possibilities.

The overall structure of (**7**) is shown in Figure 9, and the cluster has crystallographically imposed D_3 symmetry. It consists of 15 distorted tetragonal VO_5 pyramids and six trigonal AsO_3 pyramids and it encapsulates a water molecule at the center of the quasi-spherical cluster sheath. The 15 VO_5 pyramids are linked to one another through vertices. Two AsO_3 groups are joined to each other via an oxygen bridge forming a handle-like As_2O_5 moiety.

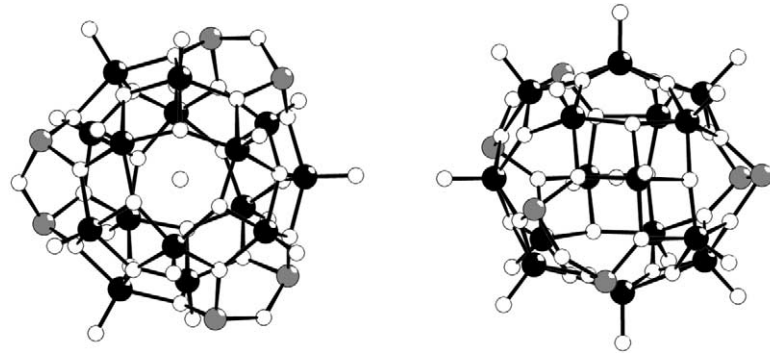

Figure 9 A representation of the structure of (**7**) from the top (left) and the side (right) view respectively. The vanadium ions are shown as black spheres, the arsenate ions by dark gray spheres and the oxygen atoms as white spheres.

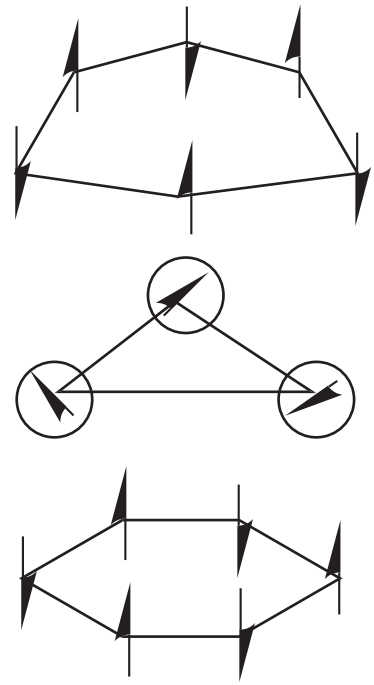

Figure 10 Scheme of the magnetic layers in $\{V_{15}\}$.

The $\{V_{15}\}$ cluster (**7**) has a room-temperature effective magnetic moment of $4.0\mu_B$, indicating strong antiferromagnetic coupling compared with the value for 15 uncoupled vanadium(IV) ions, which is $6.7\mu_B$. The effective magnetic moment decreases slowly on decreasing temperature and in the region of 100–20 K it tends to $2.8\mu_B$. Below 20 K μ_{eff} decreases again reaching $2.0\mu_B$ at 1.8 K. It would appear that the observation that the effective magnetic moment is essentially constant over a large range of temperatures is an indication that the strong antiferromagnetic coupling leaves at least three spins uncoupled at high temperature, i.e., a smaller antiferromagnetic exchange interaction couples the three spins together at low temperature, see Table 1 for details of bridging and coupling constants. Detailed analysis has shown this cluster to possess a unique multilayer magnetic structure.[102,103] Briefly, (**7**) can be considered as a small model of a multilayer structure with two external antiferromagnetic layers sandwiching an internal triangular planar layer, as schematically shown in Figure 10.

The cluster anion $[V_{14}As_8O_{42}(SO_3)]^{6-}$ (**8**), which is shown in Figure 11, is also composed exclusively of V^{IV} ions. Of these, eight, which are connected by μ_3-O and μ_3-OAs groups, define an octagon, and then two sets of three V^{IV} ions connect diametrically opposed centers on the octagons. The room-temperature effective magnetic moment is 4.45 μ_B, which is also smaller than expected for 14 uncoupled spins (6.48 μ_B) clearly indicating the presence of antiferromagnetic coupling.[102,103]

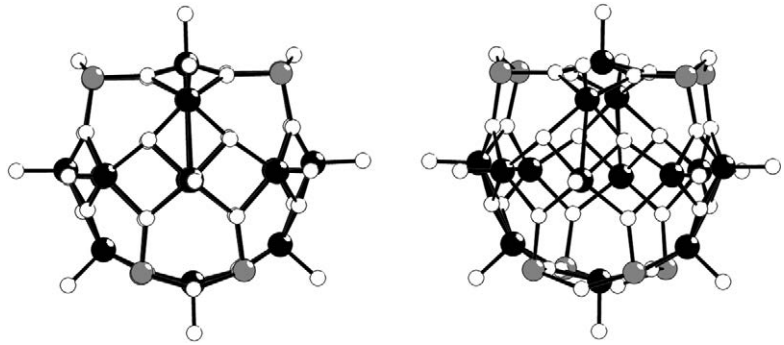

Figure 11 A representation of the structure of the $\{V_{14}\}$ cluster (**8**). The left view shows the central belt of vanadium ions and the caps above and below the belt. The right view shows that the central belt comprises eight vanadium ions and the caps of three vanadium ions above and below the central belt. The vanadium ions are shown as black spheres, the arsenate ions by dark gray spheres and the oxygen atoms as white spheres.

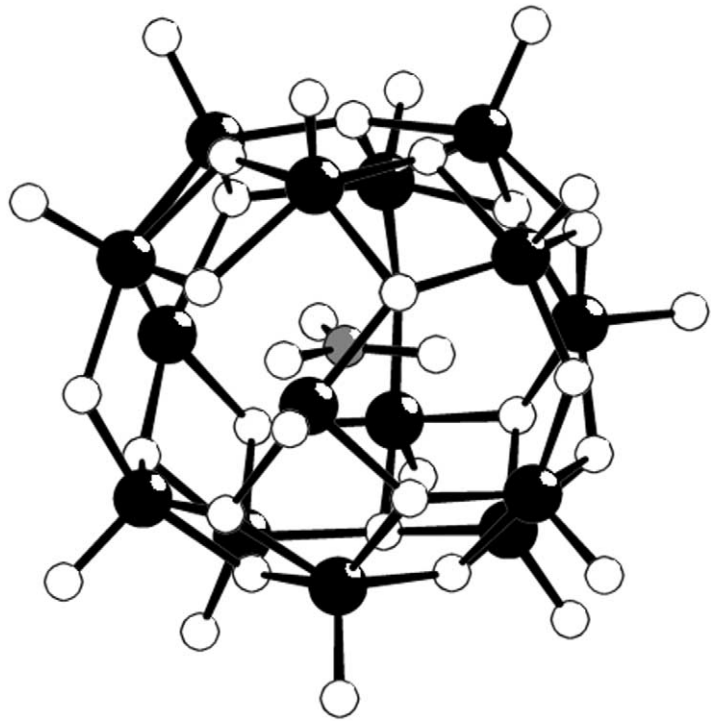

Figure 12 A representation of the structure of the $\{V_{15}\}$ (**9**) shell encapsulating a carbonate dianion. The vanadium ions are shown as black spheres and the oxygen atoms as white spheres. The carbon atom of the carbonate anion is shown as a gray sphere.

In studies by Yamase *et al.*[104] a $\{V_{15}\}$ cluster encapsulating a CO_3^{2-} was synthesized and characterized, see Figure 12. The $[V_{15}O_{36}(CO_3)]^{7-}$ anion (**9**) was synthesized by the photolysis of solutions of $[V_4O_{12}]^{4-}$ at pH = 9 adjusted by K_2CO_3. The resulting anion is a nearly spherical $\{V_{15}O_{36}\}$ cluster shell encapsulating a CO_3^{2-} anion and formally contains eight V^{IV} and seven V^{V} centers. The structure of this cluster sheath is virtually identical to a $\{V_{15}\}$ cluster (**9(a)**) synthesized by Müller in 1987 of the formula $[V_{15}O_{36}Cl]^{6-}$.[105]

7.1.2.3 $\{V_{18}\}$, $\{V_{22}\}$, $\{V_{34}\}$ Clusters—Clusters Shaped by Encapsulated Templates

It would appear that under certain reaction conditions, vanadate cluster shells can be generated by linking fragments that depend to a large extent on the size, shape, and charge of a template (in most cases the templates are anions) incorporated as a guest in the final structure. The cluster

cage...X interactions (where X is the anionic guest) appear to give a weakly repulsive surface around which the cluster can be formed (see Scheme 1), which is a schematic of the templating effect found with polyoxovanadate cluster synthesis whereby the templating molecule X helps to polymerize the OVO_4 units around itself). These weakly repulsive interactions allow the encapsulation of anions in such a way that they can almost be observed to "hover" within the cavity. A further consideration is that these interactions can often give rise to very high coordination numbers; sometimes values as high as 24 have been observed, which can be compared to the highest conventional coordination number of 12. The possibility of including so many weak interactions appears to facilitate very subtle sculpting of the resulting cluster cage. For example, it is possible to synthesize structurally equivalent $\{V_{18}\}$ cluster cages but with differing electron populations and guests encapsulated within the host.

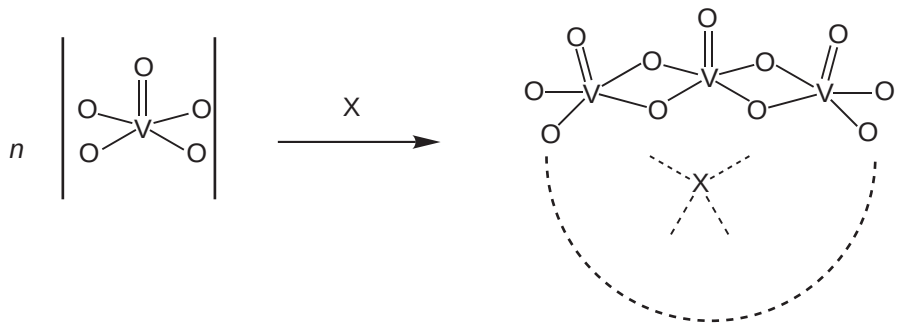

Scheme 1

It has been shown by Müller *et al*. that the $\{V_{18}O_{42}\}$ shell can exist in two different structural types.[106] The 24 μ_3 oxygen atoms form either the edges of a distorted rhombicuboctahedron or a pseudorhombicuboctahedron (the "14th" Archimedian solid), see Figure 13.[80,92] The latter polyhedron can be generated by a 45° rotation of one-half of the rhombicuboctahedron around one of its S_4 axes. Clusters corresponding to the rhombicuboctahedron can be regarded as being an enlarged Keggin ion, in which all the planes of the rhombicuboctahedron are spanned by 24 oxygen atoms and are capped by the {VO} units.

For example, the anion, $[H_7V^{IV}{}_{16}V^{V}{}_2O_{42}(VO_4)]^{6-}$ (**10**) adopts T_d symmetry due to the highly charged, tetrahedral $[VO_4]^{3-}$ "template" which seems to "force" the outer cluster shell to adopt the same symmetry, see Figure 14. This cluster is different from the other $\{V_{18}\}$ clusters reported as the $\{VO_4\}$ unit is actually bonded to the cluster shell, whereas in the other clusters guest molecules are merely included in the cluster as a nonbonded fragment.

In the case of the other guests (Table 2) such as H_2O, Cl^-, Br^-, I^-, SH^-, NO_2^-, HCO_2^- the cluster adopts the D_{4d} symmetry, see Figure 15.

Although only two structural types have been identified, within this structural classification there appear to be three types of redox states: (i) $V^{IV}{}_{18}O_{42}$ (compounds (**11a**)—(**11d**)); (ii) $V^{IV}{}_{16}V^{V}{}_2O_{42}$ (compound (**10**)); and (iii) $V^{IV}{}_{10}V^{V}{}_8O_{42}$ (compound (**12**)) see Table 2.

Type (i) clusters are fully reduced anions with $18V^{IV}$ centers and encapsulate either neutral or anionic guests; the nature of the guest is responsible for any structural variation. Compounds

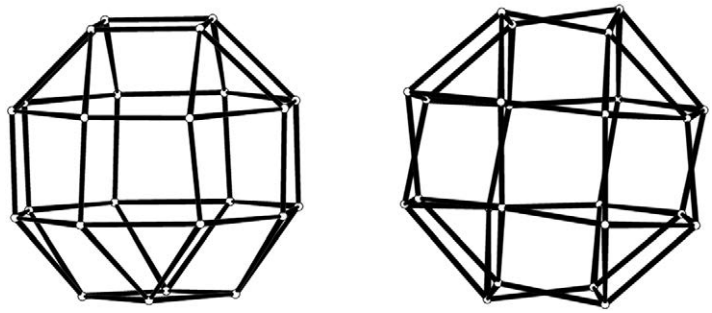

Figure 13 A schematic of the two types of polyhedron formed by the $\{V_{18}\}$ clusters. The T_d rhombicuboctahedron is shown on the LHS and the D_{4d} pseudorhombicuboctahedron is shown on the RHS.

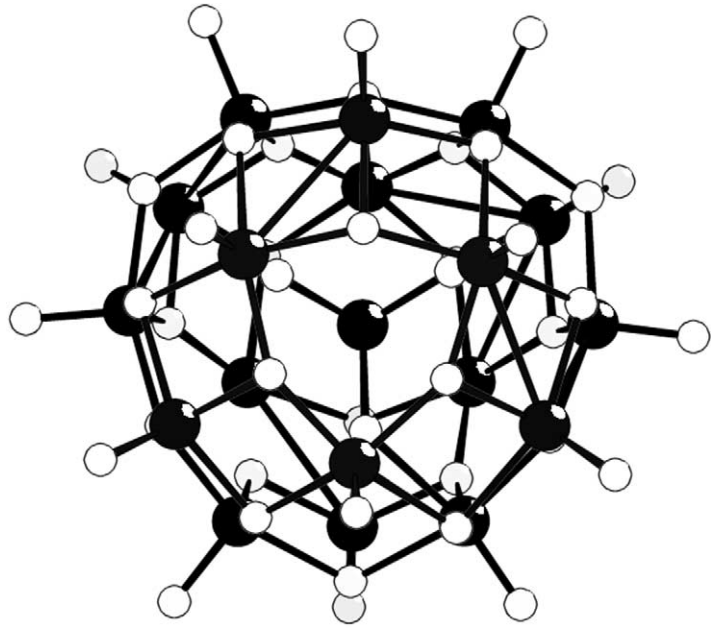

Figure 14 A representation of the $\{V_{18}{+}VO_4\}$ cluster (**10**), which includes a central $\{VO_4\}$ unit that could be implicated as a template. The vanadium ions are shown as black spheres and the oxygen atoms as white spheres.

(**11a–c**) are synthesized under anaerobic conditions at high pH values (ca. 14) from aqueous vanadates solutions and under these conditions only water molecules are enclosed within the cluster shell. The incorporation of anions in the fully reduced shell is facilitated by synthesizing the clusters at a lower pH and (ca. 10) by addition of the correct anion. Type (ii) clusters are mixed valence anions (type III according to the classification of Robin and Day)[107] with encapsulated anions. These compounds are synthesized under an inert atmosphere and at pH values 7–9. There is only one example of the type (iii) cluster (**12**) and this was synthesized from an existing[108] $\{V_{18}\}$ cluster $[V_{18}O_{42}(SO_4)]^{8-}$ by the addition of $(NEt_4)I$ in air.

It is important to note that the differences in the electron population of $\{V_{18}O_{42}\}$ were identified and confirmed structurally using BVS, EPR, and magnetochemistry.[106]

Table 2 Summary of the shell types and the formulas of the clusters characterized in each shell type.[106]

Shell type	*Compound formula*
$V^{IV}{}_{18}O_{42}$	$Cs_{12}[V^{IV}{}_{18}O_{42}(H_2O)]\cdot 14H_2O$ (**11a**)
	$K_{12}[V^{IV}{}_{18}O_{42}(H_2O)]\cdot 16H_2O$ (**11b**)
	$Rb_{12}[V^{IV}{}_{18}O_{42}(H_2O)]\cdot 19H_2O$ (**11c**)
	$K_9[H_3V^{IV}{}_{18}O_{42}(H_2O)]\cdot 14H_2O\cdot 4N_2H_4$ (**11d**)
	$K_{11}[H_2V^{IV}{}_{18}O_{42}(Cl)]\cdot 13H_2O\cdot 2N_2H_4$ (**13a**)
	$K_9[H_4V^{IV}{}_{18}O_{42}(Br)]\cdot 14H_2O\cdot 4N_2H_4$ (**13b**)
	$K_9[H_4V^{IV}{}_{18}O_{42}(I)]\cdot 14H_2O\cdot 4N_2H_4$ (**13c**)
	$K_{10}[H_3V^{IV}{}_{18}O_{42}(Br)]\cdot 13H_2O\cdot 0.5N_2H_4$ (**13d**)
	$K_9[H_4V^{IV}{}_{18}O_{42}(NO_2)]\cdot 14H_2O\cdot 4N_2H_4$ (**13e**)
	$Cs_{11}[H_2V^{IV}{}_{18}O_{42}(SH)]\cdot 12H_2O$ (**13f**)
$V^{IV}{}_{16}V^{V}{}_2O_{42}$	$K_{10}[HV^{IV}{}_{16}V^{V}{}_2O_{42}(Cl)]\cdot 16H_2O$ (**14a**)
	$Cs_9[H_2V^{IV}{}_{16}V^{V}{}_2O_{42}(Br)]\cdot 12H_2O$ (**14b**)
	$K_{10}[HV^{IV}{}_{16}V^{V}{}_2O_{42}(Br)]\cdot 16H_2O$ (**14c**)
	$Cs_9[H_2V^{IV}{}_{16}V^{V}{}_2O_{42}(I)]\cdot 12H_2O$ (**14d**)
	$K_{10}[HV^{IV}{}_{16}V^{V}{}_2O_{42}(I)]\cdot 16H_2O$ (**14e**)
	$K_{10}[HV^{IV}{}_{16}V^{V}{}_2O_{42}(HCOO)]\cdot 15H_2O$ (**14f**)
	$Na_6[H_7V^{IV}{}_{16}V^{V}{}_2O_{42}(VO_4)]\cdot 21H_2O$ (**10**)
$V^{IV}{}_{10}V^{V}{}_8O_{42}$	$(NEt)_5[V^{IV}{}_{10}V^{V}{}_8O_{42}(I)]$ (**12**)

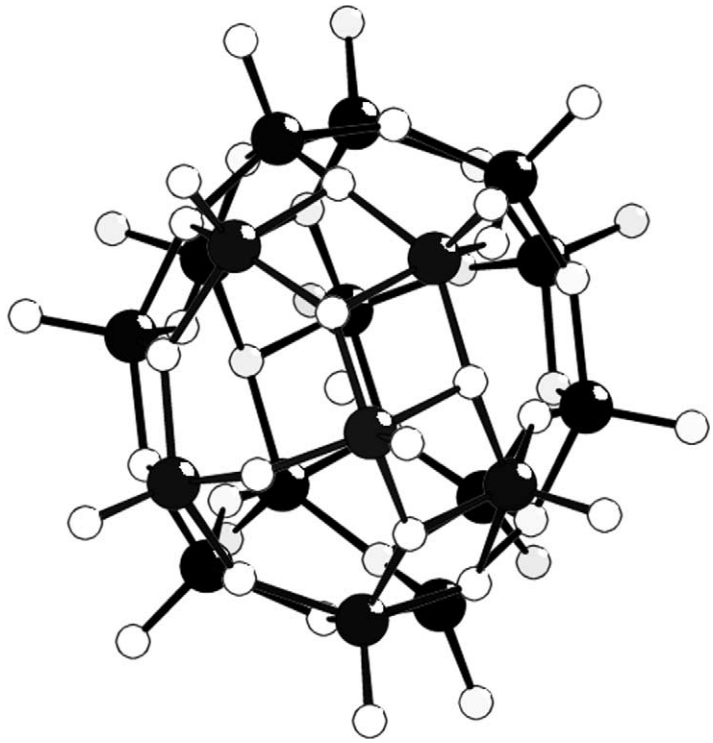

Figure 15 A representation of the $\{V_{18}\}$ cluster, which encapsulates weakly coordinated small molecules at its center (see Table 1). The vanadium ions are shown as black spheres and the oxygen atoms as white spheres.

This assembly principle can be extended to many types of anions. For example, the oxidation of $[H_9V_{19}O_{50}]^{8-}$ in the presence of NEt_4X appears to generate vanadium clusters of differing nuclearity dictated by the size of the anion, X^-. As an illustration of this, when X is azide a $\{V_{18}\}$ cluster results of the formula $[H_2V_{18}O_{44}(N_3)]^{5-}$ (**15**) see Figure 16, for X is perchlorate a $\{V_{22}\}$ cluster is produced, $[HV_{22}O_{54}(ClO_4)]^{6-}$ (**16**) and when X is thiocyanate a $\{V_{22}\}$ cluster is also produced, $[HV_{22}O_{54}(SCN)]^{6-}$ (**17**), see Figure 17.

In an alternative synthetic procedure,[97] the reaction of an aqueous solution of KVO_3 with N_2H_5OH, followed by the addition of acetic acid to a pH of ca. 8 with heating yields crystals of $[H_2V_{22}O_{54}(OAc)]^{7-}$ (**18**). Changing the anion to NO_3^-, by acidifying with HNO_3 instead of acetic acid, produces a $\{V_{18}\}$ cluster encapsulating a NO_3^- (**19**) with the formula, $[HV_{18}O_{44}(NO_3)]^{10-}$, see Figure 18. In another approach, Yamase *et al.* have used a photochemical method[109] to synthesize some mixed valence $\{V_{18}\}$ clusters with a large number of vanadium(IV) ions, and they have also chosen azide as a template, $[V_{18}O_{44}(N_3)]^{14-}$ (**20**) and one example including phosphate, $[V_{18}O_{42}(PO_4)]^{11-}$ (**21**) which exhibits the same type of super-Keggin structure as observed for (**10**), $[H_7V^{IV}{}_{16}V^{V}O_{42}(VO_4)]^{6-}$.

The cluster $[H_2V_{18}O_{44}(N_3)]^{5-}$ (**15**) has approximate D_{2h} symmetry and the cluster is built from edge- and corner-sharing tetragonal $O{=}VO_4$ pyramids. The azide ion rests in the cavity with the shortest N···O distance being ca. 3.05 Å The $\{V_{22}\}$ clusters have very similar structures and are also comprised of tetragonal OVO_4 pyramids with an overall D_{2d} symmetry. In the case of the perchlorate cluster the perchlorate anion rests in the cavity with the shortest O···O distance being around 2.96 Å. However it appears that not only weakly bound anions can be incorporated into these cluster systems. It has also been possible to identify a $[V_{34}O_{82}]^{10-}$ cluster anion (**22**) that appears to incorporate a bonded $\{V_4O_4\}O_4$ cube within a cluster shell, see Figure 19. The overall cluster anion $[V_{34}O_{82}]^{10-}$ has approximate D_{2d} symmetry and consists of an ellipsoid-shaped $\{V_{30}O_{74}\}$ sheath, which is formed by linking 30 tetragonal VO_5 pyramids, and a central V_4O_4 cube. The sheath can be divided into two identical halves that are related by a 90° rotation with respect to each other as defined by the geometry of the central cube. Geometrically each half of the anion contains 20 of the 24 oxygen atoms of a O_{24} rhombicuboctahedron. One interesting observation is that the $\{V_{18}\}$ sheath can be considered to be related to segments of a layer of vanadium pentoxide, see Figure 20.[64,65]

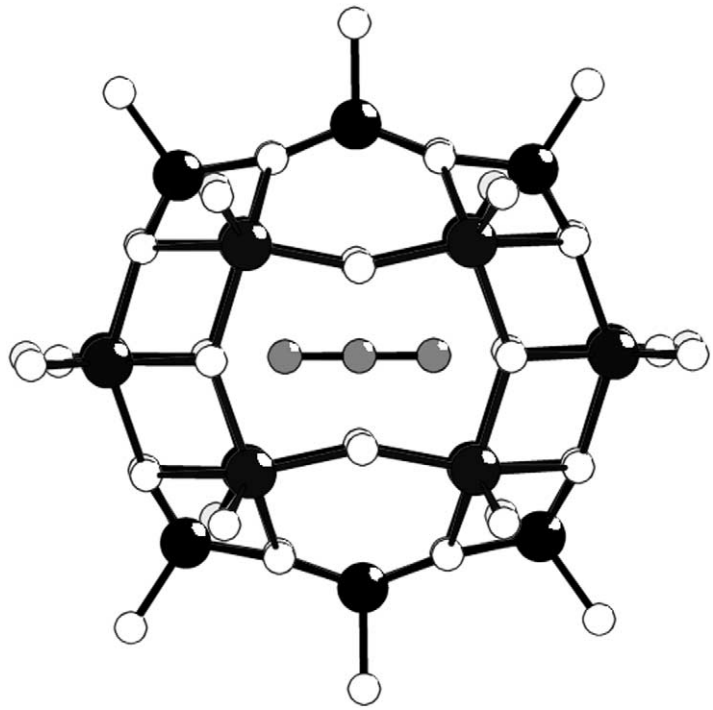

Figure 16 Structure of $\{V_{18}N_3\}$ (**20**).[73] The vanadium atoms are shown as black spheres and the oxygen atoms as white spheres, and the nitrogen atoms of the linear N_3^- anion are shown as gray spheres.

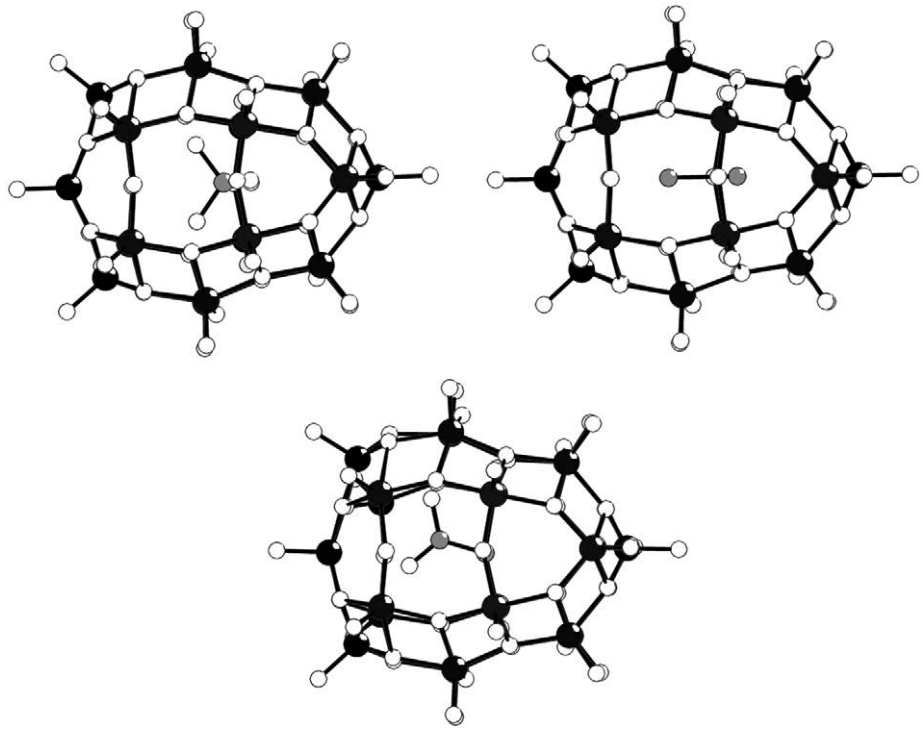

Figure 17 Structures of the $\{V_{22}ClO_4\}$ (top left), (**16**),[73,97] $\{V_{22}NCS\}$ (disordered NCS) (top right), (**17**),[97] $\{V_{22}OAc\}$[110] (**18**) bottom center. The vanadium atoms are shown as black spheres and the oxygen atoms as white spheres, and the other nonoxygen atoms of the anion are shown as gray spheres.

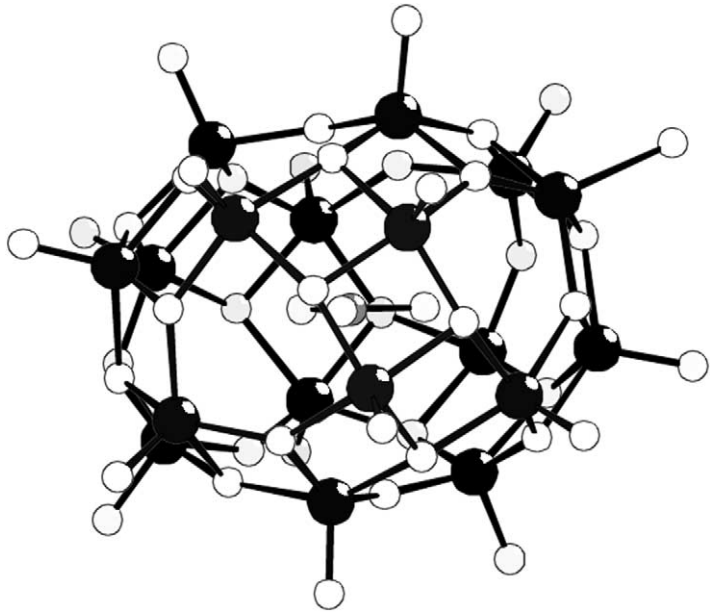

Figure 18 The structure of the $\{V_{18}NO_3\}$ cluster (**19**).[111] The vanadium atoms are shown as black spheres and the oxygen atoms as white spheres, and the non-oxygen atoms of the anion are shown as gray spheres.

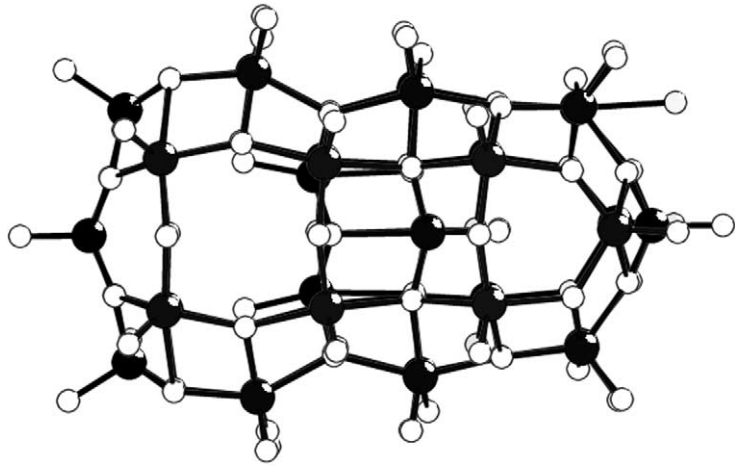

Figure 19 The structure of the $\{V_{34}\}$ cluster (**22**).[112] The vanadium atoms are shown as black spheres and the oxygen atoms as white spheres.

In summary it can be seen that linking VO_5 units in the presence of anions and other templates gives rise to several structural types that appear to be critically dependent on the nature of the anion, and this is summarized in Figure 21.

7.1.3 TUNGSTATES

The structural features of large polytungstate clusters can be visualized in terms of subunits based on lacunary fragments of the Keggin ion. In such representations many of the fragments may not actually exist independently from the cluster containing these subunits. This also applies to the building blocks identified as part of the polyoxometallate clusters discussed in Sections 7.1.4 and 7.1.5.

The Keggin ion (Figure 22) can adopt up to five skeletal isomers (α–ε),[114] and these isomers are related to each other by a rotation of one or more edge-shared $\{W_3O_{13}\}$ groups by $\pi/3$.[56]

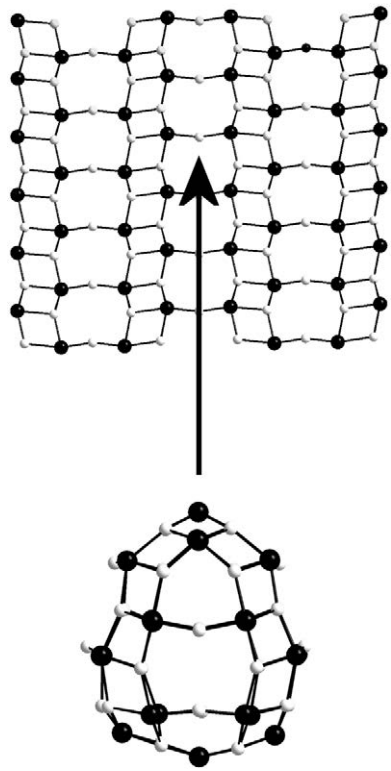

Figure 20 View of a segment of a layer of V_2O_5[113] with the terminal atoms omitted for clarity. The $\{V_{22}\}$ framework is shown below. The vanadium atoms are shown as black spheres and the oxygen atoms as white spheres.

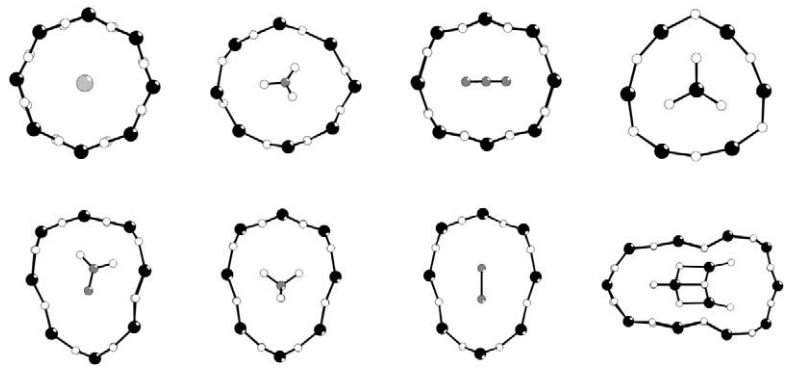

Figure 21 A schematic showing the outer vanadium–oxygen frameworks (vanadium ion shown as black spheres and oxygen atoms by white spheres) and the encapsulated molecules. The clusters depicted from; left to right (top) are the $\{V_{18}$-halide$\}$, $\{V_{18}$-nitrate$\}$, $\{V_{18}$-azide$\}$, $\{V_{18}$-$VO_4\}$; left to right (bottom) are the $\{V_{18}$-acetate$\}$, $\{V_{18}$-perchlorate$\}$, $\{V_{18}$-thiocynate$\}$ (disordered NCS), $\{V_{30}$-$V_4O_4\}$.

The relative stability of the different skeletal isomers of the Keggin ion, and indeed the equilibria that can exist between difference isomers, have been the subject of much discussion in the literature.[115,116]

Lacunary versions of these clusters geometrically result from the removal of one or more W atoms. Examples of one monovacant and two divacant lucunary derivatives of the α-Keggin ion are shown in Figure 23.

The two tri-vacant species in Figure 23 correspond to the loss of a corner-shared group of $\{WO_6\}$ octahedral (A-type) or an edge-shared group (B-type). Furthermore it can be seen that in the B-type anion the central heteroatom has an unshared terminal oxygen atom; in this respect it is easy to imagine that B-type structures are observed when the central heteroatom has an unshared pair of electrons.

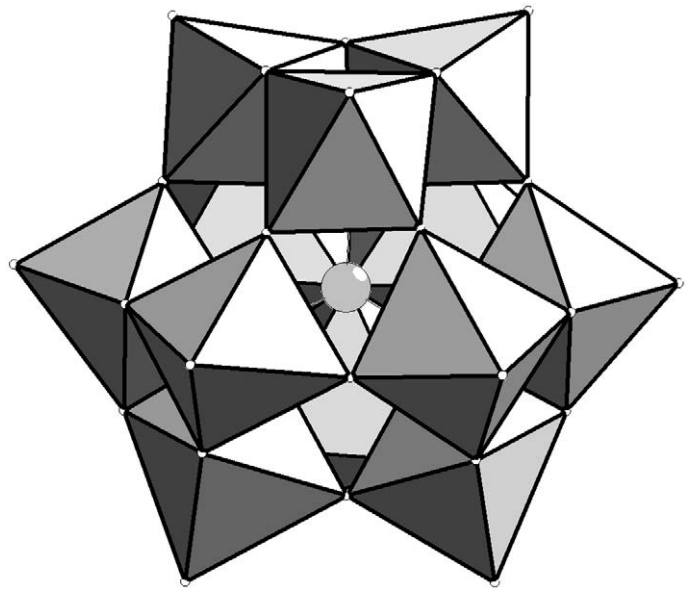

Figure 22 Polyhedral representation of the α-Keggin ion. The metal ions form the centers of the polyhedra and the oxygen atoms form the apexes of the polyhedra. The central heteroatom is shown as a gray sphere.

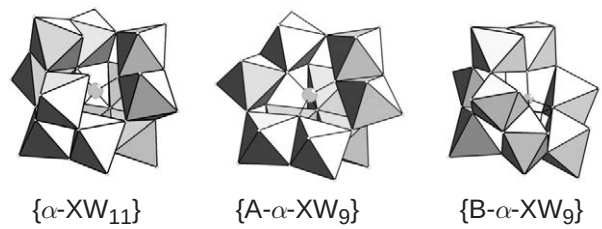

Figure 23 Polyhedral representation of the Lacunary derivatives of the α-Keggin ion; left—$\{\alpha\text{-}XW_{11}\}$, middle—$\{A\text{-}\alpha\text{-}XW_9\}$, right—$\{B\text{-}\alpha\text{-}XW_9\}$. The metal ions form the centers of the polyhedra and the oxygen atoms form the apexes of the polyhedra. The central heteroatom is shown as a gray sphere.

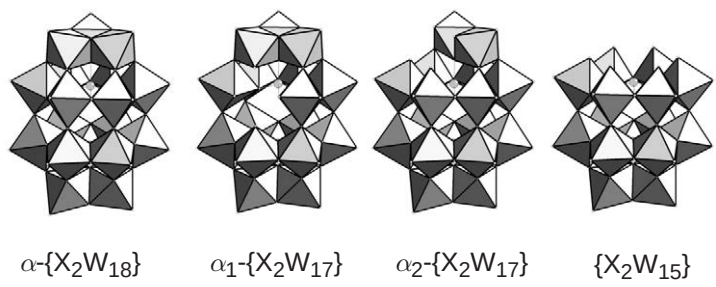

Figure 24 Polyhedral representations of the α-Dawson structure the associated three lacunary derivatives. The metal ions form the centers of the polyhedra and the oxygen atoms form the apexes of the polyhedra. The central heteroatom is shown as a gray sphere.

Linking of two $[A\text{-}PW_9O_{34}]^{9-}$ clusters (**23**) generates a Wells–Dawson anion (**24**) $[P_2W_{18}O_{62}]^6$. Six isomers of this anion are theoretically possible depending upon whether the half-units are derived from α or β-Keggin species and also whether the fragments combined in a staggered (S) or eclipsed (E) fashion.[114] Four of these isomers have been observed for $[As_2W_{18}O_{62}]^{6-}$ and three for $[P_2W_{18}O_{62}]^{6-}$.[117] As in the case of the Keggin ion, lacunary derivatives of the Wells–Dawson structure are also known. The most important of these are based on the most common isomer known as the α-Dawson anion—see Figure 24.

7.1.3.1 Clusters Incorporating Monovacant Lacunary Fragments

7.1.3.1.1 $\{XW_{11}\}_2$

Monovacant lacunary anions (mla) of the type $[PW_{11}O_{39}]^{7-}$ (**25**), $[SiW_{11}O_{39}]^{8-}$ (**26**) and $[P_2W_{17}O_{61}]^{10-}$ (**27**) form both 1:1 and 1:2 complexes with several metal cations. Such complexes were first reported by Peacock and Weakley[118] in 1971. Recently 1:1 complexes of [α-$SiW_{11}O_{39}$] units have been shown to form polymers with lanthanide ions.[119] It was suggested that the heteropolyanion ligands were tetradendate, binding to the lanthanide center through the four oxygen atoms that surround the tungsten vacancy. In this way a quasi-square antiprismatic coordination sphere is provided for the metal ion. An examination of the literature reveals many types of mla have been extremely well exploited as ligands with many combinations of metal ion (see reference[84] for a further discussion of this point). Figure 25 gives a typical representation of one such $[M(mla)_2]^{n-}$ complex (**28**), which adopts a *cis*-oid conformation with respect to the mla "ligands." This is because the polyanionic ligand only has C_s symmetry and therefore there are four possible conformations for the complexes corresponding to *cis*-oid and *trans*-oid enantiomeric pairs.[120] It would appear that all the Keggin-derived complexes are *trans*-oid whereas $[M(\alpha_2\text{-}P_2W_{17}O_{61})_2]^{(20-n)-}$ (**29**) ($M = Ce^{IV}$, Lu^{III}, U^{IV}) are *cis*-oid. 1:1 and 2:2 complexes (α_2-$P_2W_{17}O_{61}$) linked by lanthanide ions have also been recently reported.[121]

7.1.3.1.2 $\{XW_{11}\}_2\{Mo_3S_4\}_2$

It has been shown by Müller *et al.*[122] that the monovacant lacunary anion $[SiW_{11}O_{39}]^{8-}$ (**30**) reacts as an electrophile towards the nucleophile $[Mo_3S_4(H_2O)_9]^{4+}$ (**31**) to yield a bridged species $\{(SiW_{11}O_{39})_2[Mo_3S_4(H_2O)_3]_2(\mu\text{-}OH)_2\}^{10-}$ (**32**). The resulting species has C_{2v} symmetry (see Figure 26). The two nucleophilic lacunary anions, of the Keggin type $\{[SiW_{11}O_{39}]^{8-}\}$ and of the Dawson type $\{[P_2W_{17}O_{61}]^{10-}\}$, can be considered as negatively charged ligands which replace the coordinated water ligands of the electrophilic adduct. In this respect it has been suggested that the

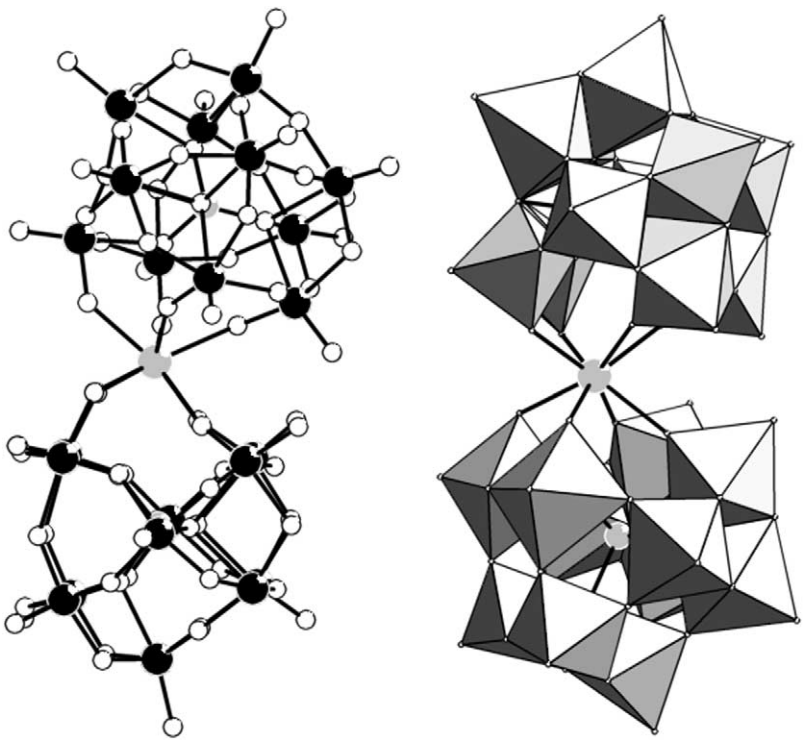

Figure 25 Structure of $[U(\alpha\text{-}GeW_{11}O_{39})_2]^{12-}$ (**28**). The ligands adopt a *trans*-oid conformation. A ball and stick representation is shown on the LHS (black spheres = W atoms, white spheres = O atoms and the visible gray sphere is the U atom). On the RHS the W atoms and the O atoms are represented as polyhedra.

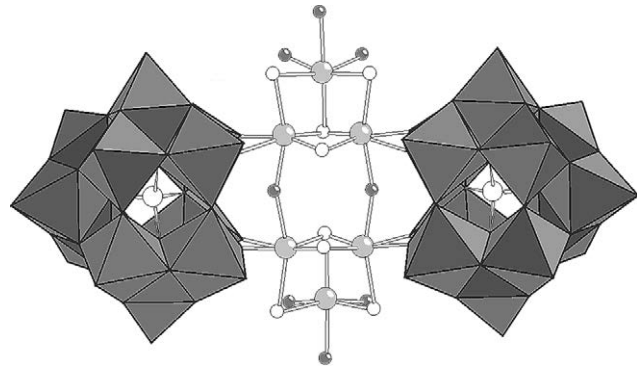

Figure 26 View of the structure of $\{(SiW_{11}O_{39})_2[Mo_3S_4(H_2O)_3]_2(\mu\text{-}OH)_2\}^{10-}$ (**32**). The lacunary Keggin-type fragments $\{\alpha\text{-}SiW_{11}\}$ are shown as polyhedra, the $\{Mo_3S_4\}$ units are in ball and stick representation.

monovacant lucanary anions with four oxygen donor atoms can be considered as an inorganic analogue of the porphyrin ligand.[122] The assembly of larger aggregates using this electronic complementarity is likely to become more significant in the drive to form "designer" solids.

7.1.3.1.3 $\{XW_{11}\}_3$

Tungstoboric acid yields two forms of crystalline product; a tetragonal form that contains a Keggin ion and a hexagonal form that comprises three lacunary $\{BW_{11}\}$ anions linked by a central $\{W_6O_{26}\}$ moiety (**33**). The overall structure has a C_{3h} symmetry, see Figure 27, and has the overall composition $H_{21}[B_3W_{39}P_{132}]$ (**33**).[123]

7.1.3.2 Clusters Incorporating Different Types of Trivacant Lacunary Fragments

7.1.3.2.1 $\{X_2W_{21}\}$

The structure of the cluster anion $[P_2W_{21}O_{71}]^{6-}$ (**34**) $\{P_2W_{21}\}$ reveals a sandwich-like arrangement of two $\{PW_9\}$ moieties around three $\{WO_5(H_2O)\}$.[124] Close examination of the structure, Figure 28, reveals a threefold rotational disorder of the anion and that two positions can be modeled for the equatorial tungsten atoms. Solution studies of this cluster anion with NMR show that two of the tungsten atoms are displaced towards the threefold axis and that one tungsten atom is

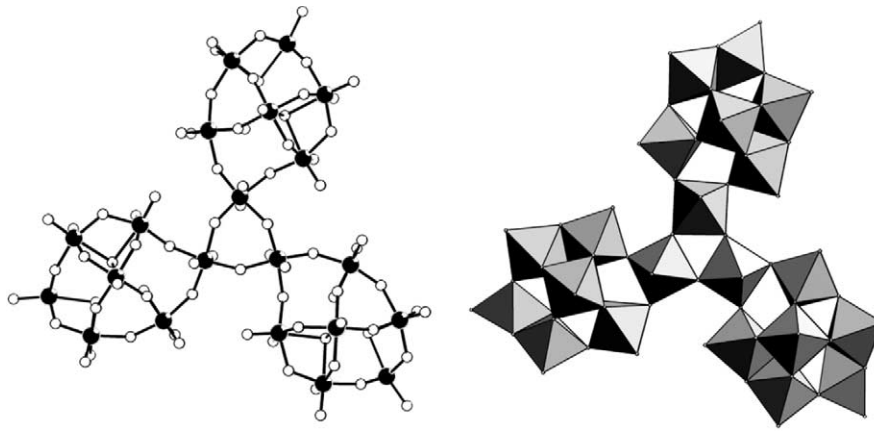

Figure 27 A ball and stick (LHS) and a polyhedral (RHS) representation of the $H_{21}[B_3W_{39}P_{132}]$ cluster (**33**). The W atoms are shown as black spheres and the oxygen atoms are shown as white spheres on the LHS. The W centers are shown as polyhedra on the RHS.

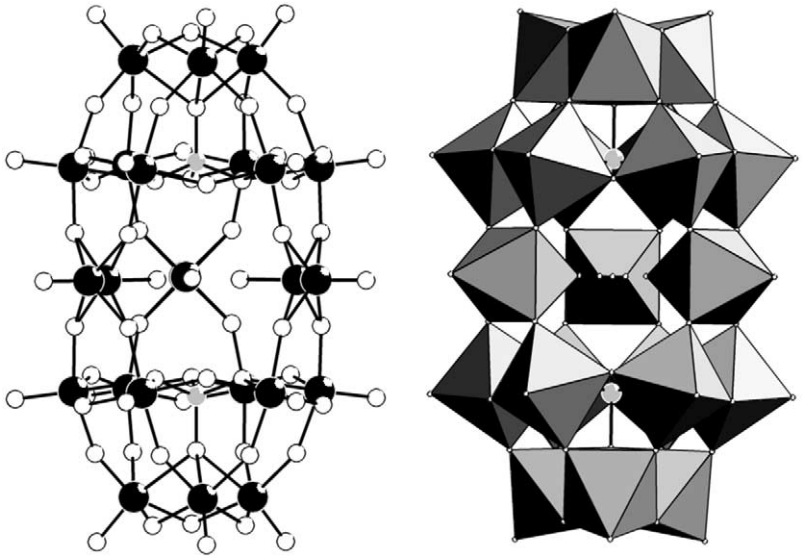

Figure 28 Structure of $[P_2W_{21}O_{71}]^{6-}$ (**34**) $\{P_2W_{21}\}$ cluster. Again, a ball and stick representation (W atoms as black spheres, O atoms as white spheres) is shown on the LHS whereas a polyhedra representation is shown on the RHS. The P atoms are visible as gray spheres in both representations.

displaced away from this axis. The center of this cluster, therefore, encloses two "terminal" oxo oxygen atoms and a water molecule that is *trans* to the terminal atom of the third tungsten center. The central water ligand undergoes slow exchange with solvent water molecules.[124]

Cluster anion (**34**) is synthesized by the acidification of the lacunary species $[P_2W_{11}O_{39}]^{7-}$, whereas acidification of the potassium salt of the lacunary species leads to a lacunary derivative of (**34**).[52] An interesting anion $\{P_2W_{20}\}$ incorporating potassium can be synthesized by the treatment of a heated suspension of $[K_3PW_{12}O_{40}]$ with potassium carbonate and yields several products[125] one of which is $K_{13}[KP_2W_{20}O_{72}]\cdot 30H_2O$ $\{P_2W_{20}\}$ (**35**). Similarly to $\{P_2W_{21}\}$, the anion comprises two A-type $\{\alpha\text{-}PW_9\}$ units linked by two tungsten atoms, but now a potassium cation occupies a center of symmetry within the cluster, see Figure 29. Indeed, the cluster can almost be viewed as acting like a crown ether moiety ligating the potassium ion. Conversely, the potassium could act to provide a template for this cluster architecture.

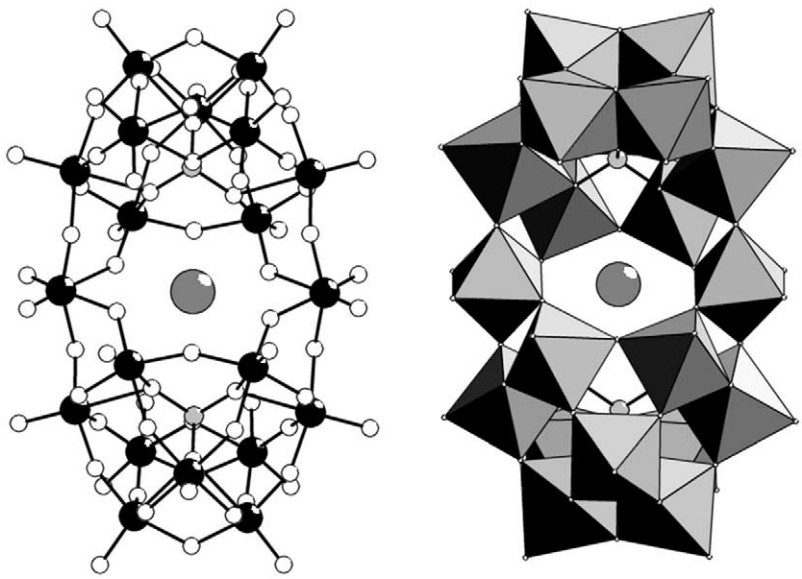

Figure 29 The structure of the $K_{13}[KP_2W_{20}O_{72}]\cdot 30H_2O$ $\{P_2W_{20}\}$ (**35**) cluster. A ball and stick representation is shown on the LHS and a polyhedral representation on the RHS. The central encapsulated potassium cation is shown in both representations as a large gray sphere.

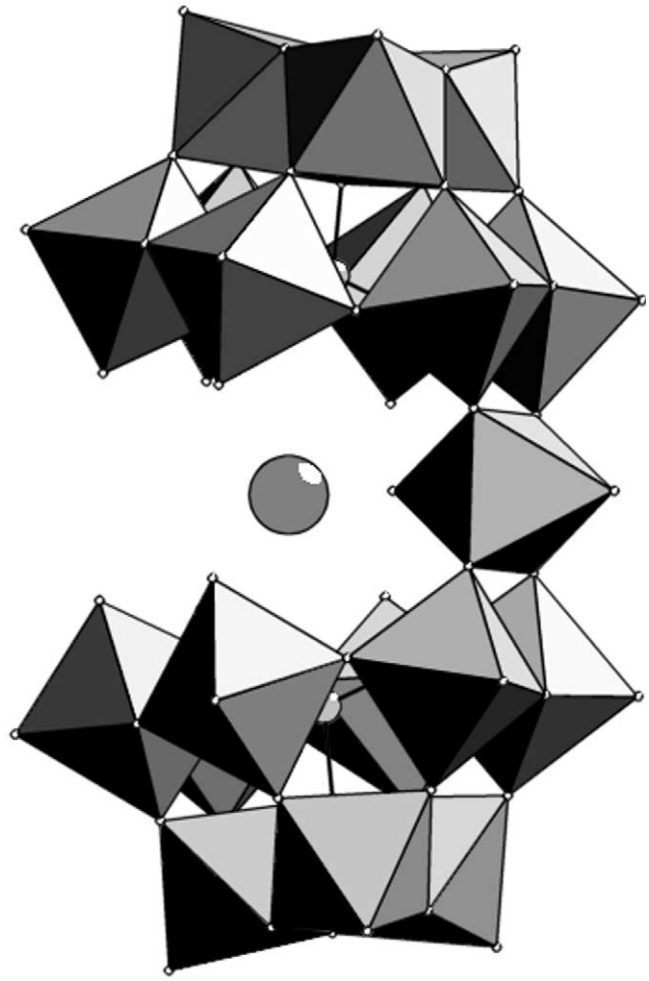

Figure 30 A polyhedra representation of the structure of $[P_2W_{19}O_{69}]^{14-}$ (**36**). The potassium cation ligated by the cleft formed by the cluster is shown as a large gray sphere.

A further derivative of $\{P_2W_{21}\}$ is the cluster anion $[P_2W_{19}O_{69}]^{14-}$ (**36**), see Figure 30.[126] This anion appears to be quite unstable, but crystallizes readily in the presence of potassium cations, which occupy equatorial sites on the anion.

7.1.3.2.2 $\{M_9P_5W_{27}\}$

The cluster anion, $[Co_9(0H)_3(H_2O)_6(HPO_4)(B\text{-}\alpha\text{-}PW_9O_{34})_3]^{16-}$ $\{Co_9P_5W_{27}\}$ (**37**) was obtained as a by-product in the synthesis of $[Co_4(H_2O)_2(PW(O_{34})]^{10-}$. This anion has D_{3h} symmetry and comprises three Keggin units $\{\alpha\text{-}PW_9Co_3\}$ linked by corner sharing $\{Co_3\}$ triads with capping axial phosphate groups, see Figure 31.[127] An analogous cluster incorporating nickel(II) instead of cobalt(II) has been synthesized and the magnetic properties of both have been studied.[128,129]

7.1.3.2.3 $\{XW_9\}_1$:$\{Eu_3SbW_{24}\}$

In 1990 an interesting europium-tungstoantimonate was reported by Yamase.[130] The cluster, $[Eu_3(H_2O)_3(Sb^{III}W_9O_{33})(W_5O_{18})_3]^{18-}$, $\{Eu_3SbW_{24}\}$ (**38**) incorporates a $\{B\text{-}\alpha\text{-}SbW_9\}$ and three $\{W_5\}$ groups which are lacunary derivatives of $[W_6O_{19}]^{2-}$. The four units are arranged in an almost tetrahedral arrangement with respect to the central $\{Eu_3\}$ unit see Figure 32.

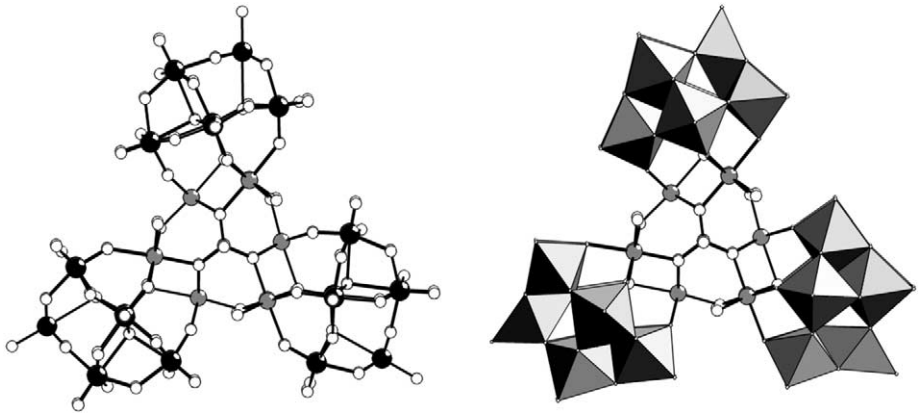

Figure 31 Representations of the cluster anion $[Co_9(0H)_3(H_2O)_6(HPO_4)(B\text{-}\alpha\text{-}PW_9O_{34})_3]^{16-}$ $\{Co_9P_5W_{27}\}$ (**37**). A ball and stick representation is shown on the LHS with the W atoms shown as black spheres, the oxygen atoms as white spheres, and the Co atoms as gray spheres. A polyhedral representation of the three $\{PW_9\}$ units is shown on the RHS with the bridging units shown as ball and stick.

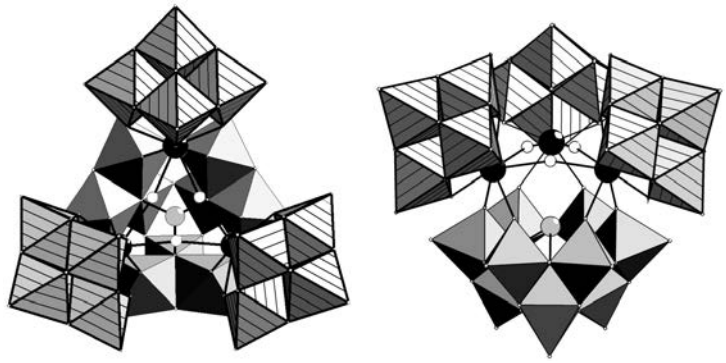

Figure 32 The structure of the cluster anion $[Eu_3(H_2O)_3(Sb^{III}W_9O_{33})(W_5O_{18})_3]^{18-}$, $\{Eu_3SbW_{24}\}$ (**38**). The Eu atoms are shown as large black spheres and the Sb atom as a gray sphere. The hatched polyhedra represent the $\{W_5\}$ units whereas the gray polyhedra represent the $\{W_9\}$ unit. A top view is shown on the LHS and the side view on the RHS.

7.1.3.2.4 {XW₉}₂:{X₂W₂₁}/{X₂W₂₂}

The structure of the anion $[As_2W_{21}O_{69}(H_2O)]^{6-}$ $\{As_2W_{21}\}$ (**39**) has been elucidated in the solid state by crystallography,[131] see Figure 33, and in the solution state by NMR.[132] The structure is analogous to $\{P_2W_{21}\}$ (see Figure 34) but, due to the lone pair of electrons on As^{III}, the $\{AsW_9\}$ units are of the B-type. The linking, equatorial tungsten atoms also adopt a different configuration with two $\{W_{out}\}$ and one $\{W_{in}\}$ due to the smaller available space.

Cluster anions, and their complexes with di- and trivalent transition metals thought to be based on $\{XW_{11}\}$ have been shown to be dimeric, based on structural studies of the salts of $[Sb_2W_{22}O_{74}(OH)_2]^{12-}$ (**40**) and related species.[133] The structure of this anionic cluster is shown in Figure 34, and comprises two $\{B\text{-}\beta\text{-}XW_9\}$ groups linked by two other tungsten atoms. Interestingly, two weakly bound tungsten atoms are bound to the periphery of the cluster and can be easily replaced by other transition metal ions.

7.1.3.2.5 {XW₉}₃

The clusters $\{Ln_2As_3W_{29}\}$ (**41**) and $\{(UO_2)_3As_3W_{29}\}$ (**42**) result from the reaction of $\{B\text{-}XW_9\}$ anions with lanthanide and actinide cations. For example the anion $[Ln_2(H_2O)_7As_3W_{29}O_{103}]^{17-}$ ($Ln^{III} = La$, Ce) (**41**) contains three $\{AsW_9\}$ fragments bridged by two additional tungsten atoms and two Ln^{III} cations. The stoichiometrically related derivative $[(UO_2)_3(H_2O)_5As_3W_{29}O_{104}]^{19-}$ also has a trimeric structure.[84]

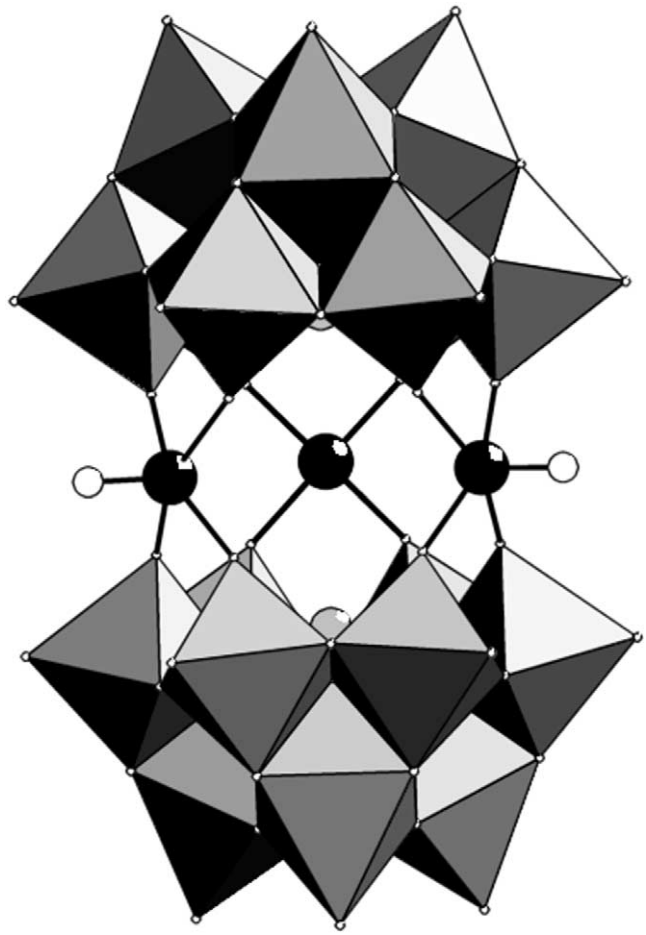

Figure 33 The structure of the anion $[As_2W_{21}O_{69}(H_2O)]^{6-}$ $\{As_2W_{21}\}$ (**39**), the W atoms in the two $\{W_9\}$ groups are shown in a polyhedra representation whereas the three linking W atoms are shown as black spheres and the associated oxygen atoms as white spheres.

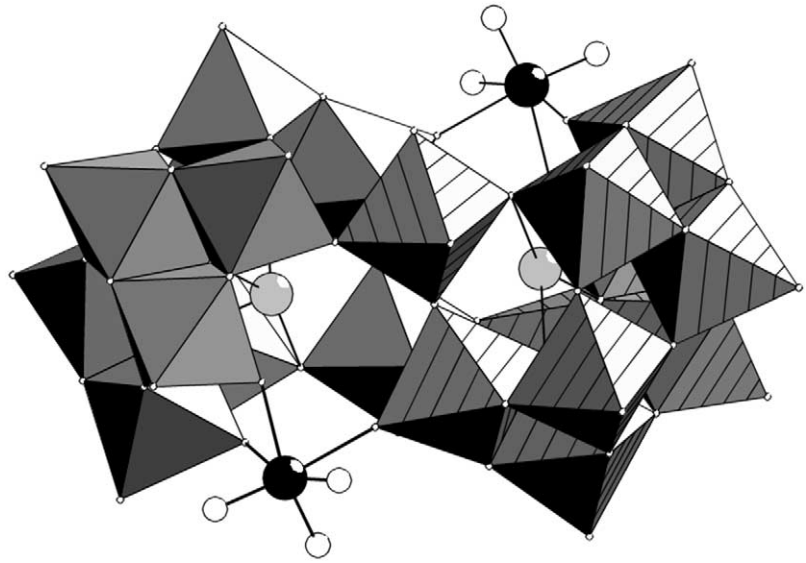

Figure 34 Structure of $[Sb_2W_{22}O_{74}(OH)_2]^{12-}$ (**40**). The two $\{B\text{-}\beta\text{-}XW_9\}$ groups are shown by the polyhedra and the Sb atoms are shown as gray spheres. The "additional" W atoms and associated oxygen ligands are shown by the black and white spheres, respectively.

7.1.3.2.6 {XW_9}$_4$

Clusters based on four linked $\{XW_9\}$ have also been identified, see Figure 35. The cluster $[As_4W_{40}O_{140}]^{28-}$ (**43**) is a cyclic anion, being composed of four $\{\alpha$-$AsW_9\}$ units linked by additional tungsten atoms; the structure shown in Figure 35 is a dicobalt derivative.[134] Derivatives of (**43**) have also been produced with lanthanide cations.[135]

A further tetramer of $\{XW_9\}$ has been reported[133] that has the composition $[Na_2Sb_8W_{36}O_{132}(H_2O)_4]^{22-}$ (**44**). The top view, see Figure 36, seems similar to (**43**) shown in Figure 35 but the side view reveals the unique structure of this cluster. This is because the $\{SbW_9\}$ groups have a β conformation and the bridging atoms are trigonal bipyramidally coordinated W^{VI} centers. Therefore the overall structure resembles that of a V-shaped cavity. The cavity contains two sodium ions and several water molecules.

7.1.3.2.7 {XW_9}$_{11}$

Recently, Pope *et al.* have synthesized a massive heteropolytungstate anion which is a dodecamer of the $\{XW_9\}$ units, $[Ln_{16}As_{12}W_{148}O_{524}(H_2O)_{36}]^{76-}$ (**45**).[61] The 12 $\{XW_9\}$ units are linked by Ln^{III} cations (Ln = La, Ce, Nd, Sm) and additional tungsten atoms to produce a folded cyclic cluster with D_{2d} symmetry. The anion is completed by the four $\{W_5O_{18}\}$ lacunary fragments and the structure is shown in Figure 37. This anion exhibits an interesting topology and exceptionally high nuclearity of metal ions.

7.1.3.3 Clusters Incorporating Hexavacant Lacunary Fragments

7.1.3.3.1 {P_8W_{48}}

One of the lacunary derivatives of the α-Dawson anion forms crystals of composition, $K_{28}Li_5H_7P_8W_{48}O_{184}{\cdot}92H_2O$ ($\{P_8W_{48}\}$, (**46**)) with the cyclic structure shown in Figure 38.[132,136] A tetramer of $\{P_2W_{12}\}$ groups leads to the D_{4h} symmetry of the structure of the $\{P_8W_{48}\}$ anion. The crystal structure reveals that the central cavity of the anion contains a number of potassium cations.

7.1.3.3.2 {P_5W_{30}}

When sodium tungstate is boiled with an excess of phosphoric acid the main heteropolytungstate products are two isomers of the Wells–Dawson anions and a smaller amount of another species (**47**). Crystallographic analysis of this species showed the composition of this anion to be $[NaP_5W_{30}O_{110}]^{14-}$ ($\{P_5W_{30}\}$, (**47**)) with the structure shown in Figure 39.[132]

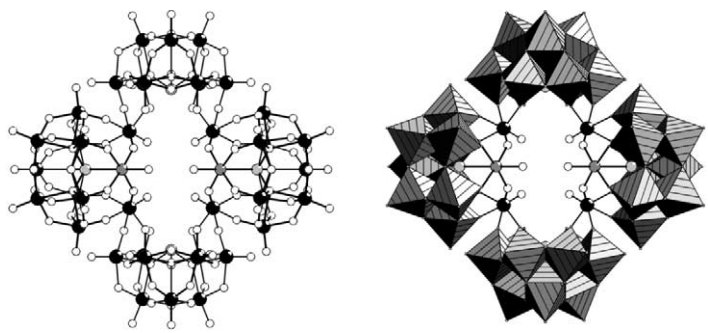

Figure 35 The structure of the cyclic anion $[As_4W_{40}O_{140}]^{28-}$ (**43**). A ball and stick representation is shown on the LHS and a polyhedral representation is shown on the RHS with the linking units shown in ball and stick. The W atoms are shown as black spheres, the As atoms as gray spheres and the O atoms as white spheres.

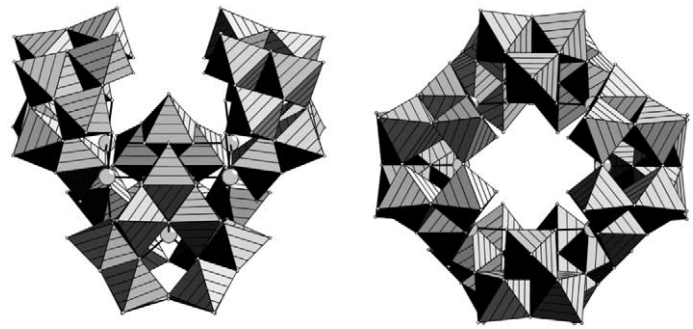

Figure 36 Two polyhedral views of the cluster $[Na_2Sb_8W_{36}O_{132}(H_2O)_4]^{22-}$. The W atoms are shown as polyhedra and the Sb atoms are shown as gray spheres.

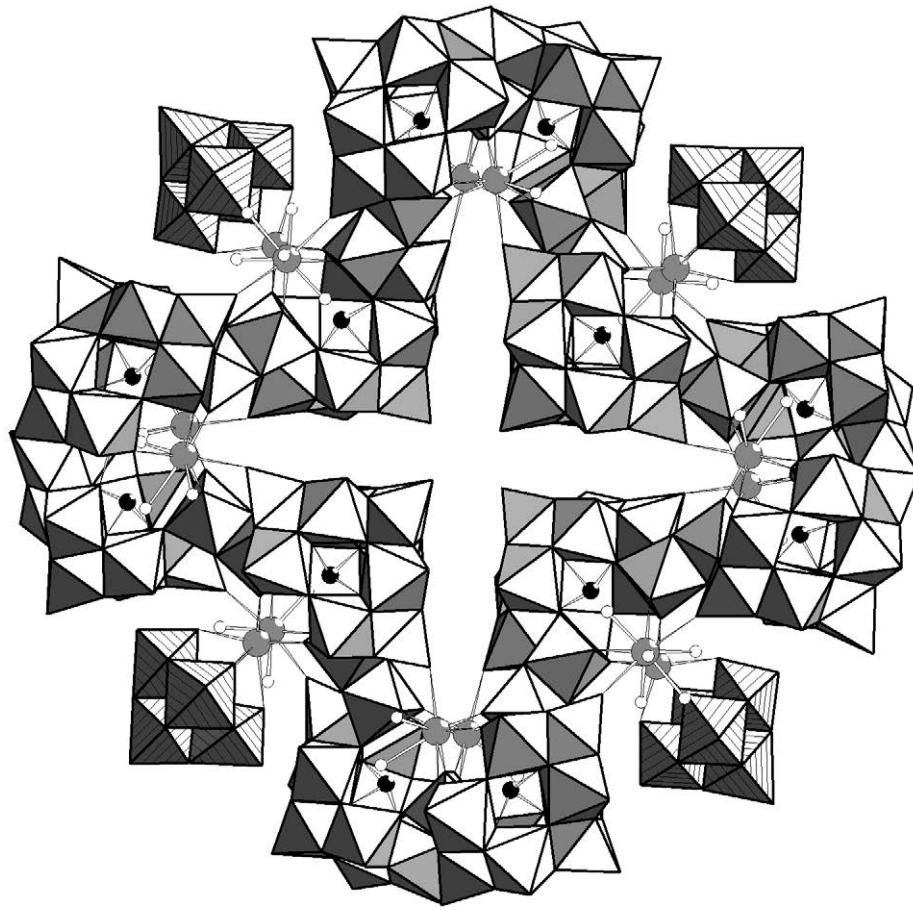

Figure 37 Structure of the anion $[Ln_{16}As_{12}W_{148}O_{524}(H_2O)_{36}]^{76-}$ (**45**) as a folded cyclic assembly of 12 {B-α-AsW_9} groups linked by additional W centers, all shown as polyhedral representations and four {LnW_5} groups. Ce(La) centers as large gray spheres and As centers as small black spheres. Finally, the water ligands are shown as white spheres.

The fivefold symmetry of this anion is completed by the linkage of five {PW_6} groups and the central sodium ion lies in the center of a plane defined by the oxygen atoms of the phosphate groups. It appears that the kinetically inert (on the NMR timescale) sodium ion is essential for the construction of the cluster.[137] The presence of the sodium cation reduces the overall anion symmetry from D_{5h} to C_{5v}. The {P_5W_{30}} anion is even more robust than the {P_8W_{48}} one (pH stability range ~0–10). Under hydrothermal conditions the central Na^+ can be replaced by other cations of similar size, e.g., Ca^{2+}, most Ln^{III}, and U^{IV}.[138–140] Reduction of Eu^{III} to Eu^{II} in these complexes occurs within the potential range at which the polytungstate framework is reduced to

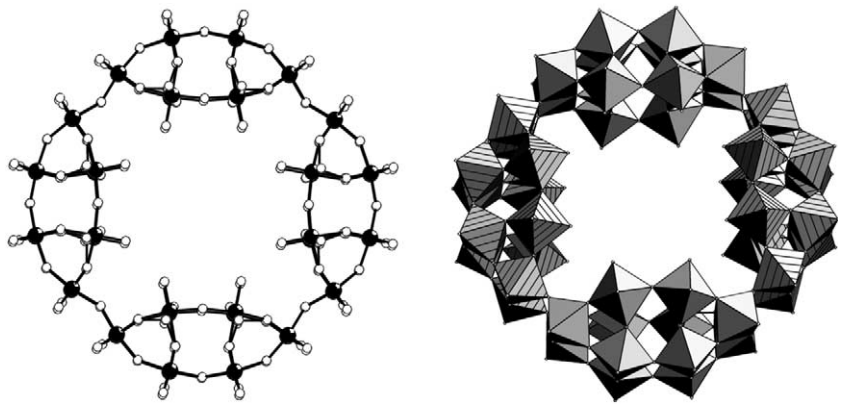

Figure 38 Structure of the anion $[P_8W_{48}O_{184}]^{40-}$, $\{P_8W_{48}\}$ (**46**) as a cyclic assembly of four lacunary $\{P_2W_{12}\}$ groups. A ball and stick representation is shown on the LHS and a polyhedral representation on the RHS.

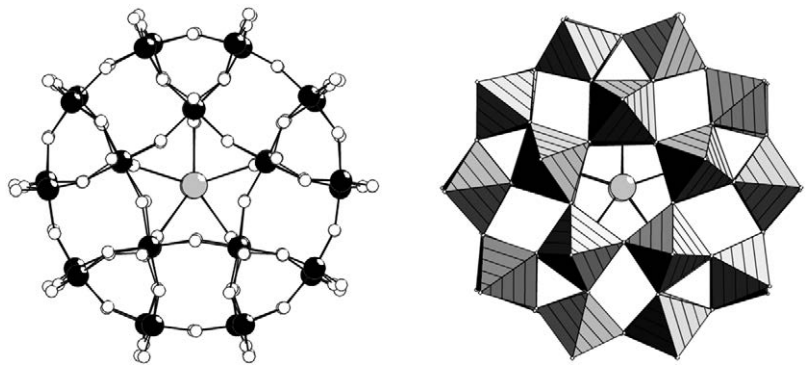

Figure 39 Structure of the anion,$[NaP_5W_{30}O_{110}]^{14-}$ ($\{P_5W_{30}\}$, **47**). A ball and stick representation is shown on the LHS and a polyhedral representation on the RHS. The central sodium ion is depicted as a large gray sphere.

heteropoly blues, and implies the possibility of generating an intermediate valence state compound.[141,142] Structures of the Eu^{III} and U^{IV} derivatives have been reported and show that these central cations are coordinated by a H_2O molecule that is enclosed in the central cavity.[143] The sodium derivative has been evaluated as a catalyst for the oxidation of H_2S to sulfur, and was the best of the polyoxometalates examined.[144,145]

7.1.4 MOLYBDATES

There is a rich chemistry of heteropolyoxomolybdates and polyoxomolybdates,[56] and it has been shown that the chemistry of these is extraordinarily versatile, which is directly related to the fact that it is very easy to reduce Mo^{VI} to Mo^{V} in aqueous solution. The generation of such "molybdenum blue" species adds a new dimension to polyoxometalate chemistry.

The history of soluble molybdenum blue (solid-state and heteropoly blues will not be considered here) dates back to Carl Wilhelm Scheele's report from 1783.[146] Solutions of molybdenum blue are almost instantaneously obtained by the reduction of Mo^{VI}-type species in acid solutions ($pH \leq 3$). Reducing agents may be metals (Al, Pb, Mo, Cu, Zn, Cd, Hg), B_2H_6, $NaBH_4$, N_2H_4, NH_2OH, H_2S, SO_2, SO_3^{2-}, $S_2O_4^{2-}$, $S_2O_3^{2-}$, $SnCl_2$, $MoCl_5$, $MoOCl_5^{2-}$, formic acid, ethanol, ascorbic acid, and it appears that the term "molybdenum blue" refers to a wide range of products.[56,147] Under stronger reducing conditions, brown species are formed which in general show the presence of Mo^{V}–Mo^{V} dumb-bells.[148] On adding electrolytes like ammonium chloride or other salts, polymerization and/or precipitation takes place. A straightforward fast identification of a molybdenum blue-type solution is possible by measuring the resonance Raman spectrum (with $\lambda_e = 1064\,nm$).

7.1.4.1 From Keggin Ions to {Mo_{37}} Clusters

The cluster anion $\{[H_{14}Mo_{37}O_{112}]^{14-}\}$ (**48**) represents a self-assembled molecular species that contains no symmetry elements, see Figure 40. The anion consists of a central $\{H_6Mo_{12}{}^{V}O_{40}(Mo^{V}O_3)_4\}$ core and two similar but nonidentical coordinated ligands, $\{Mo_{10}\}$ and $\{Mo_{11}\}$ units. The ligands differ with respect to the number of Mo centers and the degree of reduction and protonation. The core is built up from a $\{Mo_{12}{}^{V}O_{40}\}$ ε-Keggin structure[149] which is capped by four $\{Mo^{V}O_3\}$ groups.

The assembly of this anion occurs in an aqueous molybdate solution under reducing conditions and can be rationalized by assuming the initial formation of an ε-Keggin ion with T_d symmetry. Its reduction yields a highly nucleophilic ε-Keggin cluster that is stabilized by protonation and by the ligation of four electrophilic $\{Mo^{VI}O_3\}$ groups, thereby forming the anion $[H_xMo_{12}{}^{V}O_{40}(Mo^{VI}O_3)_4]^{(20-x)-}$, which has also been structurally characterized.[150] On further reduction the $\{Mo^{VI}O_3\}$ groups on the surface of the cluster now become nucleophilic and can be regarded as adopting a templating function. In the next step the $\{Mo_{10}\}$ and $\{Mo_{11}\}$ groups are assembled on the surface of the central ε-Keggin-derived unit, see Figure 40.

7.1.4.2 From {Mo_{36}} to {Mo_{57}} Clusters—Two and Three Fragment Clusters Based on {Mo_{17}} Units

The acidification of an aqueous solution of molybdate under ambient conditions has been shown to yield the $\{Mo_{36}\}$-type cluster ($[Mo_{36}(NO)_4O_{108}(H_2O)_{16}]^{12-}$) (**49**) with two $\{Mo_{17}\}$ groups linked by two MoO_2 units.[151] It appears that this is the dominant species and the cluster crystallizes readily from solution, see Figure 41. The overall structure is best understood by realizing that the $\{Mo_{17}\}$ unit can be further divided into two $\{Mo_8\}$ units and one linking $\{Mo_1\}$ unit.

If the acidified molybdate solution that forms the $\{Mo_{36}\}$ cluster is then reduced in the presence of some divalent metal ions, a three fragment cluster of the form $\{Mo_{57}M_6\}$ (**50**) type, for example, $[\{VO(H_2O)\}_6\{Mo_2(\mu\text{-}H_2O)_2(\mu\text{-}OH)\}_3\{Mo_{17}(NO)_2O_{58}(H_2O)_2\}_3]^{21-}$=$[\{VO(H_2O)\}_6\{Mo_2'\}_3(\{Mo_8\}_2\{Mo_1'\})_3]$ (Figure 6) is produced.[151–154] The $\{Mo_{57}M_6\}$-type cluster with three $\{Mo_{17}\}$

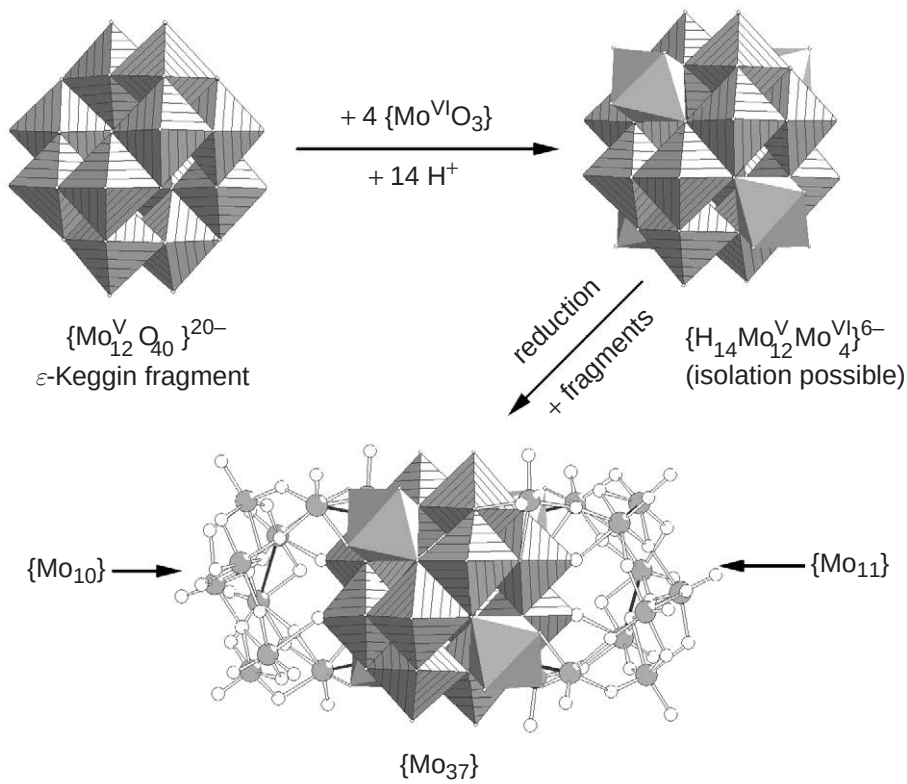

Figure 40 Summary of the stepwise assembly of the $\{Mo_{37}\}$ cluster. The ε-Keggin unit and the four added Mo units are shown as hatched and unhatched polyhedra respectively. The $\{Mo_{10}\}$ and $\{Mo_{11}\}$ units are shown in ball and stick with the Mo atoms as gray spheres and the oxygen atoms as white spheres.

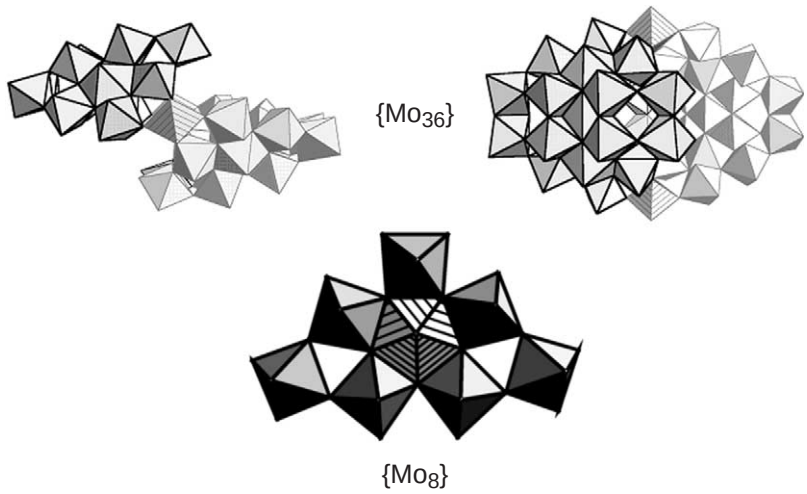

Figure 41 Polyhedral representation of the cluster anion $[Mo_{36}(NO)_4O_{108}(H_2O)_{16}]^{12-}$ ($[\{MoO_2\}_2\{H_{12}Mo_{17}(NO)_2O_{58}(H_2O)_2\}_2]^{12-}$=$[\{Mo_1^*\}_2(\{Mo_8\}_2\{Mo_1'\})_2]$). The MoO_6 octahedra that are connecting the two $\{Mo_{17}\}$ units shown as hatched polyhedra. One of the two $\{Mo_8\}$ building blocks that comprise the $\{Mo_{17}\}$ unit is also shown and the central pentagonal Mo atom is shown by the hatched polyhedron.

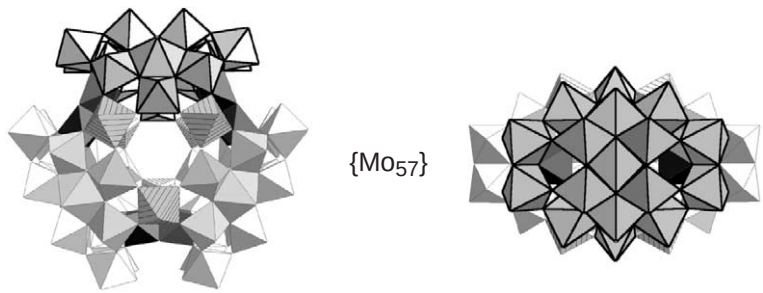

Figure 42 A polyhedral representation of the $\{Mo_{57}M_6\}$ cluster with one of the $\{Mo_8\}$ units highlighted on the left and the $\{Mo_{17}\}$ unit on the right. The divalent TM ions are shown as hatched polyhedra.

groups (see Figure 42) is formed after adding, for instance, the strong electrophilic linker $V^{IV}O^{2+}$ under reducing conditions, but other divalent metal ions can be included, e.g., Fe^{2+}. In addition, different ratios of metal ions can be included, e.g., $\{Mo57M_xM_y\}$ where $x+y=6$.[155] The $\{Mo_{57}M_6\}$ cluster comprises six $\{Mo_8\}$ units, three on each side with three $\{Mo_2'\}$ linking units and three $\{Mo_1'\}$ units which connect the two sides of the cluster together, see Figure 43. The divalent metal ions occupy three positions on the two inner rims of this cluster above and below the equator.

Another structural feature of the $\{Mo_{57}M_6\}$ are the three gaps in each of the upper and lower rims of the cluster between the ends of the $\{Mo_8\}$ units, see Figure 42. In studies by Müller *et al.*[149] it was shown that these six cavities are accessible to further coordination by the highly electrophilic $\{MoO_4\}^{4+}$ groups. This can occur under reaction conditions in which the $\{Mo_{57}M_6\}$ cluster is exposed to an excess of molybdate and gives rise to a stepwise growth process. This process allows the formation of the species $\{Mo_{57+x}V_6\}$ where x can have values between 0 and 6. Each of the $\{MoO_4\}^{4+}$ groups binds to three oxygen atoms (two terminal) of the $\{Mo_{57}V_6\}$ core resulting in a tetrahedral coordination of the incorporated Mo atoms. The degree of occupation of the cavities can be correlated with the degree of reduction of the cluster. This is because the reduction process increases the nucleophilicity of the periphery of the cluster thereby enabling the cluster to take up further electrophiles. Furthermore, this process can be reversed by the oxidation of the system so that the electrophiles are then released, see Figure 43.

7.1.4.3 $\{Mo_{154}\}$ Big Wheel Clusters

In 1995 Müller *et al.* reported the synthesis and structural characterization of a very high nuclearity cluster $\{Mo_{154}\}$ that has a ring topology.[62] The interest generated by this result is partly due to its high nuclearity and partly because of the size of this cluster; with an outer diameter

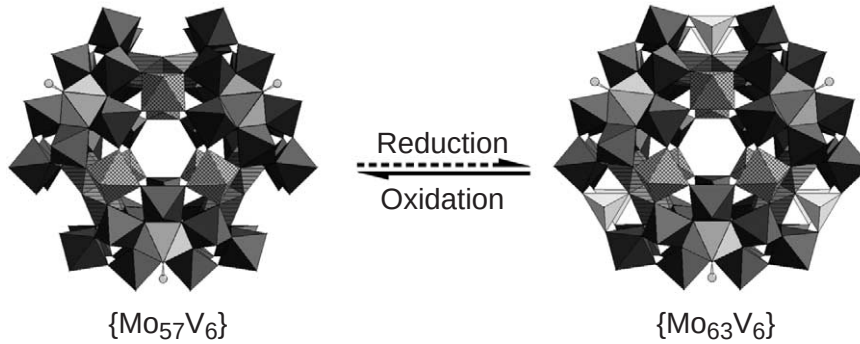

Figure 43 Polyhedral representations of the cluster ligand on the LHS and then the result of metal uptake on the RHS (tetrahedral polyhedra). The hatched polyhedra are the divalent metal ions and the pentagonal Mo polyhedra that from the $\{Mo_8\}$ units are clearly visible with the oxygen of the coordinating NO groups shown as a gray sphere.

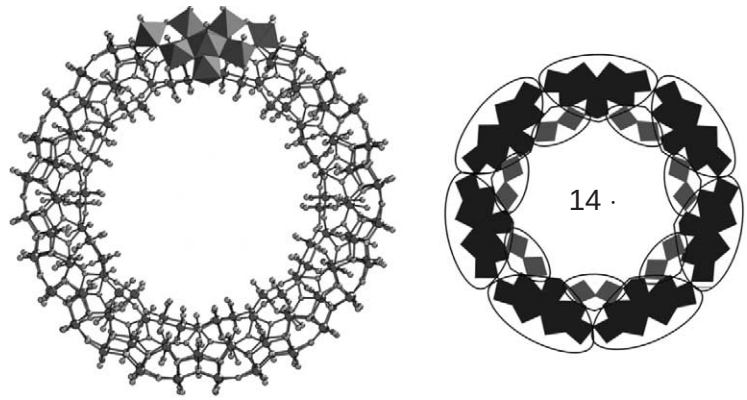

Figure 44 LHS: a ball and stick representation of $\{Mo_{154}\}$ big wheel cluster with one of the $\{Mo_8\}$ building blocks highlighted with a polyhedral representation. RHS: a polyhedral representation of the top layer of the $\{Mo_{154}\}$ cluster with the $\{Mo_8\}$ (black units) and $\{Mo_2\}$ (gray units) units clearly shown.

of ca. 34 Å, an inner diameter of 25 Å and a thickness of 14 Å it is a truly nanoscopic molecule. Using reaction conditions of pH ~ 1, with a concentration of Na_2MoO_4 of ca. 0.5 M and a degree of reduction of 1–20%, a solution is generated that yields "Giant-Wheel"-type cluster species, for example, comprising 154 Mo atoms of formula $[Mo_{154}O_{462}H_{14}(H_2O)_{70}]^{14-}$ (**51**) see Figure 44 (this can be compared to the formula of the original structure of the Giant-Wheel cluster,[62] $[Mo_{154}(NO)_{14}O_{448}H_{28}(H_2O)_{70}]^{(25\pm5)-}$; (**52**)—see Table 2). Amazingly, it is possible to synthesize gram quantities of (**51**) through a very simple "one-pot" reaction procedure in 24 hours.[156,157]

7.1.4.3.1 Construction of $\{Mo_{154}\}$-type clusters

Overall, the complete ring system consists of 140 MoO_6 octahedra and 14 pentagonal bipyramids of the type $\{MoO_7\}$, see Figure 45. The wheel can best be described as a tetradecamer comprising 14 basic $\{Mo_8\}$ units with a central $\{MoO_7\}$ group. This $\{MoO_7\}$ unit is symmetrically connected to five $\{MoO_6\}$ octahedral by edge sharing resulting in a $\{Mo/Mo_5\}$ pentagon. It should be noted that any toroidal system, such as the ring-cluster discussed here, requires a fivefold symmetry element to form the overall toroidal or spherical geometry and this is also true for clusters with a spherical topology.[58,59,63] Four of the $\{MoO_6\}$ octahedra are linked to further $\{MoO_6\}$ octahedra via corners to form the $\{Mo_8\}$ unit described above.

Continuing from the $\{Mo_8\}$ unit the complete $\{Mo_{154}\}$ cluster ring is built up as follows: (i) the two MoO_6 octahedra that are not directly connected to the central MoO7 bipyramid are fused to neighboring $\{Mo_8\}$ units through corners; (ii) neighboring $\{Mo_8\}$ groups are additionally fused together by the $\{Mo_2\}$ units, thereby completing the inner-ring parts of the upper and lower half of the ring structure; and (iii) the complete ring is constructed when the second half is rotated

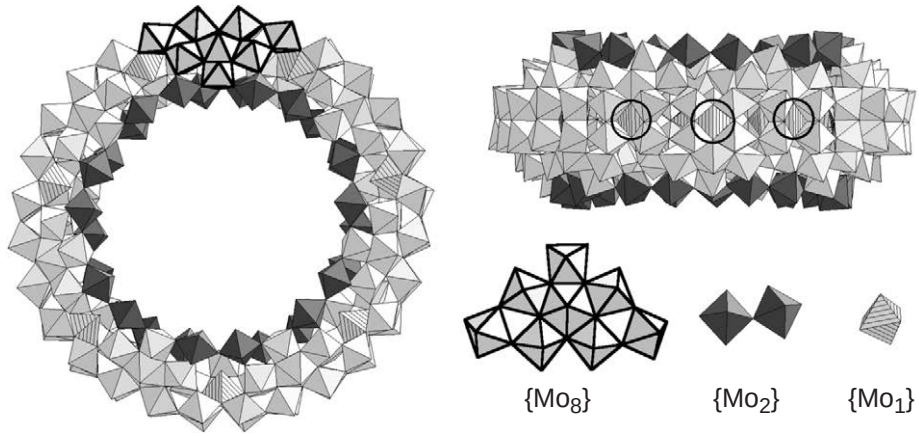

Figure 45 A polyhedral representation of the $\{Mo_{154}\}$ cluster with the component building blocks shown explicitly. The black polyhedra represent the $\{Mo_2\}$ building blocks, the hatched polyhedra represent the $\{Mo_1\}$ units that are positioned in the equator of the ring. One of the $\{Mo_8\}$ units is highlighted in the top view of the ring (LHS) for clarity. The positions of the $\{Mo_1\}$ groups are ringed on the side view of the ring (RHS) for clarity.

around 360/14° relative to the first and fused to it through the 14 $\{Mo_1\}$ groups, which are located at the equator of the complete ring, see Figure 45. Using the general architecture principle for the Giant-Wheel-type clusters the structural building blocks, e.g., for the $\{Mo_{154}\}$-type cluster, can be deduced from the formula, $[Mo_{154}O_{462}H_{14}(H_2O)_{70}]^{14-}$, in terms of the three different building blocks as $[\{Mo_2\}_{14}\{Mo_8\}_{14}\{Mo_1\}_{14}]^{14-}$.

7.1.4.3.2 Determination of the molecular formula of {Mo154}-type clusters

The deduction of the molecular formula (and the overall charge) for the first Giant-Wheel initially presented a tremendous problem. However, this information can now be routinely deduced from a combination of redox titrations, UV/Vis spectroscopy (the solution spectrum of the $\{Mo_{154}\}$ cluster gives an absorption at ca. 750 nm with a $\varepsilon \approx 6 \times 10^3$ L mol^{-1} cm^{-1}/Mo^{V} center, corresponding to an intervalence charge transfer) and analyzing structural data by calculating the bond valence sums for the molybdenum centers.[158] There are *n* electronically practically independent $\{Mo_5O_6\}$ compartments of incomplete double-cubane type, each of which carries two delocalized 4d electrons, a situation which is comparable to a so-called electronic necklace corresponding to an electron-storage system where the uncoupled storage elements are threaded like pearls on a string. These compartment-delocalized electrons are responsible for the intense blue color,[146,158] see Figure 46.

Using this information it has been found that the number of $\{Mo_8\}$ or $\{Mo_1\}$ units is equal to half the formal number of Mo^{V} centers and equal to the overall charge on the $\{Mo_{154}\}$ cluster, except in the case of the first Giant-Wheel structure which also incorporated NO as a ligand. There are formally 28 Mo^{V} centers corresponding to a charge of 14^- for the $\{Mo_{154}\}$ cluster $\equiv[\{Mo_2\}_{14}\{Mo_8\}_{14}\{Mo_1\}_{14}]^{14-}$.

At the time of discovery and publication, the $\{Mo_{154}\}$ Giant-Wheel-type cluster represented the largest cluster to be structurally characterized by single crystal X-ray diffraction. In itself, the synthesis of this giant cluster generated enormous interest, even in the popular scientific media.[159] This is because the cluster is of nanoscopic dimensions, and as such, demonstrates potential to bridge the gap between the molecular world, characterized by small molecules or ions, and a world of macroscopic bulk compounds.

7.1.4.4 Reactions of the {Mo154}-type Wheels

7.1.4.4.1 Formation of structural defects

Under certain synthetic conditions it is possible to obtain Giant-Wheel clusters based on the $\{Mo_{154}\}$ cluster that are structurally incomplete, i.e., there are defects when compared to

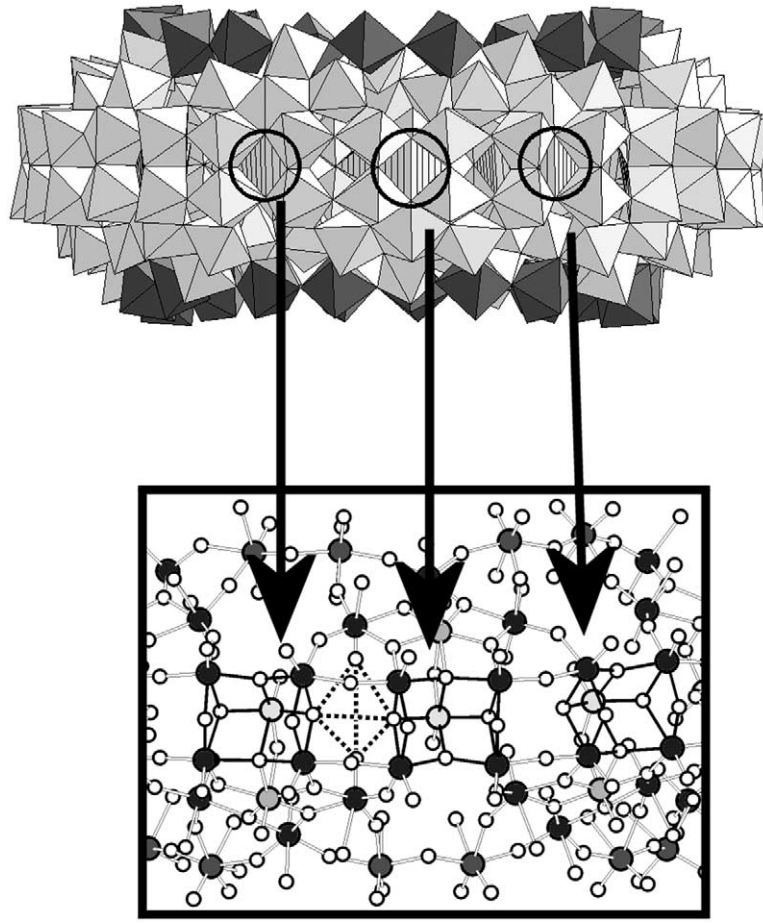

Figure 46 Polyhedral representation of the equator of the tetradecameric $\{Mo_{154}\}$-type cluster with the $\{Mo_1\}$ units that form the double-cubane-type compartments are circled. A zoom in ball and stick representation of these compartments is given below. This representation highlights (1) three of the 14 (incomplete) double-cubane-type compartments each of which is spanned by five Mo centers (Mo–Mo = 3.4–4.0 Å) belonging to $\{Mo_8\}$ as well as $\{Mo_1\}$-type groups and six O atoms (the lowered bond valence sum (BVS) values of the corresponding Mo atoms with an average value of 5.6 prove, besides other experimental data, that two 4d electrons are trapped in each compartment), and (2) one of the 14 $\{(\mu_3\text{-O})_2O_2\}$type compartments—indicated by dotted lines—which are located between two double-cubane-type compartments (the two characteristic μ_3-O atoms (dark gray, O—O = 3.07 Å) have an average BVS value of 1.2 proving protonation).

the original $\{Mo_{154}\}$ cluster. These defects manifest themselves as missing $\{Mo_2\}$ units, but statistically these defects can sometimes be seen as partially occupied $\{Mo_2\}$ units when the distribution suffers from rotational disorder or translational disorder within the crystal structure. The most extreme case found to date has six defects, three on each side of the Giant-Wheel cluster and is a $\{Mo_{142}\}$ cluster (**53**),[156,157] see Figure 47.

In this case the synthetic conditions needed to isolated the $\{Mo_{142}\}$ required a very large concentration of electrolyte (in this case ca. 2 M sodium ions present) at the time of crystallization giving a compound of formula $Na_{26}[Mo_{142}O_{432}(H_2O)_{58}H_{14}]$, $\equiv[\{Mo_2\}_8\{Mo_8\}_{14}\{Mo_1\}_{14}]^{26-}$ (**53**). This time the number of each type of building block is varied as six $\{Mo_2\}^{2+}$ groups have been removed increasing the negative charge of the Giant-Wheel by 12. The increased charge, as a consequence of the defects, increases the number of sodium ions associated with each Giant-Wheel and it is not surprising that 12 positions were found in the crystal structure that were refined as partially occupied sodium ions (a total of 6.4 sodium ions were found over 12 positions).[156,157] It is interesting that the sodium ions were found to be ligated to the oxygen atoms of the remaining $\{Mo_2\}$ units or ligated to the oxygen atoms present in the defect sites. In a recent study Yamase *et al.* also synthesized a similar species to the $\{Mo_{142}\}$ cluster species but this time the synthesis was achieved via a photochemical reduction process.[160]

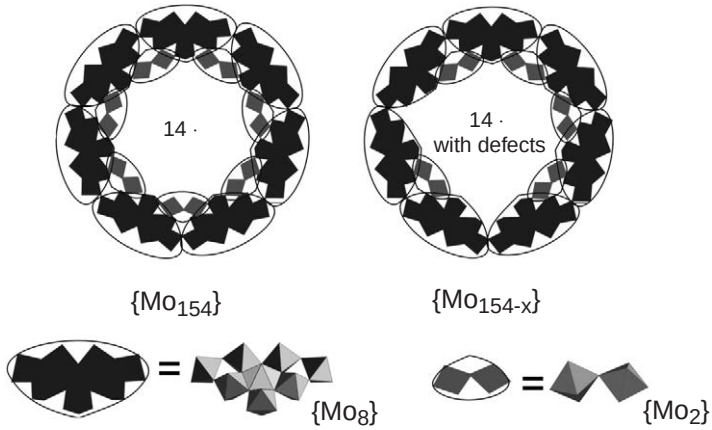

Figure 47 A representation of the building blocks that comprise the top and bottom surfaces of the wheel cluster on the LHS. On the RHS the derivative with defects is shown; literally the removal of a number of the $\{Mo_2\}$ results in a defect structure.

7.1.4.4.2 Linking of wheels to chains and layers

As the introduction of defects increases the overall negative charge of the Giant-Wheel cluster,[156–158,161] the rings can be linked together into chains and layers (see Table 3). In general, the linking reactions occur through the condensation of the terminal $\{Mo_2\}$-based $H_2O—Mo=O$ groups on the rings with the H_2O ligands on the $\{Mo_2\}$ units, $O=Mo—L$ ($L = H_2O$) (see Figure 48).

For example a defect $\{Mo_{144}\}$ cluster (**54**)[161] can be linked to chains (see Figure 49) and the other clusters $\{Mo_{144}\}$ (**55**)[156] and $\{Mo_{146}\}$ (**56**)[156] also form chains through defects. In addition to chains, a $\{Mo_{152}\}$ defect cluster (**57**)[158] can be linked to form two-dimensional layers, as can a $\{Mo_{154}\}$ (**58**) cluster derivatized with the (H_2PO_2) ligand on the inner rim, see Figure 50.[158]

The assembly of the chain shown in Figure 49 is thought to occur due to the increased negative charge resulting from the defects present in the ring, which results from the loss of $\{Mo_2\}$ units. The existence of under-occupancy at the $\{Mo_2\}$ sites is now well established[156,157,161] and has been found to be promoted by the addition of ligands which can abstract the $\{Mo_2\}$ groups. For example the formate anion has been shown to extract the $\{Mo_2\}$ units from the inner surface of the $\{Mo_{154}\}$-type cluster. This abstraction has the secondary effect of causing a higher nucleophilicity at the $O=Mo(H_2O)$ sites of the $\{Mo_2\}$ units in the surrounding area. In the case of the layered compounds[161,162] the assembly to layers has, so far, been achieved with two approaches:

By producing defects that increase the nucleophilicity by increasing the local negative charge on the terminal oxygen ligand (Mo=O) of the $\{Mo_2\}$ units that are still present on the cluster.
By introducing an electron withdrawing bidentate ligand e.g., $H_2PO_2^-$ (see Figure 48) to the $\{Mo_2\}$ units to increase the nucleophilicity on the $\{Mo_2\}$-based Mo=O group. In this case the $H_2PO_2^-$ acts as both the reducing agent (in the formation of the Giant-Wheel) as well as the bidentate ligand.

In the last process it can be considered that the reaction is facilitated by synergetically induced functional complementarity. Examination of the overall structure forms reveals the presence of a two-dimensional layer in which the cavities of the Giant-Wheel cluster stack up on each other to form nanotubes that are filled with H_2O molecules and sodium cations, see Figure 50.

7.1.4.4.3 Formation of host guest systems

The ring-shaped $\{Mo_{154}\}$-type clusters linked into chains can also act as hosts for smaller polyoxometalate guest, such as the (nonreduced) two-fragment $\{Mo_{36}\}$-type cluster.[58,59] In this supramolecular system the interaction of the guest, which fits exactly into the cavity of the host, is

Table 3 Giant-Wheel clusters and derivatives.

Compound	*Building units*	*Structure*	*References*	
$Na_{15}\{0.5[Mo_{154}O_{462}H_{14}(H_2O)_{70}]\cdot 0.5[Mo_{152}O_{457}H_{14}(H_2O)_{68}]\}$	$\{Mo_2\}_{14}\{Mo_8\}_{14}\{Mo_1\}_{14} + \{Mo_2\}_{13}\{Mo_8\}_{14}\{Mo_1\}_{14}$	Two different discrete rings, one of which possesses a defect	156	51
$(NH_4)_{28}[Mo_{154}(NO)_{14}O_{448}H_{14}(H_2O)_{70}]$	$\{Mo_2\}_{14}\{Mo_8\}_{14}\{Mo_1\}_{14}$	Discrete rings	62	52
$Na_{26}[Mo_{142}O_{432}(H_2O)_{58}H_{14}]$	$\{Mo_2\}_{8}\{Mo_8\}_{14}\{Mo_1\}_{14}$	Discrete rings	156	53
$Na_{24}[Mo_{144}O_{437}H_{14}(H_2O)_{56}]$	$\{Mo_2\}_{9}\{Mo_8\}_{14}\{Mo_1\}_{14}$	Chains built up by rings with defects	164	54
$Na_{24}\{0.5[Mo_{144}O_{437}H_{14}(H_2O)_{56}]\cdot 0.5[Mo_{144}O_{437}H_{14}(H_2O)_{60}]\}$	$\{Mo_2\}_{9}\{Mo_8\}_{14}\{Mo_1\}_{14} + \{Mo_2\}_{9}\{Mo_8\}_{14}\{Mo_1\}_{14}$	Discrete rings with defects and chains built up by rings with defects	158	55
$Na_{22}[Mo_{146}O_{442}H_{14}(H_2O)_{58}]$	$\{Mo_2\}_{10}\{Mo_8\}_{14}\{Mo_1\}_{14}$	Chains built up by rings with defects	156	56
$Na_{16}[Mo_{152}O_{457}H_{14}(H_2O)_{66.5}]$	$\{Mo_2\}_{13}\{Mo_8\}_{14}\{Mo_1\}_{14}$	Layers built up by rings with defects	157	57
$Na_{21}[Mo_{154}O_{462}H_{14}(H_2O)_{54}(H_2PO_2)_7]$	$\{Mo_2\}_{14}\{Mo_8\}_{14}\{Mo_1\}_{14}$	Layers with attached $H_2PO_2^-$ groups	158	58
$Na_{32}\{[Mo_{36}\ (NO)_4O_{108}\ (H_2O)_{16}]\subset[Mo_{148}O_{447}H_{14}(H_2O)_{64}]\}$	$\{Mo_1^*\}_2(\{Mo_8\}_2\{Mo_1'\}_2 \subset \{Mo_2\}_{11}\{Mo_8\}_{14}\{Mo_1\}_{14}$	$\{Mo_{36}\subset Mo_{148}\}$	58,59	59
$Na_3[Mo_{154}O_{462}H_{14}(H_2O)_{48}(L^{2+})_{11}]$	$\{Mo_2\}_{14}\{Mo_8\}_{14}\{Mo_1\}_{14}$	Cysteine-derived ligands attached to the inner rim	162	60
$(NH_4)_{32}[Mo_{138}O_{416}H_6(H_2O)_{58}(CH_3CO_2)_6]$	$\{Mo_2\}_6\{Mo_2Ac\}^*_2\ \{Mo_8\}_{10}\ \{Mo_8Ac\}^*_4\{Mo_1\}_{10}$	Acetate ligands attached to the wheel	154	61
$(NH_4)_{26}[Mo_{142}\ (H_4Cu^{II}_5)O_{432}(H_2O)_{58}]$	$\{Mo_2\}_{8}\{Mo_8\}_{16}\{Mo_1\}_{16}$	Copper ions distributed around the equator	165	62
$Li_{16}[Mo_{176}O_{528}H_{16}(H_2O)_{80}]$	$\{Mo_2\}_{16}\{Mo_8\}_{16}\{Mo_1\}_{16}$	Discrete rings	166,167	63
$Na_{16}[Mo_{248}O_{720}H_{16}(H_2O)_{128}]$	$\{Mo_2\}_{16}\{Mo_8\}_{16}\{Mo_1\}_{16}\{Mo_{36}\}_2$	176 wheel with hub-caps	168	64
$Na_{14}[Mo_{154}O_{462}H_{14}(CH_3OH)_8(H_2O)_{62}]$	$\{Mo_2\}_{14}\{Mo_8\}_{14}\{Mo_1\}_{14}$	Discrete rings	170	65
$Na_{16}[Mo_{176}O_{528}H_{16}(CH_3OH)_{17}(H_2O)_{63}]$	$\{Mo_2\}_{16}\{Mo_8\}_{16}\{Mo_1\}_{16}$	Discrete rings	170	66
$Na_6[Mo_{120}O_{360}(H_2O)_{60}H_{12}\{Pr(H_2O)_5\}_6]$	$\{Mo_2\}_{8}\{Mo_8\}_{12}\{Mo_1\}_{12}$	Distorted ring with six Pr^{3+} ions attached	171	67
$Eu_6A_2[Mo_{128}Eu_4O_{388}H_{10}(H_2O)_{81}]_2$ (2 A = 2 H^+ or 2 K^+)	$\{Mo_1\}_{12}\{Mo_2\}_{8}\{Mo_8\}_4\{Mo_7\}_4\{Mo_9\}_4\{Mo_2^*\}_2Eu_4$	Elliptical ring with four Eu(III) ions per ring	173	68

Table 4 Keplerate clusters and derivatives.

Compound	*Building units*	*Structure*	*References*	
$(NH_3)_{42}[Mo^{VI}_{72}Mo^{V}_{60}O_{372}(OAc)_{30}(H_2O)_{72}] = \{Mo132\}$	$\{Mo(Mo)_5\}_{12}\ \{Mo_2L\}_{30}\ L = OAc$	Discrete balls	63	69
$(NH_3)_{42}[Mo^{VI}_{72}Mo^{V}_{60}O_{372}(HCO_2)_{30}(H_2O)_{72}] = \{Mo132\}$	$\{Mo(Mo)_5\}_{12}\ \{Mo_2L\}_{30}\ L = HCO_2$	Discrete balls	177	70
$(Na)_{46}[Mo^{VI}_{66}Mo^{V}_{50}O_{331}(OAc)_{30}(H_2O)_{56}] = \{Mo132\}$	$\{Mo(Mo)_5\}_{11}\ \{Mo_2L\}_{25}\ L = OAc$	Molecular basket	178	71
$[Mo_{72}Fe_{30}O_{252}(CH_3COO)_{10}\{Mo_2O_7(H_2O)\}\{H_2Mo_2O_8(H_2O)\}_3 (H_2O)_{91}] = \{Mo_{72}Fe_{30}\}$	$\{Mo(Mo)_5\}_{12}\{Fe\}_{30}\ (L)_{10} \subset \{Mo_2\}_1\{Mo_2\}_3L = OAc$	Discrete Fe-substituted ball	181	72
$[Mo_{102}O_{282}(H_2O)_{78}(CH_3CO_2)_{12}] = \{Mo_{102}\}$	$\{Mo(Mo)_5\}_{12}\{Mo\}_{30}\ (L)_{12}\ L = OAc$	Discrete balls	179	73
$Na_{20}[\{Mo^{VI}O_3(H_2O)\}_{10}\{V^{IV}O(H_2O)\}_{20}\{Mo^{VI}/Mo^{VI}_5O_{21}(H_2O)_3\}_{10} (\{Mo^{VI}O_2(H_2O)_2\}_{5/2})_2(\{NaSO_4\}_5)_2] = \{Mo_{75}V_{20}\}$	$\{Mo(Mo)_5\}_{10}\{Mo\}_{10}\ (\{Mo\}_{5/2})_2\{V\}_{20}(NaSO_4)_5$	Barrel cluster	182	74
$[H_4Mo_{72}Fe_{30}O_{254}(CH_3COO)_{10}\{Mo_2O_7(H_2O)\}\{H_2Mo_2O_8(H_2O)\}_3 (H_2O)_{87}] = \{Mo_{72}Fe_{30}\}$-linked	$\{Mo(Mo)_5\}_{12}\{Fe\}_{30}\ (L)_{10} \subset \{Mo_2\}_1\{Mo_2\}_3L = Oac$	Balls linked to a 2d array	181	75
$[PMo_{12}O_{40} \subset \{(Mo^{VI})Mo^{VI}_5\}_{12}Fe^{III}O_{252}(H_2O)_{102}(CH_3COO)_{15}] = \{PMo_{12}\} \subset_{132}$	$Mo(Mo)_5\}_{12}\{Fe\}_{30}\ (L)_{10} \subset \{PMo_{12}\}$ $L = OAc$	Discrete ball encapsulating Keggin ion	184	76
$[PMo_{12}O_{40} \subset \{(Mo^{VI})Mo^{VI}_5\}_{12}Fe^{III}O_{252}(H_2O)_{102} (CH_3COO)_{15}] = \{PMo_{12}\} \subset_{132}$-linked	$Mo(Mo)_5\}_{12}\{Fe\}_{30}\ (L)_{12} \subset \{PMo_{12}\}$ $L = OAc$	Balls encapsulating Keggin ion linked to a 2d array	1	77
$Na_{48}[H_xMo_{368}O_{1032}(H_2O)_{240}(SO_4)_{48}] = \{Mo_{368}\}$	$[H_x\{Mo(Mo_5)\}'_8\{Mo(Mo_5)\}''_{32}\{Mo_2\}'_{16} \{Mo_2\}''_8\{Mo_2'''\}_8\{Mo_1\}_{64}]$	Lemon cluster: ball wheel hybrid cluster		78

2d = two-dimensional.

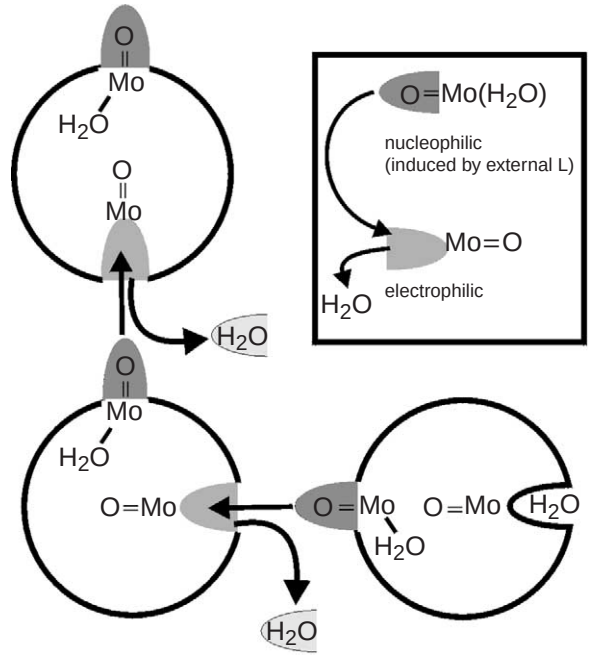

Figure 48 Schematic representation of the basic assembly principle of the Giant-Wheel-shaped cluster units forming the networks and layers. The formation is based on the synergetically induced functional complementarity of the $\{Mo_2\}$ units O═Mo(L) (e.g., L = H_2O, $H_2PO_4^{2-}$) sites of their surfaces.

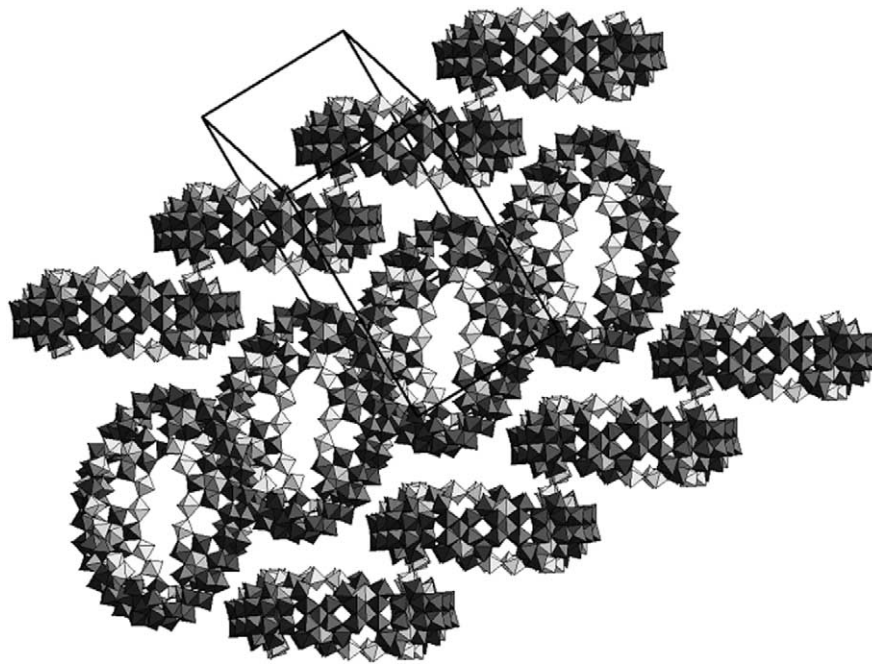

Figure 49 A polyhedral representation of $\{Mo_{144}\}$ (**54**) units linked to chains. The linking occurs via the $\{Mo_2\}$ units (see Table 3).[161]

due to 16 hydrogen bonds as well as the Coulomb interaction mediated by four sodium cations located between the negatively charged host and negatively charged guest in the formation of $\{Mo_{36} \subset Mo_{148}\}$ cluster (**59**), see Figure 51. This is an interesting system because a heavily reduced fragment has "captured" a nonreduced fragment. However, it has proved very difficult to reproduce and characterize this product further.

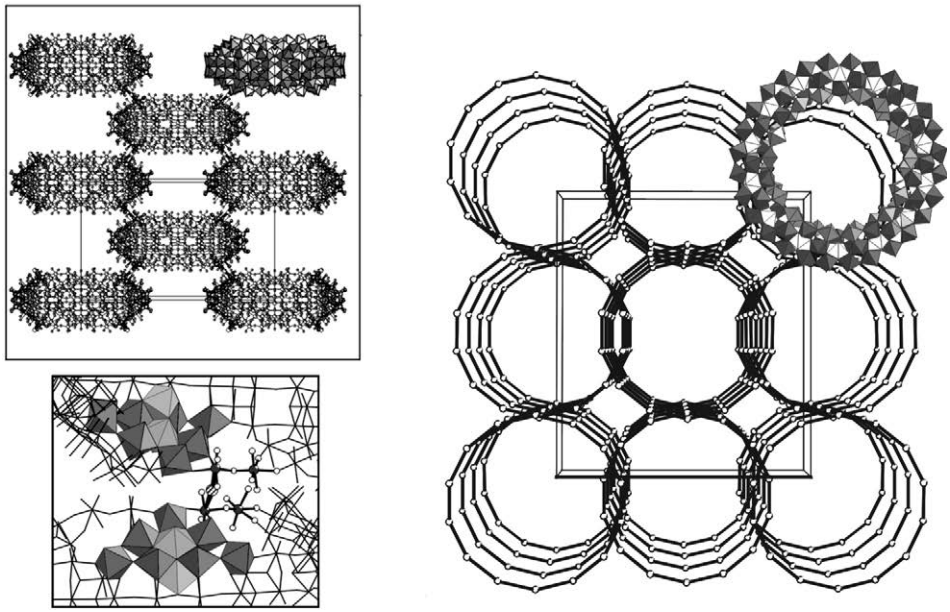

Figure 50 Ball and stick representation of the "packing" of the linked rings (in the direction of the *b*-axis) linked in crystals of $Na_{16}[Mo^{VI}_{124}Mo^{V}_{28}O_{429}(\mu_3\text{-}O)_{28}H_{14}(H_2O)_{66.5}]\cdot XH_2O$ ($X \approx 300$) ($\{Mo_{152}\}$) viewed along the crystallographic *b*-axis. Each ring is connected to surrounding rings via Mo—O—Mo bridges of the O═Mo—O—Mo—OH_2 units, thus forming layer networks parallel to the *ac* plane. One ring is shown as basic unit in polyhedral representation (LHS top). On the LHS, bottom, a detailed view of the bridging region between two cluster rings is shown. One $\{Mo_8\}$ unit of each ring along with one $\{Mo_1\}$ unit is shown in polyhedral representation and one $\{Mo_2\}^{2+}$ ($=\{Mo^{VI}_2O_5(H_2O)_2\}^{2+}$) unit per ring in ball and stick representation. On the RHS a perspective view along the crystallographic *c* showing the framework with nanotubes that are filled with H_2O molecules and sodium cations. For clarity, only one ring is shown in a polyhedral representation. To represent the other rings only the equatorial $\{Mo_1\}$ units are given and connected in the remainder of the diagram.

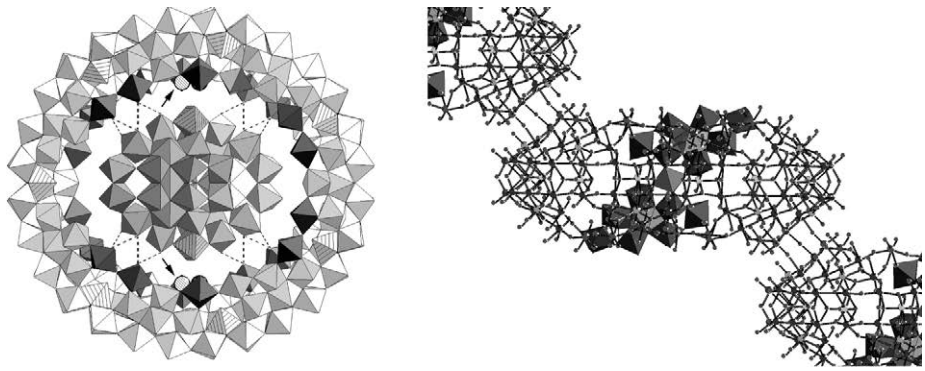

Figure 51 Structural details of the $\{Mo_{36} \subset Mo_{148}\}$ cluster system. RHS: part of the chain structure is shown, which is built up by linking ring-shaped cluster units $\{Mo_{148}\}$ (i.e., based on the $\{Mo_{154}\}$-type with three missing $\{Mo_2\}$ groups). LHS: view perpendicular to RHS; the interaction between host and guest is due to 16 hydrogen bonds (dotted lines) and (at least) four sodium cations (indicated by arrow, only two Na positions are visible in this perspective view) situated between host and guest.

7.1.4.4.4 Structural modifications of the big wheel clusters

In addition to the generation of cluster defects it has been possible to derivatize the isolated wheel clusters in other ways. For instance it has been possible to attach ligands to the inner rim of the cluster anion. This was achieved firstly by adopting reducing agents that could also act as ligands, for example cysteine,[163] which was inspired by the use of $H_2PO_2^-$ as both a reducing agent and a ligand in the formation of the wheel layers.[161,162] In the presence of cysteine a wheel cluster forms that also ligates to 11 ligands derived from the oxidation of cysteine in the formation of the species $\{Mo_{154}L_{11}\}$ (L = $HO_2C\text{-}(NH_3^+)HC\text{-}CH_2\text{-}S\text{-}S\text{-}CH_2\text{-}CH(NH_3^+)\text{-}CO_2\text{-}$) (**60**) see Figure 52.

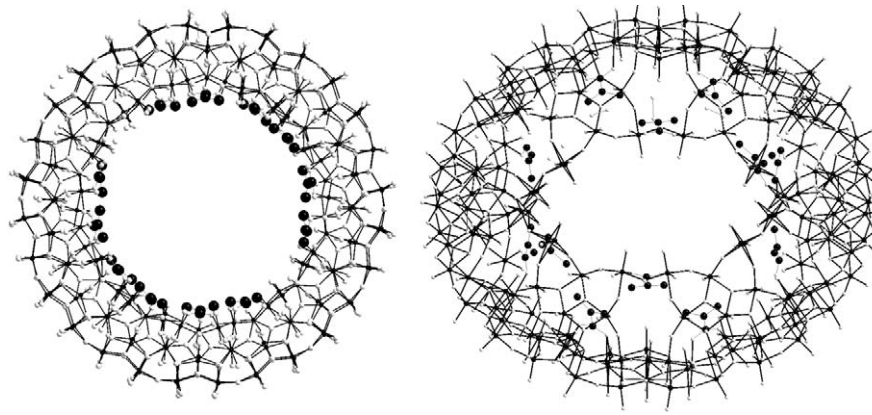

Figure 52 Ball and stick representations of the modified big wheel cluster with the oxidized cysteine ligand. Only the positions of acetate groups of the ligand were crystallographically resolved and are shown as black spheres. The LHS shows a top view looking down on the $\{Mo_{154}\}$ cluster and the RHS shows a view 45° inclined from the top view. The Mo—O framework is shown by small black and white spheres.

In an extension to this work the mixed valence cluster anion of the compound $(NH_4)_{32}[Mo^{VI}{}_{110}Mo^{V}{}_{28}O_{416}H_6(H_2O)_{58}(CH_3CO_2)_6]\cdot xH_2O$ (**1**) (x250) was synthesized under one-pot conditions. Structural analysis of this $\{Mo_{138}\}$ (**61**) cluster demonstrated that it contains well-defined, different types of defects compared to the complete parent $\{Mo_{154}\}$-type cluster. However in addition to the defects the cluster also ligates six acetate anions.[164] In further studies other derivatives and variations of the $\{Mo_{154}\}$ cluster includes the incorporation of Cu^{II} ions into a $\{Mo_{142}\}$ wheel cluster of formula $[(H_4Cu_5^{II})Mo_{28}{}^{V}Mo_{114}{}^{VI}O_{432}(H_2O)_{58}]^{26-}$ (**62**).[165]

The crystal structure reveals the presence of the cluster anions $[\{Mo_8{}^{V/VI}O_{26}(\mu\text{-}_3O)_2(H_4Cu_5)(H_2O)_3Mo^{V/VI}\}_{14}\{Mo_2{}^{VI}O_5(H_2O)_2\}_8]^{26-}$, which are derivatives of the aforementioned tetradecameric $\{Mo_{154}\}\equiv\{Mo_8\}_{14}\{Mo_1\}_{14}\{Mo_2\}_{14}$-type species (**51**). In comparison to the $\{Mo_{154}\}$ anion, (**62**) lacks six $\{Mo_2\}$-type building blocks and has the following structural additions. In the tetrahedral cavities spanned by four oxygen atoms (two μ_3 and two terminal, within the $\{Mo_8\}$ building blocks) at well-defined sites on the cluster equator, five Cu^{2+} centers are incorporated but not uniformly distributed in the cavities, the largest occupation number being 0.73. These replace some of the 14 H atoms of the parent cluster (**52**), which are bonded to several of the μ_3-O atoms that form the cavities. With high H^+ ion concentrations the maximum 14-fold protonation of the tetradecameric cluster is achieved.

7.1.4.5 $\{Mo_{176}\}$ Wheel and Derivatives

The synthesis of the $\{Mo_{176}\}$-type cluster can be related to that of the tetradecameric $\{Mo_{154}\}$ cluster. The synthesis of this larger wheel-shaped cluster was achieved by the groups of Müller[166] and Zhang in 1998.[167] The most important change is that this requires reaction conditions with a pH lower than 1 and in the presence of an increased concentration of molybdate. The $\{Mo_{176}\}$ cluster can be broadly described as a hexadecamer with two extra $\{Mo_8\}$, $\{Mo_2\}$ and $\{Mo_1\}$ units respectively with a formula of $[Mo_{176}O_{528}H_{16}(H_2O)_{80}]^{16-}$ (**63**),[166,167] which, again, can be broken into the three types of building units, $[\{Mo_2\}_{16}\{Mo_8\}_{16}\{Mo_1\}_{16}]^{16-}$, see Figure 53.

7.1.4.5.1 Comparison between the $\{Mo_{154}\}$ and $\{Mo_{176}\}$ big wheel clusters

As described in Section 7.1.4.3.1, the $\{Mo_{154}\}$ Giant-Wheel cluster, with the formula, $[Mo_{154}O_{462}H_{14}(H_2O)_{70}]^{14-}$, can be understood in terms of the three different building blocks as $[\{Mo_2\}_{14}\{Mo_8\}_{14}\{Mo_1\}_{14}]^{14-}$. It would appear the larger $\{Mo_{176}\}$ wheel, with the formula, $[Mo_{176}O_{528}H_{16}(H_2O)_{80}]^{16-}$ (**63**)[166,167] can also be broken into the three types of building units, $[\{Mo_2\}_{16}\{Mo_8\}_{16}\{Mo_1\}_{16}]^{16-}$, see Figure 54. Therefore, it is easy to see that the $\{Mo_{154}\}$ is a tetradecamer of these building blocks whilst the $\{Mo_{176}\}$ wheel is a hexadecamer, see Figure 54.

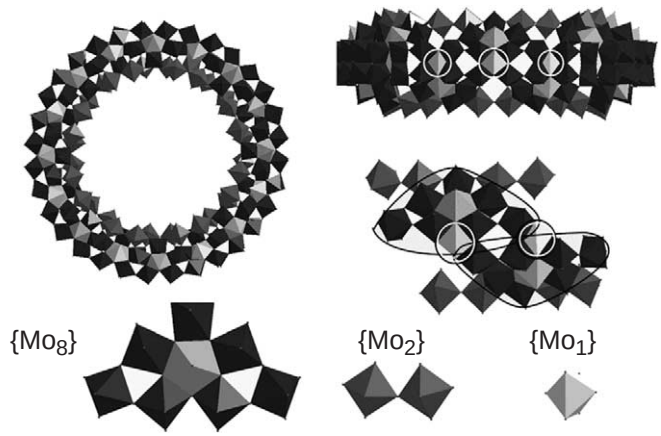

Figure 53 Top (LHS) and side (RHS) polyhedral views of the hexameric $\{Mo_{176}\}$ cluster. The $\{Mo_8\}$, $\{Mo_2\}$ and $\{Mo_1\}$ building blocks are shown below and the positions of $\{Mo_1\}$ units are ringed on the side view on the RHS.

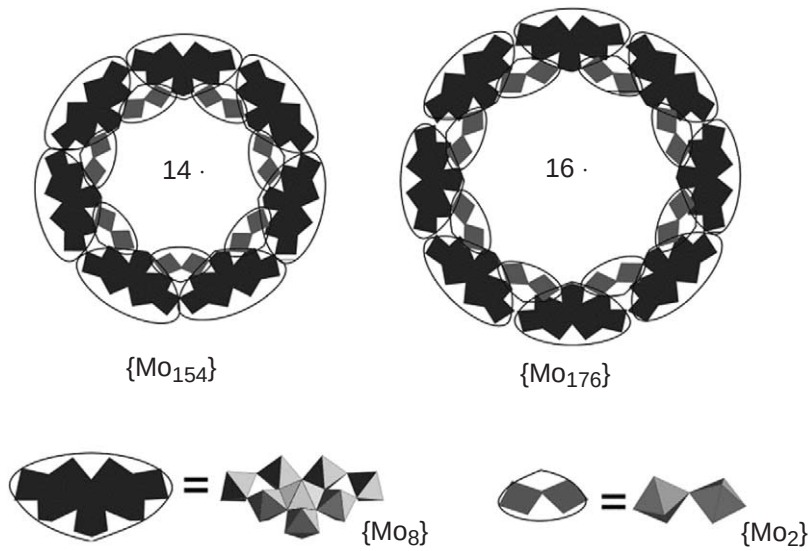

Figure 54 Comparison between the $\{Mo_{154}\}$ and $\{Mo_{176}\}$ big wheel clusters. Only the top sections of the wheels are shown which comprise half of the total number of $\{Mo_8\}$ and $\{Mo_2\}$ building blocks. The equators which contain the $\{Mo_1\}$ building blocks are omitted for clarity along with the base of the rings which contain the other $\{Mo_8\}$ and $\{Mo_2\}$ building blocks.

7.1.4.5.2 Nucleation processes within a cluster cavity—from a {Mo176} to a {Mo248} cluster

To date, despite the increasing knowledge behind the reduction and synthesis of crystalline compounds containing Giant-Wheel clusters, it is interesting that all the diverse formulations of the $\{Mo_{154}\}$-type analogues have not been reproduced with the larger $\{Mo_{176}\}$ ring structure. One possible explanation for this observation is that the $\{Mo_2\}$ groups are more strained in the $\{Mo_{154}\}$ than the $\{Mo_{176}\}$ wheel due to the inclusion of more building groups. This is because the overall curvature in the $\{Mo_{176}\}$ is less than in the $\{Mo_{154}\}$ cluster. Therefore, any reactions that remove the $\{Mo_2\}$ groups from the $\{Mo_{176}\}$ cluster may be energetically unfavorable under the conditions that have been studied. This idea would also explain why no example of a defect or chain $\{Mo_{176}\}$ cluster has been observed.

It is extraordinary, therefore, that under special types of reducing conditions, using ascorbic acid as a reducing agent,[168] the $\{Mo_{176}\}$ cluster can be observed to grow. During this process a further two $\{Mo_{36}\}$ units are added to each side of the cluster forming a spherical disk-shape cluster comprising 248 Mo atoms of the formula $[Mo_{248}O_{720}H_{16}(H_2O)_{128}]^{16-}$ (**64**), where the "hub-caps" were found to have a occupancy of 50%, see Figure 55. This appears to be a remarkable result when it is considered that the larger wheel cluster "cap" $[Mo_{36}O_{96}(H_2O)_{24}]$-type

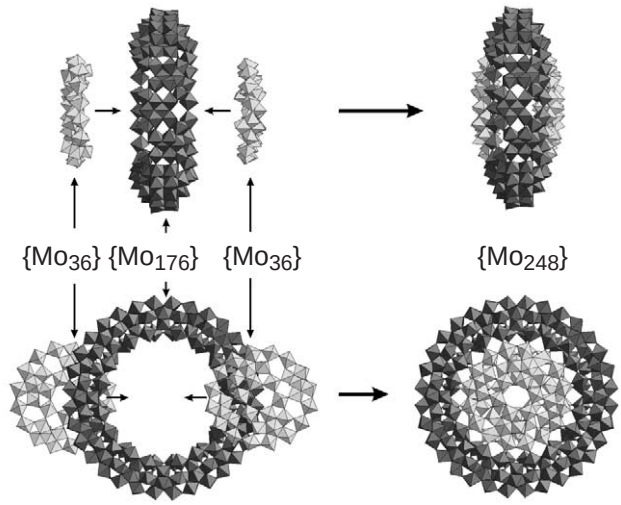

Figure 55 A schematic representation of the growth process $\{Mo_{176}\} \rightarrow \{Mo_{248}\}$. The structure of one $\{Mo_{248}\}$ cluster can formally be decomposed into one $\{Mo_{176}\}$ ring and two $\{Mo_{36}O_{96}(H_2O)_{24}\}$ hub-caps.

fragment is nearly identical to a segment of the solid-state structure of the compound $\{Mo_5O_{14}\}$.[169] This extraordinary structure offers the possibility to model crystal growth under boundary conditions, especially nucleation processes. Of particular note is that the growth event can be considered to start from the inner $\{Mo_2\}$ groups, see Figure 55.

7.1.4.5.3 Surface ligand exchange on the big wheel clusters

Both types of the Giant-Wheel clusters have a very large number of H_2O ligands present on the surface of the cluster; the $\{Mo_{154}\}$ cluster supports 70 H_2O ligands and the $\{Mo_{176}\}$ cluster supports 80 H_2O ligands. As a result, it appears possible to exchange these ligands by those with similar donor properties, for example, CH_3OH. In the presence of CH_3OH it has been found that the $\{Mo_{154}\}$ and the $\{Mo_{176}\}$ rings can take up eight and 17 CH_3OH molecules, respectively, in the formation of $\{Mo_{154}{\cdot}8MeOH\}$ (**65**) and $\{Mo_{176}{\cdot}17MeOH\}$ (**66**), displacing H_2O ligands, as observed by single crystal X-ray crystallography (see Figure 56).[170] It is interesting to note that in both structures the CH_3OH ligands are only observed to replace the H_2O ligands that exist on one type of site, although the CH_3OH molecules were found to occupy only one type of site by X-ray crystallographic studies this does not rule out the possibility of disorder over other sites—both in solution and the solid state.[170] This site occurs on the $\{Mo_8\}$ unit between the Mo polyhedra

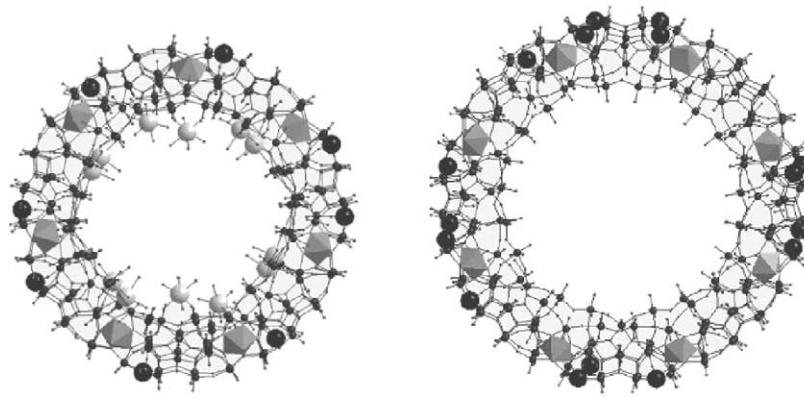

Figure 56 Ball and stick representations of $\{Mo_{154}\}{\cdot}8MeOH$ (LHS) and $\{Mo_{176}\}{\cdot}17MeOH$ (RHS with surface exchanged methanol molecules shown in black and the central pentagonal unit of the $\{Mo_8\}$ unit shown in polyhedra). The lower section shows a schematic showing the location of the methanol molecules on the $\{Mo_8\}$ unit. The positions of the located sodium ions in the crystal structure of $\{Mo_{154}\}{\cdot}8MeOH$ are shown as gray spheres.

adjacent to the hole formed below the $\{Mo_2\}$ units. Furthermore, in the case of the $\{Mo_{154}\}\cdot 8MeOH$ several sodium ions were also located in the crystal structure. These are coordinated with 50% occupancy to the $\{Mo_2\}$ units. These results have indicated that by modeling (pattern matching, donor matching) the sites amenable to surface exchange it should be possible to utilize ligands with more that one donor atom. For example, by functionalizing the ring with multi-donor ligands advantage of the chelate effect can be taken. Such derivatives can then be extended to incorporate amphiphilic ligands with the head part exchanging the H_2O ligands that can in turn allow the complexation of other species on to and into the wheel by the tail of the ligand.

7.1.4.6 Synthesis of Wheels with Electrophiles

Formally, the removal of a $\{Mo_2\}$ unit, introducing defects into the Giant-Wheel-type clusters, should result in the negative charge increasing by two providing a route to the specific derivatization of the inner side of the cluster (the defects only occur at the $\{Mo_2\}$-type sites on the inside of the cluster) and should allow the incorporation of electrophilic substrates.

7.1.4.6.1 Synthesis of the big wheel-type clusters with Pr^{III} salts

In a recent derivatization of the $\{Mo_{154}\}$ cluster it has been shown that a smaller dodecameric cluster (rather than a tetradecameric cluster, as in the case of the $\{Mo_{154}\}$) can be produced when the synthesis of the cluster is conducted in the presence of Pr^{III} ions of the formula $[Mo_{120}O_{360}(H_2O)_{60}H_{12}\{Pr(H_2O)_5\}_6]^{6-}$ (**67**). However in the case of this smaller dodecameric cluster, six of the $\{Mo_2\}$ groups are completely replaced by $\{Pr(H_2O)_5\}^{3+}$ moieties,[171,172] resulting in a $\{Mo_{120}Pr_6\}$-type Giant-Wheel cluster, see Table 3 and Figure 57.

The $\{Mo_{120}Pr_6\}$-type cluster consists of 12 sets of the three characteristic building blocks $\{Mo_2\}$, $\{Mo_8\}$, and $\{Mo_1\}$ corresponding to the formula of the dodecameric cluster. Therefore, the incorporation of Pr^{3+} into the ring system has resulted in a ring with increased curvature. The main consequence of the increased curvature is shown as a decreased average diameter and ring size, as the number of building blocks that can be incorporated is smaller than compared to the $\{Mo_{154}\}$ Giant-Wheel cluster, see Table 3.

7.1.4.6.2 Synthesis of the big wheel clusters with Eu^{III} salts

Synthesis of the cluster in the presence of Eu^{III} rather than Pr^{III} salts instead results in a new type of elliptical cluster, see Figure 58.

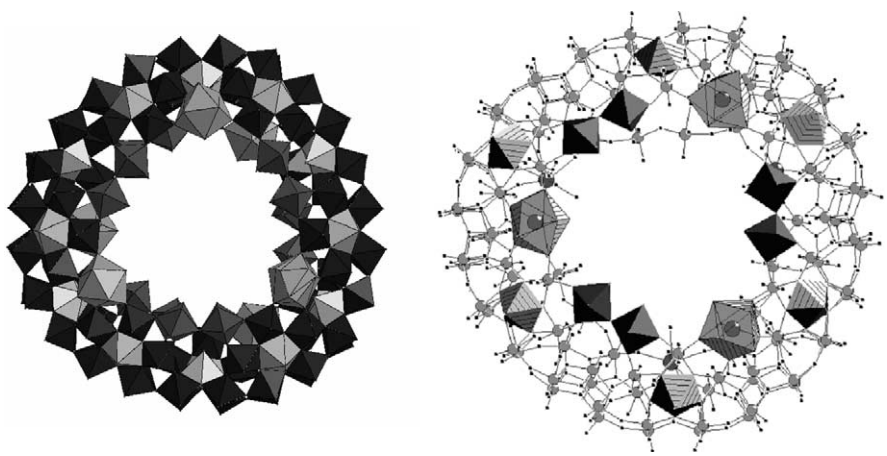

Figure 57 A schematic showing the structure of $\{Mo_{126}Pr_6\}$ Giant-Wheel cluster in polyhedral representation (LHS) and in ball and stick presentation (RHS) (view along the crystallographica *a*-axis). On the RHS, the PrO_9 polyhedra (the Pr atoms are shown in the center of polyhedra with hatched sides and open faces), the pentagonal bipyramids (shown as hatched polyhedra) and the $\{Mo_2\}$ units (shown as filled polyhedra) on the upper half of the wheel are shown in polyhedral representation.

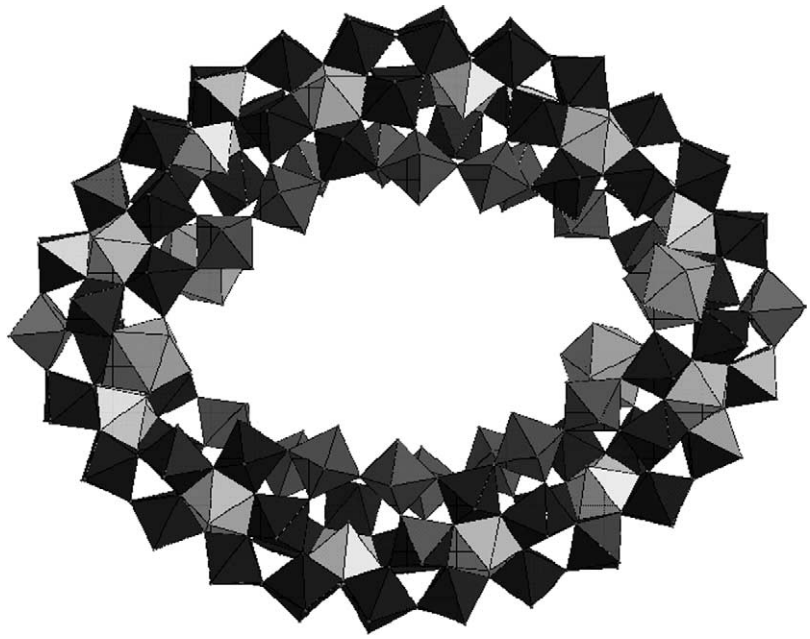

Figure 58 Polyhedral representation of the structure of the $\{Mo_{128}Eu_4\}$ cluster. The pentagonal centers in the $\{Mo_8\}$ units are shown as the hatched polyhedra and the Eu^{III} ions are shown as hatched polyhedra.

This cluster was structurally characterized as dimer of two giant clusters with the formula $Eu_6A_2[Mo_{128}Eu_4O_{388}H_{10}(H_2O)_{81}]_2$ ($2A = 2H^+$ or $2K^+$) (**68**).[173] The dimer contains two elliptical molybdenum oxide-based units, linked together by two Eu—O—Mo bonds, each unit incorporates 128 $Mo^{VI/V}$ and four Eu^{III} centers and includes large fragments of the $\{Mo_{154}\}$ "parent" cluster, see Figure 59. One explanation of this is that these dimers are formed by Eu^{III} centers acting as symmetry breakers which prevent the corresponding highly symmetrical parent-ring closure.[146,173] In addition, it is important to realize that such large fragments can, in principle, be used as synthons. The ability to connect or assemble clusters in

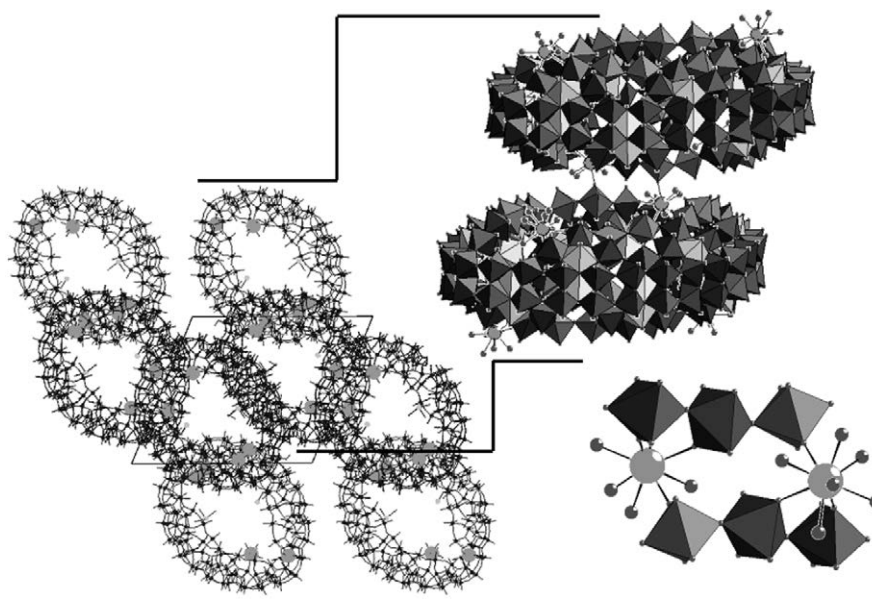

Figure 59 On the left a packing diagram of the cluster units in ball and stick representation is shown looking down the "cavities" (Eu^{III} ions in gray). On the right a representation of the "dimeric" unit (**68**) is shown with the Mo-oxide-based units displayed as polyhedra ($\{Mo_1\}$ units, $\{Mo_2\}$ groups, $\{Mo_8\}$ units with pentagonal units; Eu^{III} coordination spheres in ball and stick representation). An expanded view of the Mo—O—Eu groups linking the two cluster rings is also shown.

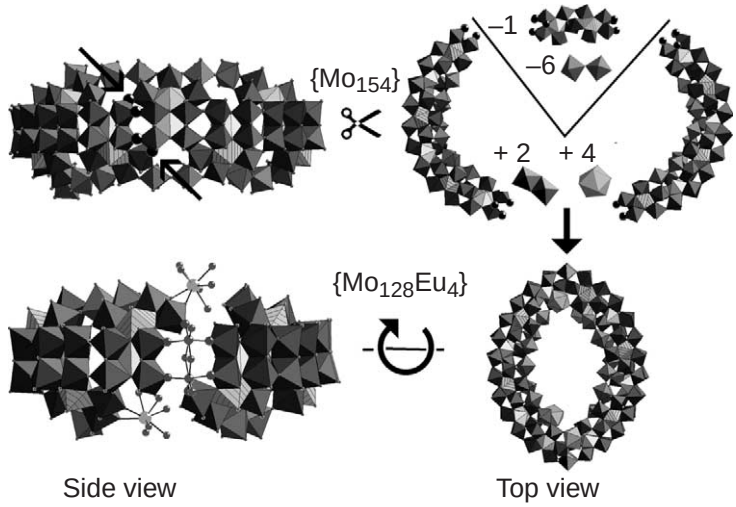

Figure 60 Demonstration of a formal $\{Mo_{128}Eu_4\}$ ring construction from a parent $\{Mo_{154}\}$-type cluster by a "cutting" process giving two large fragments. A side view of the $\{Mo_{154}\}$ ring (top left) shows the cutting positions marked as large black spheres and the top right view those units which have to be removed from the $\{Mo_{154}\}$ ring and those which have to be added to the resulting two large fragments (left and right) to generate the $\{Mo_{128}Eu_4\}$cluster unit which are shown in a side and top view at the bottom (the new $\{Mo_2{*}\}$ units are shown on the left side together with the EuO_9 in ball and stick representation).

a predefined manner may allow for the design of nanoscopic devices using the "bottom up" approach.

The giant ring-shaped parent clusters (see above) obtained from molybdenum blue solutions are based on the three different building blocks $\{Mo_1\}$, $\{Mo_2\}$, and $\{Mo_8\}$.[146] The remarkable feature in (**68**) is that this has undergone critical structural changes as a result of the incorporation of Eu^{III} (compare the Pr^{III} substituted cluster).[171] This situation could be explained in that the presence of Eu^{III} ions, which have a smaller ionic radius than Pr^{III} ions, prevent ring closure to the parent ring type as the accompanying increase of the curvature destabilizes the system.

The two ellipsoidal cluster entities of $Eu_6A_2[Mo_{128}Eu_4O_{388}H_{10}(H_2O)_{81}]_2 \cdot$ ca. 600 H_2O ($A = H^+$ or K^+) can be approximately described by the building-block scheme used for the formation of the $\{Mo_{154}\}$- and $\{Mo_{176}\}$-type species, which comprise not only the building blocks $\{Mo_1\}$, $\{Mo_2\}$, and $\{Mo_8\}$, but also the additional "new" units of the $\{Mo_2{*}\}$, $\{Mo_7\}$, and $\{Mo_9\}$ type ($\{Mo_2{*}\}\{Mo_2{}^{V/VI}O_7(H_2O)\}^{3-}$): the fragments are (formally) cut, as shown in Figure 60, from the $\{Mo_{154}\}$-type Giant-Wheel at four positions. The "cutting" process takes place between those polyhedra showing the least number of bonds. The large fragments obtained (Figure 60) have the composition $[\{Mo_1\}_6\{Mo_2\}_4\{Mo_8\}_2\{Mo_7\}_2\{Mo_9\}_2]$, that is, they include the two new $\{Mo_7\}$ and $\{Mo_9\}$ units, which are formally generated by "cutting" asymmetrically two neighboring $\{Mo_8\}$ units at the above-mentioned positions to produce the two major parts of the new ellipsoidal ring. The complete ellipsoidal ring unit is formed when the two fragments are combined with two new $\{Mo_2{*}\}$ units and four Eu^{III} ions (Figure 60).

7.1.4.7 $\{Mo_{132}\}$ Big Ball Keplerate Clusters

In 1998, Müller *et al*. synthesized and structurally characterized a polyoxometalate that can best be described as a molecular sphere with an outer diameter of 30 Å, and an inner diameter of 25 Å.[63] This molecular sphere, or inorganic super fullerene was given the name "Keplerate" corresponding to Kepler's model of the cosmos and his concept of planetary motion, as described in his early opus *Mysterium Cosmographicum*.[174] In accordance with this speculative model, Kepler believed that the distances between the orbits of the planets could be explained if the ratios between the successive orbits were designed to be equivalent to the spheres successively circumscribed around and inscribed within the five Platonic solids. In analogy, the cluster correspondingly shows a spherical shell of terminal oxygen atoms in which an icosahedron spanned by the centers of the 12 $\{(Mo)Mo_5\}$ pentagons—the Mo atoms of the central MoO_7 bipyramids—is inscribed (see Figure 61).

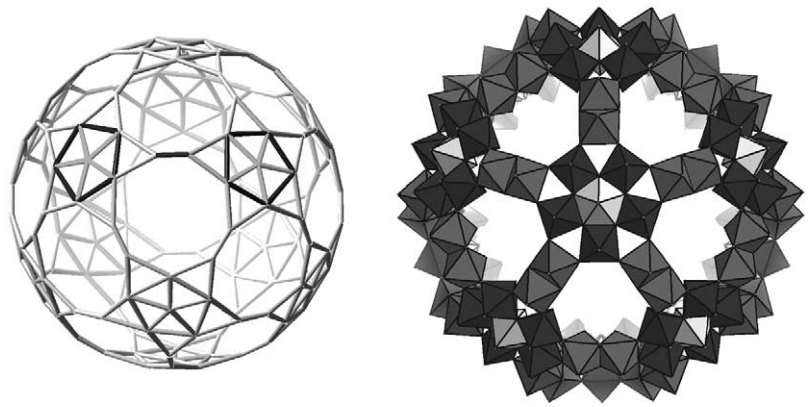

Figure 61 Representations of the spherical Keplerate $\{Mo_{132}\}$ cluster. LHS: schematic representation of the 132 molybdenum atom framework of the Keplerate cluster highlighting its spherical nature. Two pentagonal units $\{(Mo)Mo_5\}$ groups linked by an $\{Mo^V–Mo^V\}$ bridge (red) are emphasized. RHS: polyhedral representation of the cluster. The pentagonal Mo centers are shown by the white polyhedra, the rest of the $\{(Mo)Mo_5\}$ groups are shown as the very dark (almost black) polyhedra and the $\{Mo^V–Mo^V\}$ or $\{Mo_2\}$ linker groups are shown as the lighter colored polyhedra.

7.1.4.7.1 Building block scheme for the Keplerate clusters

The overall Keplerate clusters have the formula $[Mo^{VI}{}_{72}Mo^{V}{}_{60}O_{372}(MeCO_2)_{30}(H_2O)_{72}]^{42-}$ ($\{Mo_{132}\}$) (**69**) and consist of two types of building block (Figure 61): 12 pentagonal $\{Mo(Mo)_5\}$ units and 30 linking$\{Mo^V{}_2\}$ units, where this type of $\{Mo_2\}$ unit can be formulated as $\{Mo^V{}_2O_4(OOR)^+\}$ ($R = CCH_3$, CH, PO_2). In geometrical terms this type of cluster can be described as $(Pentagon)_{12}(Linker)_{30}$; $Pentagon = \{Mo(Mo)_5\}$ and $Linker = \{Mo^V{}_2O_4(OOR)^+\}$, $\{OMo(H_2O)\}^{3+}$, $\{Fe(H_2O)_2\}^{3+}$. Unlike the $\{Mo_{154}\}$ cluster system, this cluster is synthesized at pH 4 (aqueous conditions) in an ammonia/acetate buffer using ammonium heptamolybdate with $N_2H_4{\cdot}H_2SO_4$ as a reducing agent. Sufficient reducing agent is used to reduce 45% of the total number of Mo centers from Mo^{VI} to Mo^V. Under these conditions crystals of the $\{Mo_{132}\}$ cluster result in four days.

It is interesting that the $\{Mo^V{}_2\}$ building unit can only be formed in the presence of stabilizing bidentate ligands and it is these units that are able to direct the formation of the $\{(Mo)(Mo_5)\}$ pentagon, which does not exist as an independent unit. Furthermore the $\{(Mo)(Mo_5)\}$ pentagon found in the Keplerate can be considered to be almost identical to the $\{(Mo)(Mo_5)\}$ pentagons found in the $\{Mo_8\}$ units, of which the $\{Mo_{57}\}$ and Giant-Wheel clusters are comprised, Figure 62. In addition to the building units already mentioned it is possible to describe both the wheel and ball clusters in terms of $\{Mo_{11}\}$ units.[58,59]

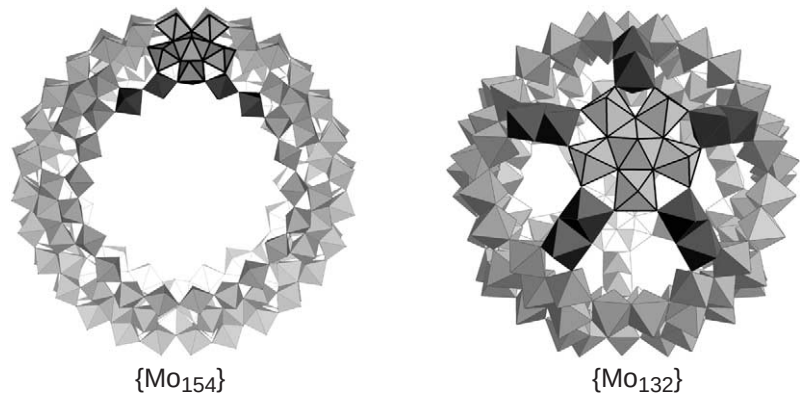

Figure 62 Comparison of the polyhedral representations of the $\{Mo_{132}\}$ Keplerate with the $\{Mo_{154}\}$ cluster (not to scale) with the pentagonal $\{Mo(Mo)_5\}$ (in thick lines) and the adjacent $\{Mo_2\}$ (dark gray) units emphasized in each. It is important to know, in the context of synthesis, that the $\{Mo_2\}$ units have a different structure in each class of cluster, but it is only these units, which have been observed to be exchangeable for other metal ions.

7.1.4.7.2 Construction of spherical species with icosahedral symmetry

To synthesize giant molecular species the most obvious starting point appears to be in finding a reaction system in which pentagonal units[60] with C_5 symmetry can first be generated, then become linked and be placed at the 12 corners of an icosahedron. In the case of polyoxomolybdates these pentagonal units ({(Mo)Mo_5} groups) can consist of a central pentagonal bipyramidal MoO_7 unit-sharing edges with five MoO_6 octahedra. As stated earlier, the {(Mo)Mo_5} unit is itself a constituent of the {Mo_8}-type unit abundant in many giant polyoxometalates (see Figure 62) in which two additional MoO_6 octahedra are bound (sharing corners) to the {(Mo)Mo_5} unit. In the presence of linkers, units which are capable of bridging two (or more) building blocks, for instance those of the classical $[Mo^{V}{}_2O_4]^{2+}$ type[3] (typically formed in reduced molybdate solutions in the presence of bidentate ligands), the icosahedral molecular system with 12 such pentagons and 30 such linkers is formed. When, for example, acetate anions act as bridging ligands for the $Mo^{V}{}_2O_4{}^{2+}$ groups, the spherical cluster with the stoichiometry $[Mo^{VI}{}_{72}Mo^{V}{}_{60}O_{372}(CH_3COO)_{30}(H_2O)_{72}]^{42-}$ ({Mo_{132}}) results. The central Mo positions of the 12 {(Mo)Mo_5} pentagons define the 12 corners, and the 30 $Mo^{V}{}_2O_4{}^{2+}$ groups the 30 edges of an icosahedron, in agreement with Euler's well-known formula. This corresponds to the formulation $[\{(Mo)Mo_5O_{21}(H_2O)_6\}_{12}\{Mo^{V}{}_2O_4(CH_3COO)\}_{30}]^{42-}$. Figure 63 describes the assembly, only in a geometrical sense, and this is vitally important if one is to both understand and design further spherical species.

7.1.4.7.3 Changing the bridging ligands in the Keplerate clusters

On substituting the bridging acetate ligands with formate groups this smaller ligand allows a special type of organization of the H_2O molecules encapsulated inside the cluster: a hydrogen-bonded water cluster as guest system with an "onion-type" structure which is induced by the peripheral spherical cluster shell, see Figure 64, in the synthesis of $\{(H_2O)_n \subset Mo_{132}\}$ (**70**)

This type of inclusion compound is of particular interest in the study of the influence of the outer spherical shell (including the different types of coordinated ligands) on the organization of encapsulated, weakly bonded, guest molecules, in this case water molecules.[175,176] In addition to derivatives (**69**) {$Mo_{132}(OAc)_{30}$} and (**70**)[177] {Mo_{132}(formate)$_{30}$} it is, in principle, possible to change the bidentate ligand that stabilizes the {$Mo_2{}^{V}$} group for other ligands as long as they will fit in the cavity created by the formation of the Keplerate. In addition it is possible to exchange the acetate ligands present in (**69**) with ligands like phosphate, hypophosphite, and partially for sulfate.[178]

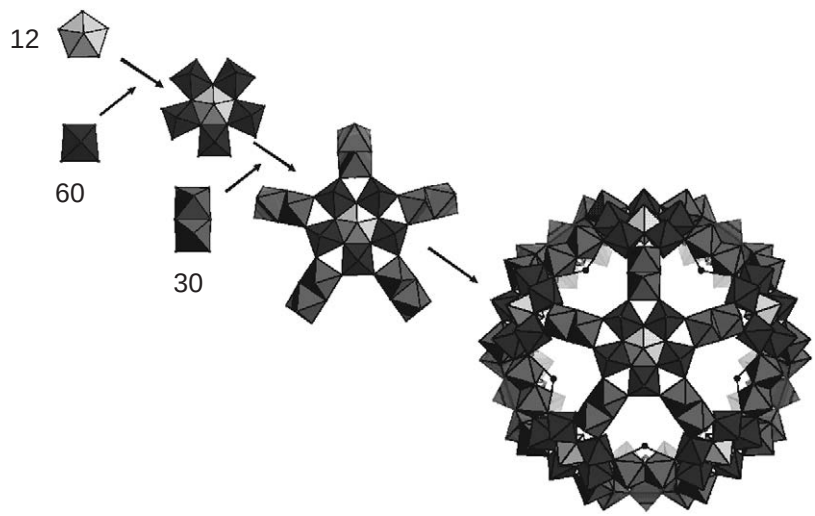

Figure 63 A basic geometrical description of the construction of the spherical Keplerate. Going down the diagonal from the upper left to the bottom right: the pentagonal {Mo} unit is shown by the white polyhedra and the remaining five Mo groups are colored dark gray. The formation of one of 12 {(Mo)Mo_5} building blocks is shown and then in the next step five {$Mo_2{}^{V}$} linkers are added (lighter gray polyhedra). In total 12 {(Mo)Mo_5} units and 30 {Mo_2} units combine to form the overall {Mo_{132}} cluster. NOTE this is not a mechanism for cluster formation, but a geometrical description.

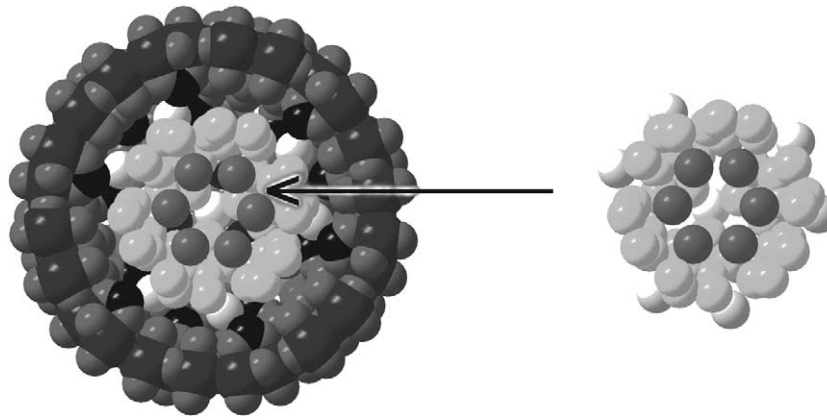

Figure 64 Space filling representation of the cross-section of the cluster showing the central cavity with the organized water molecules inside. There are three shells of water molecules visible and these are depicted on the RHS. The framework of the cluster is depicted by the dark gray close-packed spheres on the LHS and the carbon atoms of the formate anions are shown by the black close-packed spheres.

7.1.4.7.4 Structural derivatives: removing the lid of the Keplerate

In the same way as it is possible to form derivatives of the $\{Mo_{154}\}$ wheel cluster with defects, it is possible to remove the "lid" from the $\{Mo_{132}\}$ Keplerate cluster in the formation of a molecular basket, see Figure 65.[178]

This molecular basket has the composition $[Mo_{116}O_{331}(OAc)_{30}(H_2O)_{56}]^{46-}$, (**71**) and, by using the building block principle described earlier, the $\{Mo_{132}\}$ cluster loses one $\{Mo(Mo)_5\}$ unit and five $\{Mo_2\}$ units to yield the basket anion, see Figure 66. The $\{Mo_{116}\}$ species comprises 66 Mo^{VI} centers and 50 Mo^{V} compared to 72 Mo^{VI} and 60 Mo^{V} species in the $\{Mo_{132}\}$. Therefore the reaction of $\{Mo_{132}\}$ to the $\{Mo_{116}\}$ cluster can be considered to be a partial oxidation. The reaction conditions for the synthesis of the $\{Mo_{116}\}$ cluster are similar to that of the Keplerate species (**69**), but a very high concentration of NaCl is introduced into the reaction mixture and the solution is left to stand in air over a period of weeks.[178]

The reaction of $\{Mo_{132}\}$ to the $\{Mo_{116}\}$ presents some intriguing possibilities to remove the lid, deposit a guest molecule and then reseal the lid by careful reduction of the species to make a kind of "molecular hostage," see Figure 66.

7.1.4.7.5 From $\{Mo_{132}\}$ to $\{Mo_{72}M_{30}\}$ spherical clusters (M = Fe, Mo)

In an interesting extension to the chemistry of the $\{Mo_{132}\}$ (**69**) Müller *et al.* have succeeded in exchanging the $\{Mo_2\}$ groups present in the Keplerate species with Fe^{III} and Mo^{V} atoms in the formation of the neutral $\{Mo_{72}Fe_{30}\}$ cluster (**72**)[179] $[Mo_{72}Fe_{30}O_{252}(CH_3COO)_{10}\{Mo_2O_7(H_2O)\}$

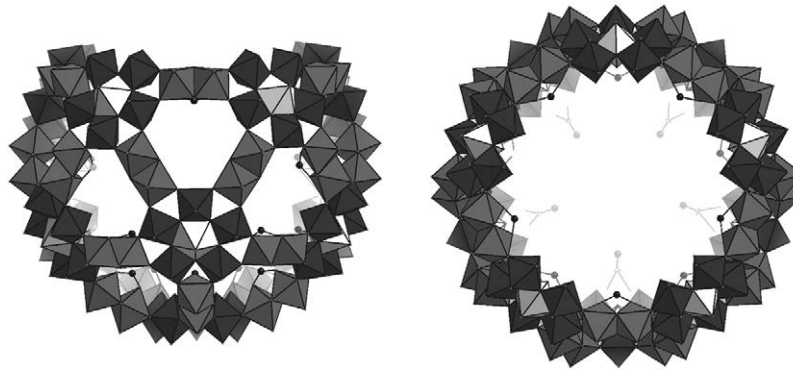

Figure 65 Polyhedral representations of the basket-derived Keplerate $\{Mo_{116}\}$ (**71**). A side view is shown on the LHS and the top view is shown on the RHS. The pentagonal centers of the $\{Mo(Mo)_5\}$ units are shown as white polyhedra whereas the appended Mo atoms are shown as very dark gray polyhedra. The $\{Mo_2\}$ groups are shown by the lighter gray polyhedra.

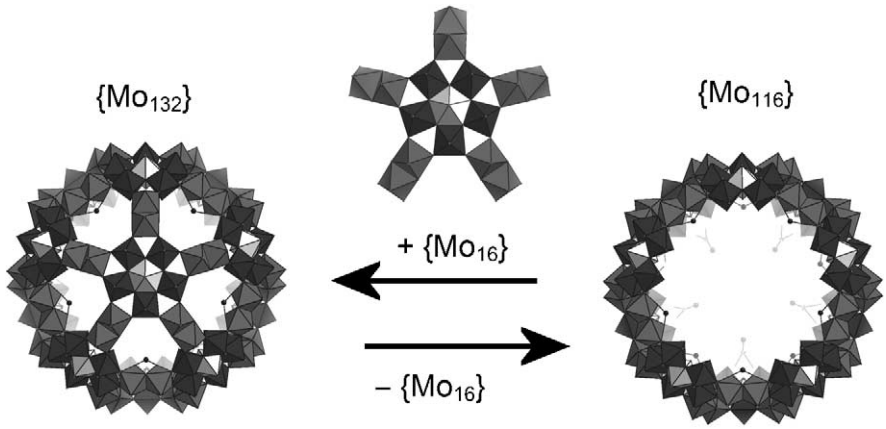

Figure 66 A schematic representation of the loss of the lid to form the basket species. The $\{Mo_{132}\}$ Keplerate cluster is shown on the LHS and the $\{Mo_{116}\}$ is shown on the RHS. The pentagonal centers of the $\{Mo(Mo)_5\}$ units are shown as white polyhedra whereas the appended Mo atoms are shown as very dark gray polyhedra. The $\{Mo_2\}$ groups are shown by the lighter gray polyhedra.

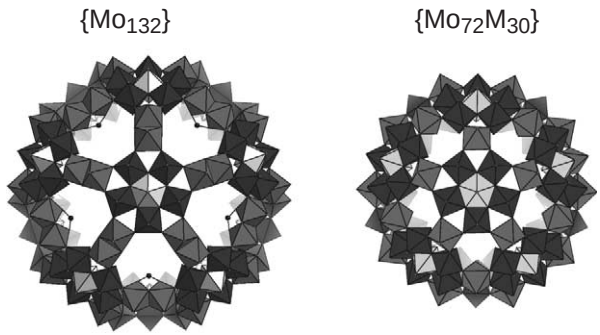

Figure 67 A representation of the structure of the $\{Mo_{72}M_{30}\}$cluster on the RHS and a comparison with the $\{Mo_{132}\}$ Keplerate cluster on the LHS. The pentagonal centers of the $\{Mo(Mo)_5\}$ units are shown as white polyhedra whereas the appended Mo atoms are shown as very dark gray polyhedra. The lighter gray polyhedra in the $\{Mo_{132}\}$ refer to the $\{Mo_2\}$ units whereas the lighter gray polyhedra in the $\{Mo_{72}M_{30}\}$ refer to the $\{M\}$ units.

$\{H_2Mo_2O_8(H_2O)\}_3(H_2O)_{91}]$ and a neutral $\{Mo_{102}\}$ cluster (**73**)[179] $[Mo_{102}O_{282}(H_2O)_{78}(CH_3CO_2)_{12}]$, respectively, see Figure 67. These spheres are smaller than the parent $\{Mo_{132}\}$ with outer diameters of ca. 24 Å and inner diameters of ca. 18 Å. The $\{Mo_{72}Fe_{30}\}$ cluster is comprised of only Mo^{VI} atoms whereas the $\{Mo_{72}Mo_{30}\}$ cluster contains 36 reduced Mo^{V} centers where the 30 linking units are reduced and the remaining six centers are delocalized of the 12 pentagonal centers present in the cluster. It is, however, not possible to produce (**72**) in a one pot reaction and assemble the cluster from its constituent components. One must instead react the Keplerate cluster (**69**) with iron salts followed by heating and adjusting the pH to ca. 2.5. Similarly, the synthesis of (**73**) is achieved by acidification of a solution of the Keplerate cluster (**69**) with HCl followed by the addition of a large amount of NaCl. Crystals of (**73**) form after the solution is left for three days.

In essence the reaction of the $\{Mo_{132}\}$ cluster to the $\{Mo_{72}Fe_{30}\}$ species probably proceeds via a stepwise substitution of the $\{Mo_2\}$ groups although no intermediates have been isolated. Remarkably, because it is possible to produce mono-anions of (**72**) and (**73**) it has even been possible to observe molecular ions of these species in the gas phase using MALDI mass spectrometry.[180] Such a result offers the interesting possibility that such a cluster can be "screened" with different guests included rather than resorting to full crystallographic analysis. Furthermore it may be possible to deposit such clusters from the gas phase to produce novel thin layer materials, perhaps with applications in molecular electronics, etc.[36]

7.1.4.7.6 Formation of molecular barrels $\{Mo_{75}V_{20}\}$

If vanadyl sulfate is added to an acidified molybdate solution, the compound $Na_{20}[\{Mo^{VI}O_3(H_2O)\}_{10}\{V^{IV}O(H_2O)\}_{20}\{Mo^{VI}/Mo^{VI}{}_5O_{21}\}(H_2O)_3\}_{10}(\{Mo^{VI}O_2(H_2O)_2\}_{5/2})_2(-\{NaSO_4\}_5)_2]\cdot xH_2O$

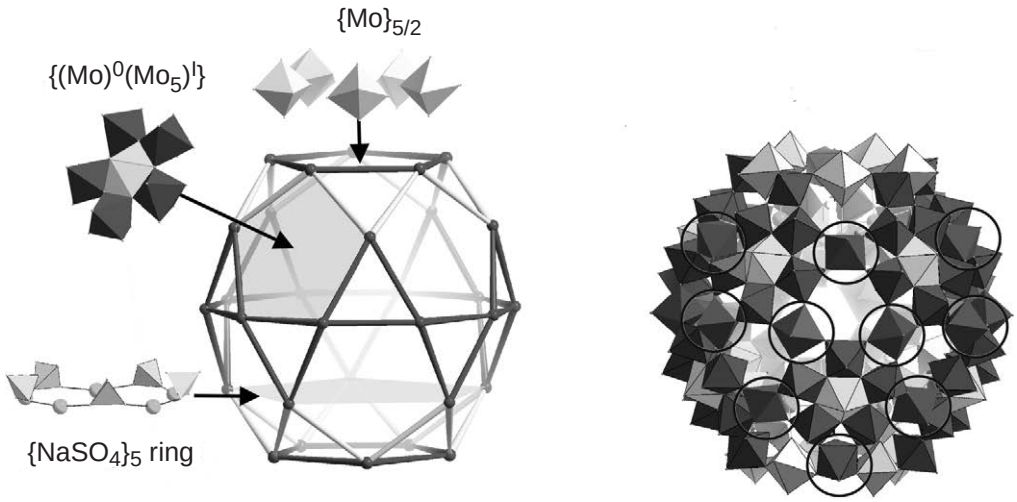

Figure 68 The basic framework of (**74**) shown as a distorted icosidodecahedron with 20 triangles and 12 pentagons and the $\{Na(SO_4)\}_5$ is also shown on the LHS. On the RHS a polyhedral representation of the overall cluster is shown. The vanadium centered polyhedra are shown by the black circles and the pentagonal centers of the $\{Mo(Mo)_5\}$ units are shown by the light gray polyhedra; the other polyhedra are the five appended Mo atoms of the $\{Mo(Mo)_5\}$ unit.

($x = 70$) (**74**) precipitates when the electrolyte concentration is high enough. This anionic cluster has a barrel shape, being ca. 23 Å high and ca. 25 Å in diameter and is best described with reference to a distorted icosidodecahedron formed by 20 triangular and 12 pentagonal faces built up by Mo^{VI} and 20 V^{IV} centers, see Figure 68. Ten triangles spanned by 20 V^{IV} centers form an unusual equatorial magnetic ring shaped band. The remaining 10 triangles above and below this equatorial band, each formed by one V^{IV} and two Mo^{VI} centers, complete the (distorted) icosidodecahedron. Ten of the 12 pentagonal faces, each formed by one Mo^{VI} and four V^{IV} centers, are capped by a $\{Mo(Mo)_5\}$ pentagonal unit.[182]

7.1.4.7.7 Formation of solid-state structures with $\{Mo_{72}Fe_{30}\}$

The solid-state chemistry based upon the spherically shaped Keplerate clusters is versatile. In crystals of the $\{Mo_{132}\}$-type species (space group $Fm\bar{3}$), the spheres are ordered according to the cubic closed packing scheme.[63] This packing, similar to hard spheres, is simply due to the spherical shape of the cluster's van der Waals surface. In contrast, in the case of a monoclinic crystal modification of the functionalized Keplerate system $\{Mo_{72}Fe_{30}\}$,[181] distinct solid-state reactions, i.e., the linking of these icosahedral spherical clusters to layers, can take place even at room temperature. During the dehydration process of crystals comprising $\{Mo_{72}Fe_{30}\}$ units, crystal water molecules are expelled in a first, slow step and the cluster shells approach each other until a minimum distance between the Fe—$OH_2\cdots H_2O$—Fe groups (on adjacent clusters) is reached (Figure 69). This first step is followed by a second, faster one in which a condensation reaction takes place at four Fe sites on each cluster unit to produce a linked cluster, (**75**). This reaction mechanism is known for the formation of inorganic polycations at low activation energies.

This reaction finally results in a two-dimensional grid structure found in the compound $[H_4Mo_{72}Fe_{30}O_{254}(CH_3COO)_{10}\{Mo_2O_7(H_2O)\}\{H_2Mo_2O_8(H_2O)\}_3(H_2O)_{87}] \cdot$ ca. 80 H_2O. The four Fe—O—Fe links (Fe—Fe = 3.79 Å) interconnect each cluster unit with four neighboring shells.[42] This also leads to a decrease of the effective magnetic moment from nearly 30 uncoupled Fe(III) centers to approximately 26 uncoupled Fe(III) centers as the iron centers of the nearly linear Fe—O—Fe groups are strongly coupled. This situation is typical for structurally similar (linear) (μ-O)Fe_2 complexes.[183]

It is possible to isolate the intermediate compound containing the spherical clusters as discrete entities: $[Mo_{72}Fe_{30}O_{252}(CH_3COO)_{10}\{Mo_2O_7(H_2O)\}\{H_2Mo_2O_8(H_2O)\}_3(H_2O)_{91}] \cdot$ ca. 100 H_2O (Fe—Fe = 5.35 Å), which crystallizes in the same space group ($P2_1/n$) as the freshly prepared precipitated compound, before the dehydration (drying) process. In this compound the short

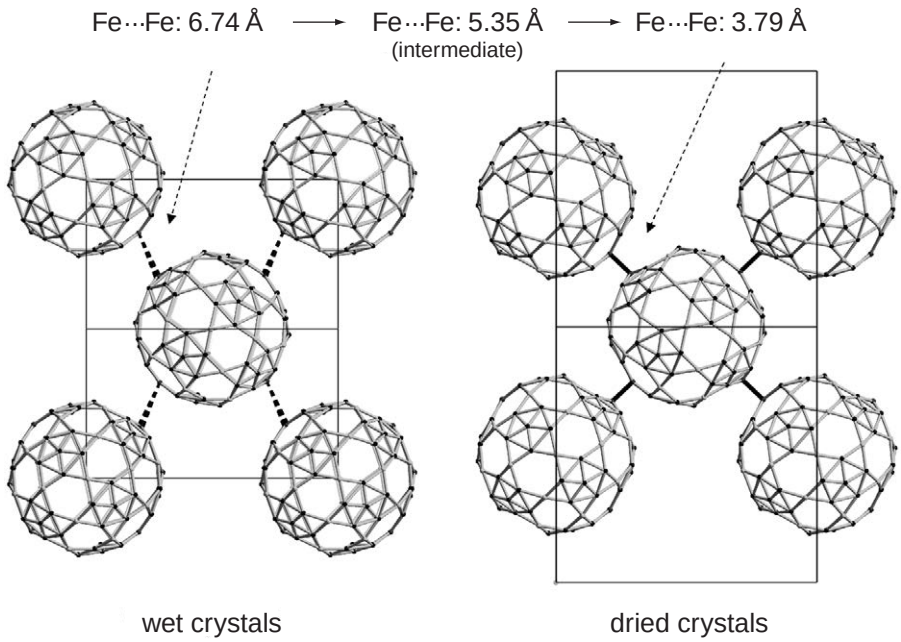

Figure 69 Representation of the metal skeletons of the cluster units in the $\{Mo_{72}Fe_{30}\}$ layer compound with emphasized links (right side). The condensation reaction proceeds from discrete cluster units (as present in freshly prepared crystals of $\{Mo_{72}Fe_{30}\}$; left side) via an intermediate, in which discrete units are approached to each other reaching a minimum distance. This geometry is stabilized by hydrogen bonds between the Fe—OH_2···H_2O—Fe groups, which finally react to the Fe–O–Fe linkers.

Fe···Fe distances are stabilized by hydrogen bonds (Fe—OH_2···OH_2—Fe of 2.77 Å), see Figure 69.

In addition, the tiling of icosahedral units in a two-dimensional grid in principle collides with classical crystallography, which excludes the presence of C_5 axes. In the layer compound that crystallizes in the space group *Cmca*, the symmetry is broken by the linking of the icosahedral units via oxygen atoms, thus enabling the arrangement in a two-dimensional grid.

7.1.4.7.8 Molecular hostages and networks of molecular hostages

In a dramatic extension to the chemistry of the iron-substituted Keplerates, it has been possible to assemble a Keggin ion inside the $\{Mo_{72}Fe_{30}\}$ cluster in the formation of the hostage complex $\{PMo_{12}\} \subset \{Mo_{132}\}$ (**76**) with the formula, $[PMo_{12}O_{40} \subset \{(Mo^{VI})Mo^{VI}{}_5\}_{12}Fe^{III}O_{252}(H_2O)_{102}(CH_3COO)_{15}] \cdot$ ca. 120 H_2O, see Figure 70.[184,185] This possibility was first realized by a modeling investigation resulting in the initial synthetic approach, which involved mixing the Keggin ion and $\{Mo_{72}Fe_{30}\}$ together in aqueous solution. Initial crystallographic studies were ambiguous but an electron density synthesis helped indicate the presence of a low percentage of the Keggin ion encapsulated inside the $\{Mo_{72}Fe_{30}\}$ sphere.[186]

In further studies it was realized that the synthesis of the cluster could be observed if a solution of the Keggin ion, Fe^{III} salts, molybdate, and acetate was taken to a pH of around 2 and left for five days, after which time (**76**) precipitates. Furthermore, if just a solution of NaH_2PO_4 was added to the above solution (without the Keggin ion) the same cluster (**76**) will precipitate after seven days. This evidence clearly points to the Keggin ion as having a vital templating role in the formation of $\{PMo_{12}\} \subset_{132}$ (**76**) and it has not yet been possible to generate an empty $\{Mo_{72}Fe_{30}\}$ cluster from the constituent ingredients of molybdate, Fe^{III} salts and acid, see Figure 71. Finally, it also appears that reaction of the $\{PMo_{12}\}$ Keggin ion with Fe^{III} also results in the hostage complex (**76**).[184]

Similar to the observation that $\{Mo_{72}Fe_{30}\}$ clusters form a two-dimensional network on dehydration, the hostage complex also undergoes a dehydration resulting in a remarkable two-dimensional network of spheres encasing weakly bonded Keggin ions, (**77**), see Figure 72.[185]

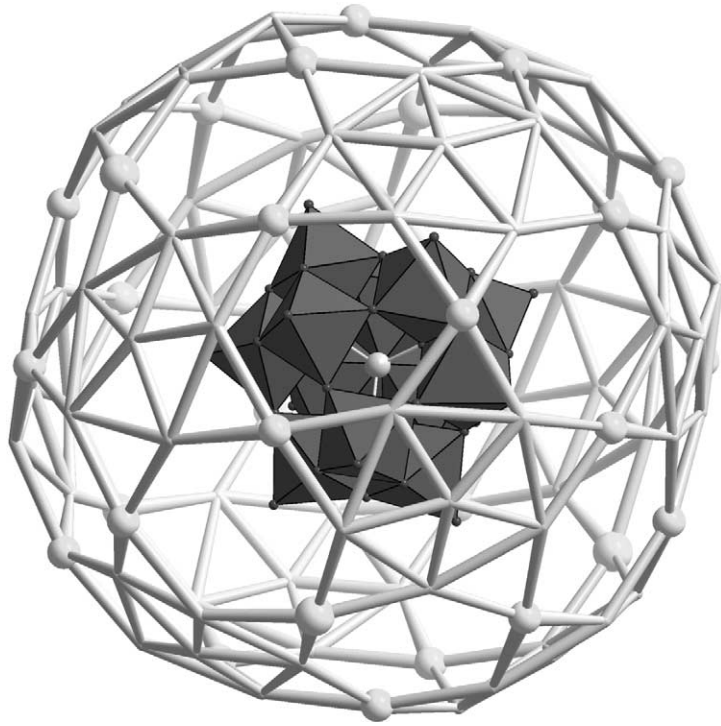

Figure 70 A representation of the crystal structure of $\{PMo_{12}\}\subset_{132}$(**76**). A wireframe representation of the $\{Mo_{72}Fe_{30}\}$ cluster shell is shown with a polyhedral representation of the encapsulated Keggin ion.

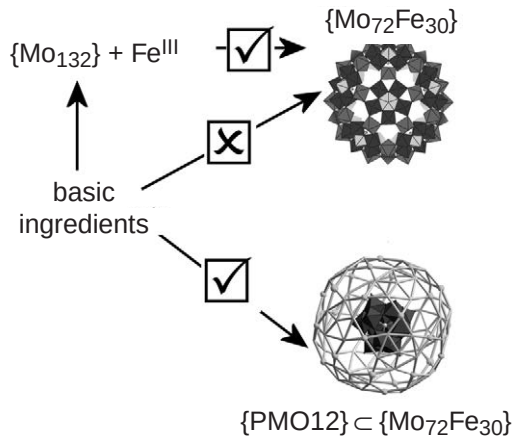

Figure 71 A schematic showing the reaction processes leading to the $\{PMo_{12}\}\subset_{132}$ and $\{Mo_{72}Fe_{30}\}$. The molecular hostage complex can be synthesized directly from the most basic units but the empty $\{Mo_{72}Fe_{30}\}$ cluster must be synthesized from the $\{Mo_{132}\}$ cluster. These observations strongly suggest a role for the Keggin ion as a template to assemble the outer sphere.

7.1.4.8 $\{Mo_{368}\}$ Clusters: a Hybrid Between Wheel- and Ball-shaped clusters

In a very recent result, Müller *et al.*[1] have reported the largest molecular cluster to be characterized by single crystal X-ray diffraction to date. In this case the molybdenum oxide based nanocluster is the size of hemoglobin, with an approximate diameter of 6 nm, and contains 368 metal (1,880 nonhydrogen) atoms formed by the linking of 64 $\{Mo_1\}$-, 32 $\{Mo_2\}$-, and 40 $\{Mo(Mo_5)\}$-type units with the formula $[H_xMo_{368}O_{1032}(H_2O)_{240}(SO_4)_{48}]^{48-}$ (**78**). Once again, the role of the pentagonal $\{Mo(Mo_5)\}$ units in creating a curved surface cannot be overstated. The overall structure of the cluster is unprecedented, insofar as it incorporates two oppositely curved surfaces, i.e., a positive surface that goes through an inflexion point to a negative surface. The result is a cluster that resembles the shape of a lemon, see Figure 73.

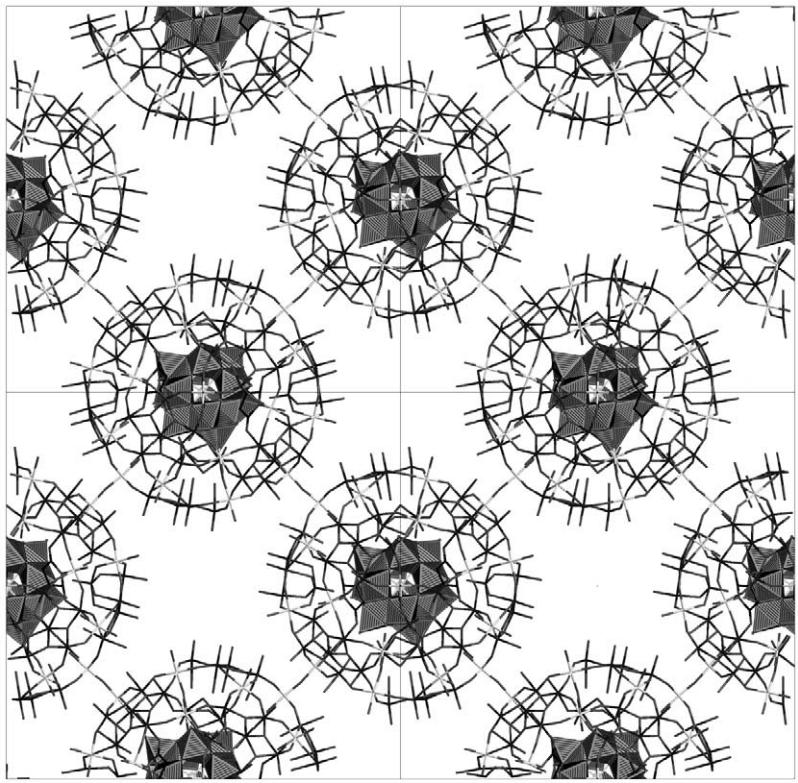

Figure 72 Schematic structural representation of a layer of the two-dimensional network of (**77**) with the outer case, $\{Mo_{72}Fe_{30}\}$ shown as a wire frame and the encapsulated Keggin ion shown as a polyhedral representation.

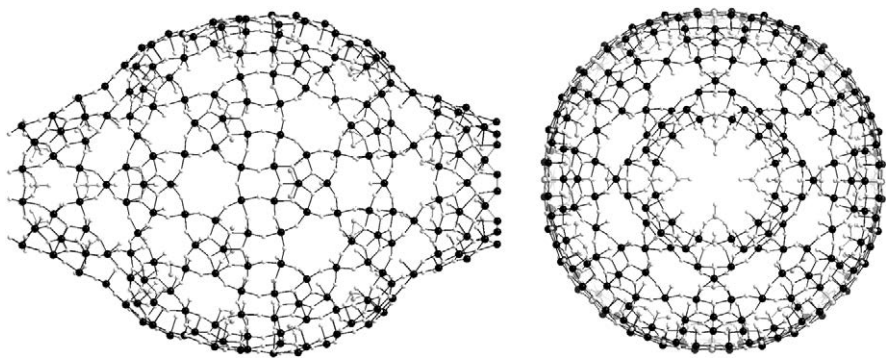

Figure 73 A ball and stick representation of the structure of the $\{Mo_{368}\}$ cluster; the molybdenum atoms are shown as black spheres, the oxygen atoms as white spheres and the sulfur atoms of the sulfate groups (inside the sphere) are shown as gray spheres. A side view is shown on the LHS, which shows the longest dimension of the cluster, being ca. 54 Å and a height of ca. 37 Å. A top view is shown on the RHS, which shows the opening at the top of the cluster of ca. 14 Å.

In terms of building blocks the $\{Mo_{368}\}$ can be described as $[H_x\{Mo(Mo_5)\}'_8\{Mo(Mo_5)\}''_{32}\{Mo_2\}'_{16}\{Mo_2\}''_8\{Mo_2\}'''_8\{Mo_1\}_{64}]^{48-}$ and has an approximate D_4 symmetry with a central ball-shaped fragment, $\{Mo_{288}O_{784}(H_2O)_{192}(SO_4)_{32}\}$, and two capping units, $\{Mo_{40}O_{124}(H_2O)_{24}(SO_4)_8\}$, see Figure 74. Interestingly, there are three rather large areas, with different local symmetries: D_{8d} in the central part and C_{4v} in the two capping areas (Figure 74). The presence of the bidentate SO_4^{2-} appears to allow the construction of this cluster, the coordination type of the SO_4^{2-} ligands: 40 with SO_4^{2-} ligands and eight without located in the C_{4v} areas. The dinuclear units $\{Mo_2\}$ not only differ with respect to the number of bidentate SO_4^{2-} ligands but also, for those at the ends of both caps, that is, the borderlines, both Mo centers have two terminal O

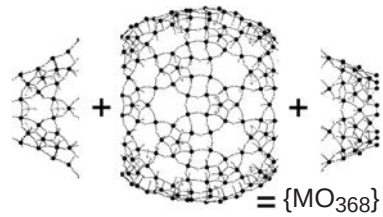

Figure 74 Ball and stick representation of the $\{Mo_{368}\}$ split into the three distinct units, the central cylinder and the two caps, all of which have different local symmetries.

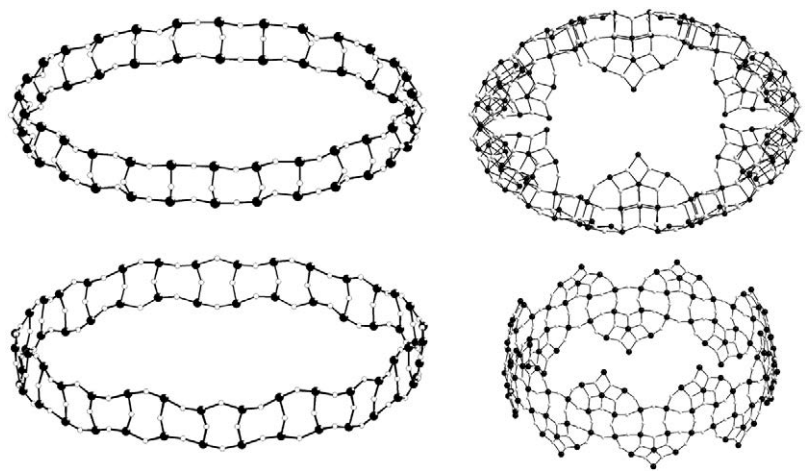

Figure 75 Comparison of the equator frameworks of the $\{Mo_{154}\}$ wheel (top section) and $\{Mo_{368}\}$-type clusters (bottom section). The equator associated with the $\{Mo_{368}\}$ appears to be more corrugated than that of the wheel but the pentagonal units associated with the equator rim (bottom RHS) rise more closely to the vertical, perpendicular to the plane dissecting the equator than those of the wheel (top RHS).

atoms in a situation characteristic for stopping growth. The $\{Mo_1\}$ units are of the classical type $\{OMo^{V}(H_2O)\}^{3+}$ and contribute correspondingly to the highly reduced state of (**78**). The other formally Mo^{V}-type centers are distributed over several parts of the cluster areas, which causes a widespread delocalization of the Mo 4d electrons.

The structure of (**78**) can be considered as a hybrid between the Giant-Wheel ($\{Mo_{154}\}$-type/$\{Mo_{176}\}$-type) and ball ($\{Mo_{102}\}$-type) clusters.[187] Examination of these two clusters and comparison with the $\{Mo_{368}\}$ cluster is revealing; the $\{Mo(Mo_5)\}$ and $\{Mo_1\}$ units of the $\{Mo_{102}\}$ ball-type cluster as well as $\{Mo(Mo_5)\}$ and $\{Mo_2\}$ units of the wheel-type species are all present in (**78**). In addition, this cluster has a definable equator, the framework of which can be compared to that of the wheel-shaped cluster, see Figure 75.

The high reduction state (ca. 112 Mo^{V}, 256 Mo^{VI}), which is much higher than that in the wheel systems (e.g., 28 Mo^{V}, 126 Mo^{VI}) seems to confirm the importance of Mo^{V} centers in the construction of clusters displaying extraordinary structural versatility. The $\{Mo_{368}\}$ cluster is synthesized by reducing a solution of molybdate with $Na_2S_2O_4$ acidified with H_2SO_4. It is important to note that this cluster appears to be constructed at higher reducing values, ca. 30%, i.e., 30% of the total number of the Mo centers in $\{Mo_{368}\}$ cluster are Mo^{V} compared with 18–20% in the $\{Mo_{154}/Mo_{176}\}$ clusters, 45% in the Keplerate $\{Mo_{132}\}$, and 35% in the $\{Mo_{102}\}$ ball.

7.1.4.9 Building Block Principles

In this section, high nuclearity clusters with sizes ranging from that of a normal molecule to a size approaching that of a small protein are described. A common theme that links all these systems is that almost all of these molecules can be synthesized under one-pot reaction conditions. Even more strikingly, these conditions need only to be adjusted in one or two respects to encourage

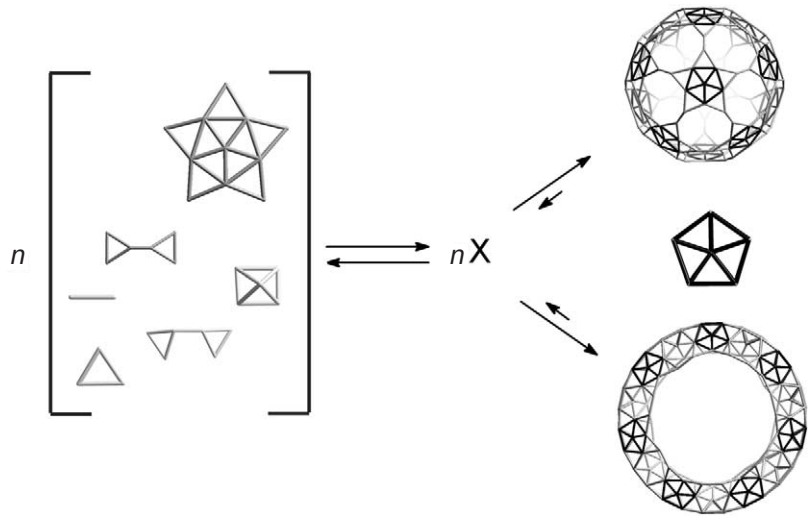

Figure 76 A schematic showing the potential for many types of polyoxometalate building blocks in solution with the pentagon-based units forming closed units (and therefore more difficult to decompose, all things being equal, than a cluster system that had well defined edges and corners). On the LHS the vast number of hypothesized different building units present in solution, along with the pentagonal units are shown. Then our hypothesized equilibrium between these units and various clusters in solution is shown. Finally on the RHS the clusters with pentagonal building blocks with closed geometries are depicted with an equilibrium which is in favor of the close-spherical/ring-shaped cluster system.

growth of, for example, a $\{Mo_{368}\}$ cluster rather than a $\{Mo_{36}\}$ cluster (in this case the addition of reducing agent and a ligand). In the case of polyoxomolybdates chemistry, the use of pentagonal-type building groups, with different symmetries, plays a key role in the synthesis of these systems. This can be taken further by considering that edge-sharing (condensed) pentagons cannot be used to tile an infinite plane,[188] whereas exactly 12 pentagons are required, in connection with well-defined sets of hexagons, to construct spherical systems such as that observed in the truncated icosahedron—the most spherical Archimedean solid—in polyhedral viruses, or in the geodesic Buckminster–Fuller domes.[189] Therefore the use of pentagonal building blocks is absolutely essential in chemistry for the production of curved species—the paradigm of which is C_{60}.

However, the question of exactly why these cluster systems were discovered at all still remains. This can be highlighted by considering the simplicity of the constituent building blocks and, therefore, the literally hundreds, maybe thousands, of condensed metal oxygen fragments with varying charges and symmetries that could exist in a solution of partly reduced molybdate at certain pH values. To answer this question we must consider a solution with many hundreds of different types of linkable units present with smaller building block species in equilibrium with large species (it should be noted that in poloxomolybdate chemistry this equilibrium is attained in a matter of minutes or hours).

Perhaps the answer can be found in the fact that the pentagonal unit facilitates the formation of a curved geometrical system with no edges. However, when one considers the formation of rigid pentagonal units in solution and the reaction through to the product, one can see that a closed cluster with no edges is uniformly reactive and, therefore, harder to decompose (if it is rigid) than a cluster with many edges and no rigidity. In summary, the combination of rigid units with pentagonal symmetry may result in many hundreds of species, but it is likely that only the structurally uniform, most stable species are likely crystallize. In this way the equilibrium can be pushed towards the precipitation of closed geometrical systems with no edges, i.e., clusters with ring or spherical topology. This hypothesis is summarized in Figure 76.

7.1.5 OUTLOOK

In recent years there has been an unprecedented increase in the number of interesting polyoxometalate clusters that have been structurally characterized by single crystal X-ray crystallography and, of course, the absolute size of the molecules characterized. Indeed, the elucidation of the

structure of the $\{Mo_{368}\}$ represents the largest nonbiologically derived macromolecule to be structurally characterized to date and there is no reason to suppose that the discoveries in this area will stop at this nuclearity.[1]

Polyoxometalates, with all their relevance to catalysis, reactivity, electronic structure, materials science, and medicine are set to become a paradigm for those working in nanoscience. This is because the polyoxometalate clusters described here are ideal candidates for the development of a new type of supramolecular chemistry based upon the building-block ideas already established. Using these ideas it should be possible to work towards designer nanomolecules of ever increasing size and complexity.[190–192] Such clusters, for instance, are being proposed for the design of molecular magnets[17] that could behave as super-paramagnets and electron storage devices that could be used in molecular electronics. Maybe such systems could be used to probe and even discover new physics at the quantum classical limit or examine molecular growth processes.[168] In addition, researchers could begin to answer the fundamental questions about the self-assembly processes that underpin the creation of such structures and ask what influence could our concept of building geometrical and real building blocks have in the design of these molecules.[60] If we are able to devise some rules for cluster design then it may be possible to design new types of molecular hostage complexes that could be used in information storage or even in light-harvesting systems, as well as potential applications as robust sequestering agents. For example, there is the potential to design polyoxometalate clusters that can selectively assemble into a given structural type in the presence of the ion to be sequestered, e.g., actinide ions to give a system for sequestering radioactive elements. The design/discovery of polyoxometalate nanotubes and junctions would also be an important aspect and provide an interesting alternative to the carbon-based analogues.[193] Whatever the future, one thing is sure—that researchers will be captivated and motivated by the beauty and complexity of polyoxometalate structures that will be discovered during the coming years.

ACKNOWLEDGMENTS

I would like to thank Professor A. Müller for introducing me to polyoxometalate chemistry and Dr. D. Long for proof-reading and helpful comments.

7.1.6 REFERENCES

1. Müller, A.; Beckmann, E.; Bögge, H.; Schmidtmann, M.; Dress, A. *Angew. Chem.,Int. Ed.* **2002**, *41*, 1162–1167.
2. Al-Zahrani, S. M.; Jibril, B. Y.; Abasaeed, A. E. *J. Mol. Catal. A,Chem.* **2001**, *175*, 259–265.
3. Comuzzi, C.; Dolcetti, G.; Trovarelli, A.; Cavani, F.; Trifiro, F.; Llorca, J.; Finke, R. G. *Catal. Lett.* **1996**, *36*, 75–79.
4. Hu, C. W.; He, Q. L.; Zhang, Y. H.; Liu, Y. Y.; Zhang, Y. F.; Tang, T. D.; Zhang, J. Y.; Wang, E. B. *Chem. Commun.* **1996**, 121–122.
5. Indovina, V.; Occhiuzzi, M.; Ciambelli, P.; Sannino, D.; Ghiotti, G.; Prinetto, F. *11th Int. Cong. Catal.—40th Ann., Parts A and B* **1996**, *101*, 691–700.
6. MoroOka, Y.; Ueda, W. *Adv. Catal.* **1994**, *40*, 233–273.
7. Pozniczek, J.; Bielanski, A.; Kulszewiczbajer, I.; Zagorska, M.; Kruczala, K.; Dyrek, K.; Pron, A. *J. Mol. Catal.* **1991**, *69*, 223–233.
8. Sadakane, M.; Steckhan, E. *J. Mol. Catal. A,Chem.* **1996**, *114*, 221–228.
9. Weiner, H.; Finke, R. G. *J. Am. Chem. Soc.* **1999**, *121*, 9831–9842.
10. Yang, X. Y.; Xia, X. Q.; Wu, N. Z. *Chin. J. Catal.* **2001**, *22*, 358–360.
11. Yang, Y. L.; Guo, Y. H.; Wang, Y. H.; Hu, C. W.; Wang, E. B.; Feng, S. H. *Prog. Nat.Sci.* **2002**, *12*, 153–157.
12. Zhang, X.; Sasaki, K.; Hill, C. L. *J. Am. Chem. Soc.* **1996**, *118*, 4809–4816.
13. Zhang, X. Y.; Pope, M. T. *J. Mol. Catal. A, Chem.* **1996**, *114*, 201–208.
14. Xiang, D. F.; Tan, X. S.; Zhang, S. W.; Han, Y.; Yu, K. B.; Tang, W. X. *Polyhedron* **1998**, *17*, 2095–2100.
15. Aebersold, M.; Andres, H. P.; Buttner, H.; BorrasAlmenar, J. J.; Clemente, J. M.; Coronado, E.; Gudel, H. U.; Kearley, D. *Physica B* **1997**, *234*, 764–765.
16. Chiorescu, I.; Wernsdorfer, W.; Müller, A.; Bögge, H.; Barbara, B. *J. Magn. Magn. Mater.* **2000**, *221*, 103–109.
17. Clemente-Juan, J. M.; Coronado, E. *Coord. Chem. Rev.* **1999**, *195*, 361–394.
18. Dhaussy, A. C.; Abraham, F.; Mentre, O.; Steinfink, H. *J. Solid State Chem.* **1996**, *126*, 328–335.
19. Gatteschi, D.; Pardi, L. *Mol. Cryst. Liq. Cryst.* **1993**, *232*, 577–590.
20. Müller, A.; Beugholt, C.; Kögerler, P.; Bögge, H.; Bud'ko, S.; Luban, M. *Inorg. Chem.* **2000**, *39*, 5176–5177.
21. Müller, A.; Kögerler, P.; Dress, A. W. M. *Coord. Chem. Rev.* **2001**, *222*, 193–218.
22. Müller, A.; Luban, M.; Schroder, C.; Modler, R.; Kögerler, P.; Axenovich, M.; Schnack, J.; Canfield, P.; Bud'ko, S.; Harrison, N. *Chem. Phys. Chem* **2001**, *2*, 517–520.
23. Wei, Y. G.; Zhang, S. W.; Shao, M. C.; Tang, Y. Q. *Polyhedron* **1997**, *16*, 1471–1475.
24. Volkmer, D.; Du Chesne, A.; Kurth, D. G.; Schnablegger, H.; Lehmann, P.; Koop, M. J.; Müller, A. *J. Am. Chem. Soc.* **2000**, *122*, 1995–1998.

25. Apblett, A. W.; Reinhardt, L. E. *Abstr. Pap. Am. Chem. Soc.* **1996**, *212*, 259.
26. Coronado, E.; GalanMascaros, J. R.; GimenezSaiz, C.; GomezGarcia, C. J.; Laukhin, V. N. *Adv. Mater.* **1996**, *8*, 801–811.
27. Evans, J.; Pillinger, M.; Zhang, J. J. *J. Chem. Soc.,Dalton Trans.* **1996**, 2963–2974.
28. Nazar, L. F.; Koene, B. E.; Britten, J. F. *Chem. Mater.* **1996**, *8*, 327–329.
29. Coronado, E.; Gomez-Garcia, C. J. *Chem. Rev.* **1998**, *98*, 273–296.
30. Livage, J.; Bouhedja, L.; Bonhomme, C. *J. Sol-Gel Sci. Technol.* **1998**, *13*, 65–70.
31. Vaidhyanathan, B.; Balaji, K.; Rao, K. J. *Chem. Mater.* **1998**, *10*, 3400–3404.
32. Barton, T. J.; Bull, L. M.; Klemperer, W. G.; Loy, D. A.; McEnaney, B.; Misono, M.; Monson, P. A.; Pez, G.; Scherer, G. W.; Vartuli, J. C.; Yaghi, O. M. *Chem. Mater.* **1999**, *11*, 2633–2656.
33. Duraisamy, T.; Ojha, N.; Ramanan, A.; Vittal, J. J. *Chem. Mater.* **1999**, *11*, 2339–2349.
34. LaDuca, R. L.; Finn, R.; Zubieta, J. *Chem. Commun.* **1999**, 1669–1670.
35. Cronin, L.; Kögerler, P.; Müller, A. *J. Solid State Chem.* **2000**, *152*, 57–67.
36. Kurth, D. G.; Lehmann, P.; Volkmer, D.; Müller, A.; Schwahn, D. *J. Chem. Soc., Dalton Trans.* **2000**, 3989–3998.
37. Kurth, D. G.; Volkmer, D.; Ruttorf, M.; Richter, B.; Müller, A. *Chem. Mater.* **2000**, *12*, 2829–2832.
38. LaDuca, R. L.; Desciak, M.; Laskoski, M.; Rarig, R. S.; Zubieta, J. *J. Chem. Soc., Dalton Trans.* **2000**, 2255–2257.
39. Law, T. S. C.; Sung, H. H. Y.; Williams, I. D. *Inorg. Chem. Commun.* **2000**, *3*, 420–423.
40. Mayer, C. R.; Thouvenot, R.; Lalot, T. *Chem. Mater.* **2000**, *12*, 257–263.
41. Muhr, H. J.; Krumeich, F.; Schonholzer, U. P.; Bieri, F.; Niederberger, M.; Gauckler, L. J.; Nesper, R. *Adv. Mater.* **2000**, *12*, 231–235.
42. Müller, A.; Das, S. K.; Krickemeyer, E.; Kögerler, P.; Booge, H.; Schmidtmann, M. *Solid State Sci.* **2000**, *2*, 847–854.
43. Zeng, H. D.; Newkome, G. R.; Hill, C. L. *Angew. Chem., Int. Ed.* **2000**, *39*, 1772–1775.
44. Ito, T.; Inumaru, K.; Misono, M. *Chem. Mater.* **2001**, *13*, 824–831.
45. Johnson, B. J. S.; Schroden, R. C.; Zhu, C. C.; Stein, A. *Inorg. Chem.* **2001**, *40*, 5972–5978.
46. Liu, T. B.; Wan, Q.; Xie, Y.; Burger, C.; Liu, L. Z.; Chu, B. *J. Am. Chem. Soc.* **2001**, *123*, 10966–10972.
47. Murakami, H.; Kozeki, T.; Suzuki, Y.; Ono, S.; Ohtake, H.; Sarukura, N.; Ishikawa, E.; Yamase, T. *Appl. Phys. Lett.* **2001**, *79*, 3564–3566.
48. Cheng, L.; Cox, J. A. *Chem. Mater.* **2002**, *14*, 6–10.
49. Devi, R. N.; Zubieta, J. *Inorg. Chim. Acta* **2002**, *332*, 72–78.
50. Liu, S. Q.; Kurth, D. G.; Mohwald, H.; Volkmer, D. *Adv. Mater.* **2002**, *14*, 225–230.
51. Wang, Y. H.; Wang, X. L.; Hu, C. W.; Shi, C. S. *J. Mater. Chem.* **2002**, *12*, 703–707.
52. Tourne, G. F.; Tourne, C. M. In *Polyoxometalates: from Platonic Solids to Anti-retoviral Activity*; Pope, M. T., Müller A., Eds.; Kluwer: Dordrecht, The Netherlands, 1994, 1–414.
53. Fukuma, M.; Seto, Y.; Yamase, T. *Antiviral Res.* **1991**, *16*, 327–339.
54. Judd, D. A.; Nettles, J. H.; Nevins, N.; Snyder, J. P.; Liotta, D. C.; Tang, J.; Ermolieff, J.; Schinazi, R. F.; Hill, C. L. *J. Am. Chem. Soc.* **2001**, *123*, 886–897.
55. Pope, M. T.; Müller, A. *Angew. Chem., Int. Ed. Engl.* **1991**, *30*, 34–48.
56. Pope, M. T. *Heteropoly and Isopoly Oxometalates*; Springer-Verlag: Berlin, 1983.
57. Pope, M. T. *Comprehensive Coordination Chemistry* : lsopolyanions and Heteropolyanions; Wilkinson, G., Gillard, R. D., McCleverty, J. A., Eds.; Pergamon Press, 1987; Vol. 3, 1023–1057.
58. Müller, A.; Kögerler, P.; Kuhlmann, C. *Chem. Commun.* **1999**, 1347–1358.
59. Müller, A.; Kögerler, P.; Bögge, H. *Mol. Self-assembly* **2000**, *96*, 203–236.
60. Cronin, L. In *Inorganic Chemistry Highlights*; The Potential of Pentagonal Building Blocks : From Giant Ring-shaped to Sperical Polyoxometallate Cluster. Wiley: Weinhiem, Germany 2002, 113–121.
61. Wassermann, K.; Dickman, M. H.; Pope, M. T. *Angew.* Weinhien, Germany *Chem., Int. Ed. Engl.* **1997**, *36*, 1445–1448.
62. Müller, A.; Krickemeyer, E.; Meyer, J.; Bögge, H.; Peters, F.; Plass, W.; Diemann, E.; Dillinger, S.; Nonnenbruch, F.; Randerath, M.; Menke, C. *Angew. Chem., Int. Ed. Engl.* **1995**, *34*, 2122–2124.
63. Müller, A.; Krickemeyer, E.; Bögge, H.; Schmidtmann, M.; Peters, F. *Angew. Chem., Int. Ed.* **1998**, *37*, 3360–3363.
64. Klemperer, W. G.; Marquart, T. A.; Yaghi, O. M. *Angew. Chem., Int. Ed. Engl.* **1992**, *31*, 49–51.
65. Müller, A.; Reuter, H.; Dillinger, S. *Angew. Chem., Int. Ed. Engl.* **1995**, *34*, 2328–2361.
66. Müller, A.; Penk, M.; Krickemeyer, E.; Bögge, H.; Walberg, H. J. *Angew. Chem., Int. Ed. Engl.* **1988**, *27*, 1719–1721.
67. Hayashi, Y.; Fukuyama, K.; Takatera, T.; Uehara, A. *Chem. Lett.* **2000**, 770–771.
68. Day, V. W.; Klemperer, W. G.; Yaghi, O. M. *J. Am. Chem. Soc.* **1989**, *111*, 5959–5961.
69. Khan, M. I.; Zubieta, J. *Angew. Chem., Int. Ed.* **1994**, *33*, 760.
70. Priebsch, W.; Rehder, D.; von Oeynhausen, M. *Chem. Ber.* **1991**, *124*, 761.
71. Huan, G.; Jacobsen, A. J.; Day, V. W. *Angew. Chem., Int. Ed.* **1991**, *30*, 422.
72. Heinirch, D. D.; Folting, K.; Streib, W. E.; Huffman, J. C.; Christou, G. *J. Chem. Soc., Chem. Commun.* **1989**, 1411.
73. Müller, A.; Krickemeyer, E.; Penk, M.; Rohlfing, R.; Armatage, A.; Bögge, H. *Angew. Chem., Int. Ed. Engl.* **1991**, *30*, 1674–1677.
74. Khan, M. I.; Lee, Y. S.; O'Connor, C. J.; Haushalter, R. C.; Zubieta, J. *J. Am. Chem Soc.* **1994**, *116*, 4525.
75. Haushalter, R. C.; Wang, Z.; Thompson, M. E.; Zubieta, J.; O'Connor, C. J. *Inorg. Chem.* **1993**, *32*, 3966.
76. Soghomonian, V.; Chen, Q.; Haushalter, R. C.; Zubieta, J. *Angew. Chem., Int. Ed. Engl.* **1993**, *32*, 610.
77. Lonnroth, P.; Eriksson, J. W.; Posner, B. I.; Smith, U. *Diabetologia* **1993**, *36*, 113–116.
78. Goldfine, A. B.; Simonson, D. C.; Folli, F.; Patti, E.; Kahn, C. R. *Mol. Cell. Biochem.* **1995**, *153*, 217–231.
79. Anonymous, *Chem. Br.* **1988**, *24*, 754–755.
80. King, R. B. *Theochem, J. Mol. Struct.* **1995**, *336*, 165–174.
81. Menke, C.; Diemann, E.; Müller, A. *J. Mol. Struct.* **1997**, *437*, 35–47.
82. Müller, A.; Doring, J. *Z. Anorg. Allg. Chem.* **1991**, *595*, 251–274.
83. Müller, A.; Rohlfing, R.; Barra, A. L.; Gatteschi, D. *Adv. Mater.* **1993**, *5*, 915–917.
84. Müller, A.; Peters, F.; Pope, M. T.; Gatteschi, D. *Chem. Rev.* **1998**, *98*, 239–271.
85. Ueda, Y. *Chem. Mater.* **1998**, *10*, 2653–2664.
86. Chiang, M. H.; Huffman, J. C.; Streib, W. E.; Bollinger, J.; Christou, G. *Abstr. Pap. Am. Chem. Soc.* **1999**, *217*, 290.

87. Gatteschi, D.; Pardi, L.; Barra, A. L.; Müller, A. *Mol. Eng.* **1993**, *3*, 157–169.
88. Gatteschi, D.; Tsukerblat, B. S.; Fainzilberg, V. E. *Appl. Magn. Reson.* **1996**, *10*, 217–249.
89. Lin, B. Z.; Liu, S. X. *J. Chem. Soc., Dalton Trans.* **2002**, 865–869.
90. Livage, J. *Coord. Chem. Rev.* **1998**, *180*, 999–1018.
91. Day, V. W.; Klemperer, W. G.; Yaghi, O. M. *Abstr. Pap. Am. Chem. Soc.* **1989**, *197*, 320.
92. Müller, A.; Penk, M.; Doring, J. *Inorg. Chem.* **1991**, *30*, 4935–4939.
93. Barra, A. L.; Gatteschi, D.; Tsukerblatt, B. S.; Doring, J.; Müller, A.; Brunel, L. C. *Inorg. Chem.* **1992**, *31*, 5132–5134.
94. Brown, I. D.; Kang, K. W. *Acta Crystallogr. Sect. B, Struct. Commun.* **1976**, *B32*, 1957–1958.
95. Müller, A.; Doring, J.; Bögge, H. *J. Chem. Soc., Chem. Commun.* **1991**, 273–274.
96. Gatteschi, D.; Tsukerblatt, B.; Barra, A. L.; Brunel, L. C.; Müller, A.; Doring, J. *Inorg. Chem.* **1993**, *32*, 2114–2117.
97. Müller, A.; Rohlfing, R.; Krickemeyer, E.; Bögge, H. *Angew. Chem., Int. Ed. Engl.* **1993**, *32*, 909–912.
98. Klemperer, W. G.; Marquart, T. A.; Yaghi, O. M. *Mater. Chem. Phys.* **1991**, *29*, 97–104.
99. Kawanami, N.; Ozeki, T.; Yagasaki, A. *J. Am. Chem. Soc.* **2000**, *122*, 1239–1240.
100. Winpenny, R. E. P. *J. Chem. Soc., Dalton Trans.* **2002**, 1–10.
101. Müller, A.; Doring, J. *Angew. Chem., Int. Ed. Engl.* **1988**, *27*, 1721–1721.
102. Barra, A. L.; Gatteschi, D.; Pardi, L.; Müller, A.; Doring, J. *J. Am. Chem. Soc.* **1992**, *114*, 8509–8514.
103. Gatteschi, D.; Pardi, L.; Barra, A. L.; Müller, A.; Doring, J. *Nature* **1991**, *354*, 463–465.
104. Yamase, T.; Ohtaka, K. *J. Chem. Soc., Dalton Trans.* **1994**, 2599–2608.
105. Müller, A.; Krickemeyer, E.; Penk, M.; Walberg, H. J.; Bögge, H. *Angew. Chem., Int. Ed. Engl.* **1987**, *26*, 1045–1046.
106. Müller, A.; Sessoli, R.; Krickemeyer, E.; Bögge, H.; Meyer, J.; Gatteschi, D.; Pardi, L.; Westphal, J.; Hovemeier, K.; Rohlfing, R.; Doring, J.; Hellweg, F.; Beugholt, C.; Schmidtmann, M. *Inorg. Chem.* **1997**, *36*, 5239–5250.
107. Robin, M. B.; Day, P. *Adv. Inorg. Chem. Radiochem.* **1967**, *10*, 247–248.
108. Müller, A.; Doring, J.; Bögge, H.; Krickemeyer, E. *Chimia* **1988**, *42*, 300–301.
109. Yamase, T.; Suzuki, M.; Ohtaka, K. *J. Chem. Soc., Dalton Trans.* **1997**, 2463–2472.
110. Chirayil, T.; Zavalij, P. Y.; Whittingham, M. S. *Acta Crystallogr. Sect. C, Cryst. Struct. Commun.* **1998**, *54*, 1441–1444.
111. Müller, A. *Nature* **1991**, *352*, 115.
112. Müller, A.; Rohlfing, R.; Doring, J.; Penk, M. *Angew. Chem., Int. Ed. Engl.* **1991**, *30*, 588–590.
113. Shklover, V.; Haibach, T.; Ried, F.; Nesper, R.; Novak, P. *J. Solid State Chem.* **1996**, *123*, 317–323.
114. Baker, L. C. W.; Figgis, J. S. *J. Am. Chem Soc.* **1970**, *92*, 3794–3795.
115. Weinstock, I. A.; Cowan, J.; Barbuzzi, E. M. G.; Zeng, H.; Hill, C. L. *J. Am. Chem Soc.* **1999**, *121*, 4608–4617.
116. Teze, A.; Cadot, E.; Bereau, V.; Herve, G. *Inorg. Chem.* **2001**, *40*, 2000–2004.
117. Contant, R.; Thouvenot, R. *Inorg. Chim. Acta* **1993**, *212*, 41–50.
118. Peacock, R. D.; Weakley, T. J. R. *J. Chem. Soc.* **1971**, 1836–1838.
119. Sadakane, M.; Dickman, M. H.; Pope, M. T. *Angew. Chem., Int. Ed.* **2000**, *39*, 2914–2916.
120. Termes, S. C.; Pope, M. T. *Transit. Met. Chem.* **1978**, *3*, 103–105.
121. Sadakane, M.; Ostuni, A.; Pope, M. T. *J. Chem. Soc., Dalton Trans.* **2002**, 63.
122. Müller, A.; Fedin, V. P.; Kuhlmann, C.; Fenske, H. D.; Baum, G.; Bögge, H.; Hauptfleisch, B. *Chem. Commun.* **1999**, 1189–1190.
123. Herve, G.; Michelon, M.; Teze, A. *Inorg. Chem.* **1997**, *36*, 505–509.
124. Tourne, C. M.; Tourne, G. F.; Weakley, T. J. R. *J. Chem. Soc., Dalton Trans.* **1986**, 2237–2242.
125. Fuchs, J.; Palm, R. *Z. Naturforsch* **1984**, *39b*, 757–762.
126. Tourne, C. M.; Tourne, G. F. *J. Chem. Soc. Chem. Dalton Trans.* **1988**, 2411–2420.
127. Weakley, T. J. R. *J. Chem. Soc., Chem. Commun.* **1984**, 1406–1407.
128. Galan-Mascaros, J. R.; Gomez-Garcia, C. J.; Borras-Almenar, J. J.; Coronado, E. *Adv. Mater.* **1994**, *6*, 221–223.
129. Coronado, E.; Gomez-Garcia, C. J. *Comments Inorg.* **1995**, *17*, 255–256.
130. Yamase, T.; Naruke, H.; Sasaki, Y. *J. Chem. Soc., Dalton Trans.* **1990**, 1687–1696.
131. Jeannin, Y.; Martin-Frere, J. *J. Am. Chem. Soc.* **1981**, *103*, 1664–1667.
132. Jeannin, Y. *J. Cluster Sci.* **1992**, *3*, 55–58.
133. Bosing, M.; Loose, I.; Pohlmann, H.; Krebs, B. *Chem. Eur. J.* **1997**, *3*, 1232–1237.
134. Herve, G.; Teze, A. *Inorg. Synth.* **1990**, *27*, 118–120.
135. Wassermann, K.; Pope, M. T. *Inorg. Chem.* **2001**, *40*, 2763–2768.
136. Contant, R.; Teze, A. *Inorg. Chem.* **1985**, *24*, 4610–4614.
137. Alizadeh, M. H.; Harmalker, S. P.; Jeannin, Y.; Martin-Frere, J.; Pope, M. T. *J. Am. Chem. Soc.* **1985**, *107*, 2662–2669.
138. Creaser, I.; Heck, M. C.; Neitz, R. J.; Pope, M. T. *Inorg. Chem.* **1993**, *32*, 1573–1578.
139. Antonio, M. R.; Soderholm, L. *Inorg. Chem.* **1994**, *33*, 5988–5993.
140. Soderholm, L.; Liu, G. K.; Muntean, J.; J, M.; Antonio, M. R. *J. Phys. Chem.* **1995**, *99*, 9611–9616.
141. Antonio, M. R.; Soderholm, L. *J. Cluster Sci.* **1996**, *7*, 585–587.
142. Antonio, M. R.; Soderholm, L. *J. Alloys Compd.* **1997**, *250*, 541.
143. Dickman, M. H.; Gama, G. J.; Kim, K. C.; Pope, M. T. *J. Cluster Sci.* **1996**, *7*, 567–573.
144. Harrup, M. K.; Hill, C. L. *Inorg. Chem.* **1994**, *33*, 5448–5455.
145. Topsoe, H.; Clausen, B. S.; Topsoe, N. Y.; Pedersen, E.; Niemann, W.; Müller, A.; Bögge, H.; Lengeler, B. *J. Chem. Soc., Faraday Trans. I* **1987**, *83*, 2157–2167.
146. Müller, A.; Serain, C. *Accounts Chem. Res.* **2000**, *33*, 2–10.
147. Müller, A.; Meyer, J.; Krickemeyer, E.; Diemann, E. *Angew. Chem., Int. Ed. Engl.* **1996**, *35*, 1206–1208.
148. Chae, H.; Klemperer, W. G.; Marquart, T. A. *Coord. Chem. Rev.* **1993**, *128*, 209–224.
149. Müller, A.; Meyer, J.; Krickemeyer, E.; Beugholt, C.; Bögge, H.; Peters, F.; Schmidtmann, M.; Kögerler, P.; Koop, M. J. *Chem., Eur. J.* **1998**, *4*, 1000–1006.
150. Müller, A.; Dillinger, S.; Krickemeyer, E.; Bögge, H.; Plass, W.; Stammler, A.; Haushalter, R. C. *Z. Naturforsch. (B)* **1997**, *52*, 1301–1306.
151. Müller, A.; Krickemeyer, E.; Dillinger, S.; Bögge, H.; Plass, W.; Proust, A.; Dloczik, L.; Menke, C.; Meyer, J.; Rohlfing, R. *Z. Anorg. Allg. Chem.* **1994**, *620*, 599–619.
152. Zhang, S.-W.; Huang, G.-Q.; Shao, M.-C.; Tang, Y.-Q. *J. Chem. Soc., Chem. Commun.* **1993**, 37–38.

153. Müller, A.; Krickemeyer, E.; Dillinger, S.; Bögge, H.; Proust, A.; Plass, W.; Rohlfing, R. *Naturwissenschaften* **1993**, *80*, 560–564.
154. Müller, A.; Bögge, H.; Krickemeyer, E.; Dillinger, S. *Bull. Pol. Acad. Sci., Chem.* **1994**, *42*, 291–298.
155. Müller, A.; Plass, W.; Krickemeyer, E.; Sessoli, R.; Gatteschi, D.; Meyer, J.; Bögge, H.; Krockel, M.; Trautwein, A. X. *Inorg. Chim. Acta* **1998**, *271*, 9–12.
156. Müller, A.; Das, S. K.; Fedin, V. P.; Krickemeyer, E.; Beugholt, C.; Bögge, H.; Schmidtmann, M.; Hauptfleisch, B. *Z. Anorg. Allg. Chem.* **1999**, *625*, 1187–1192.
157. Müller, A.; Beugholt, C.; Koop, M.; Das, S. K.; Schmidtmann, M.; Bögge, H. *Z. Anorg. Allg. Chem.* **1999**, *625*, 1960–1962.
158. Müller, A.; Krickemeyer, E.; Bögge, H.; Schmidtmann, M.; Beugholt, C.; Das, S. K.; Peters, F. *Chem., Eur. J.* **1999**, *5*, 1496–1502.
159. Bradley, D. *News Scientist* **1995**, *18*, 18.
160. Yamase, T.; Prokop, P. V. *Angew. Chem., Int. Ed.* **2002**, *41*, 466–469.
161. Müller, A.; Krickemeyer, E.; Bögge, H.; Schmidtmann, M.; Peters, F.; Menke, C.; Meyer, J. *Angew. Chem., Int. Ed. Engl.* **1997**, *36*, 484–486.
162. Müller, A.; Das, S. K.; Bögge, H.; Beugholt, C.; Schmidtmann, M. *Chem. Commun.* **1999**, 1035–1036.
163. Müller, A.; Das, S. K.; Kuhlmann, C.; Bögge, H.; Schmidtmann, M.; Diemann, E.; Krickemeyer, E.; Hormes, J.; Modrow, H.; Schindler, M. *Chem. Commun.* **2001**, 655–656.
164. Müller, A.; Maiti, R.; Schmidtmann, M.; Bögge, H.; Das, S. K.; Zhang, W. J. *Chem. Commun.* **2001**, 2126–2127.
165. Müller, A.; Krickemeyer, E.; Bögge, H.; Schmidtmann, M.; Kögerler, P.; Rosu, C.; Beckmann, E. *Angew. Chem., Int. Ed.* **2001**, *40*, 4034–4038.
166. Müller, A.; Krickemeyer, E.; Bögge, H.; Schmidtmann, M.; Beugholt, C.; Kögerler, P.; Lu, C. Z. *Angew. Chem., Int. Ed.* **1998**, *37*, 1220–1223.
167. Jiang, C. C.; Wei, Y. G.; Liu, Q.; Zhang, S. W.; Shao, M. C.; Tang, Y. Q. *Chem. Commun.* **1998**, 1937–1938.
168. Müller, A.; Shah, S. Q. N.; Bögge, H.; Schmidtmann, M. *Nature* **1999**, *397*, 48–50.
169. Cotton, F. A.; Wikinson, G. *Advanced Inorganic Chemistry*; 4th ed.; John Wiley: New York, 1980.
170. Müller, A.; Koop, M.; Bögge, H.; Schmidtmann, M.; Beugholt, C. *Chem. Commun.* **1998**, 1501–1502.
171. Müller, A.; Beugholt, C.; Bögge, H.; Schmidtmann, M. *Inorg. Chem.* **2000**, *39*, 3112–3114.
172. Cronin, L.; Beugholt, C.; Müller, A. *J. Mol. Struct. Theochem* **2000**, *500*, 181–193.
173. Cronin, L.; Beugholt, C.; Krickemeyer, E.; Schmidtmann, M.; Bögge, H.; Kögerler, P.; Luong, T. K. K.; Müller, A. *Angew Chem., Int. Ed.* **2002**, *41*, 2805–2808.
174. Kemp, M. *Nature* **1998**, *393*, 123.
175. Viant, M. R.; Cruzan, J. D.; Lucas, D. D.; Brown, M. G.; Liu, K. J.; Saykally, R. J. *J. Phys. Chem. A.* **1997**, *101*, 9032–9041.
176. Ludwig, R.; Weinhold, F.; Farrar, T. C. *J. Chem. Phys.* **1997**, *107*, 499–507.
177. Müller, A.; Fedin, V. P.; Kuhlmann, C.; Bögge, H.; Schmidtmann, M. *Chem. Commun.* **1999**, 927–928.
178. Müller, A.; Polarz, S.; Das, S. K.; Krickemeyer, E.; Bögge, H.; Schmidtmann, M.; Hauptfleisch, B. *Angew. Chem., Int. Ed.* **1999**, *38*, 3241–3245.
179. Müller, A.; Shah, S. Q. N.; Bögge, H.; Schmidtmann, M.; Kögerler, P.; Hauptfleisch, B.; Leiding, S.; Wittler, K. *Angew. Chem., Int. Ed.* **2000**, *39*, 1614–1616.
180. Müller, A.; Diemann, E.; Shah, S. Q. N.; Kuhlmann, C.; Letzel, M. C. *Chem. Commun.* **2002**, 440–441.
181. Müller, A.; Sarkar, S.; Shah, S. Q. N.; Bögge, H.; Schmidtmann, M.; Kögerler, P.; Hauptfleisch, B.; Trautwein, A. X.; Schunemann, V. *Angew. Chem., Int. Ed.* **1999**, *38*, 3238–3241.
182. Müller, A.; Koop, M.; Bögge, H.; Schmidtmann, M.; Peters, F.; Kögerler, P. *Chem. Commun.* **1999**, 1885–1886.
183. Müller, A.; Krickemeyer, E.; Das, S. K.; Kögerler, P.; Sarkar, S.; Bögge, H.; Schmidtmann, M. *Angew. Chem., Int. Ed.* **2000**, *39*, 1612–1614.
184. Müller, A.; Das, S. K.; Bögge, H.; Schmidtmann, M.; Botar, A.; Patrut, A. *Chem. Commun.* **2001**, 657–658.
185. Müller, A.; Das, S. K.; Kögerler, P.; Bögge, H.; Schmidtmann, M.; Trautwein, A. X.; Schunemann, V.; Krickemeyer, E.; Preetz, W. *Angew. Chem., Int. Ed.* **2000**, *39*, 3414–3418.
186. Cronin, L.Das, S. K.Müller, A. *Unpublished results* **2000**.
187. Müller, A.; Kögerler, P.; Bögge, H. *Struct. Bonding* **2000**, *96*, 203–211.
188. Coxeter, H. S. M. *Introduction to Geometry* **1969**, Wiley: New York.
189. Kroto, H. W.; Heath, J. R.; O'Brien, S. C.; Curl, R. F.; Smalley, R. E. *Nature* **1985**, *318*, 162–163.
190. Müller, A.; Kögerler, P. *Bull. Pol. Acad. Sci., Chem.* **1998**, *46*, 207–219.
191. Müller, A.; Kögerler, P. *Coord. Chem. Rev.* **1999**, *182*, 3–17.
192. Müller, A.; Kögerler, P. *Coord. Chem. Rev.* **2000**, *199*, 335–341.
193. Cronin, L.Yamase, T. *Personal communication* **2002**.

Comprehensive Coordination Chemistry II
ISBN (set): 0-08-0437486

Volume 7, (ISBN 0-08-044329X); pp 1–56